VAAL UNIVERSITY OF TECHNOLOGY

SYNTHESIS AND CHARACTERIZATION OF PINE CONE CARBON SUPPORTED IRON OXIDE CATALYST FOR DYE AND PHENOL DEGRADATION

MMELESI OLGA KELEBOGILE

Student number: 210114940

BTech: Chemistry

Dissertation submitted in fulfilment of the requirement for the degree of

MAGISTER TECHNOLOGIAE: CHEMISTRY

FACULTY OF APPLIED AND COMPUTER SCIENCES

DEPARTMENT OF CHEMISTRY

SUPERVISOR: Prof. A. E OFOMAJA (BSc Hons, MSc, DTech Chemistry)

CO-SUPERVISOR: Dr. E. L VILJOEN (BSc Hons, MSc, Ph.D. Chemistry)

JUNE 2017

DECLARATION

I declared that unless indicated otherwise, this dissertation is my own work. It is being submitted for the Degree Magister Technologiae in Chemistry to the Department of Chemistry, Vaal University of Technology, Vanderbijlpark and has not been submitted before for any degree or examination to any other university.

DEDICATION

This work is dedicated to my parents, S. I. & G. R. Mmelesi.

ACKNOWLEDGEMENTS

I would like to express my profound appreciation and gratitude to the following for their contributions to this work:

- ✓ My supervisors, Prof. A. E. Ofomaja & Dr. E. L. Viljoen for their educative and constructive comments, guidance, inputs, and support throughout this research.
- ✓ The Vaal University of Technology through the Research Directorate for providing the research funding. The Department of Chemistry for providing the necessary structures for the research.
- ✓ The National Research Foundation (NRF) & SASOL for my fees funding, which made my life easier
- ✓ My fellow postgraduate students in the research laboratories for creating a supportive and a friendly working environment.
- ✓ My family for their undying support and for believing in me. Thank you for being the rock in my life.
- ✓ The God almighty for giving me life and strength tackle this task.

RESEARCH OUTPUTS

Presentations

The results of this study were presented in the following conferences:

- "Adsorption of methylene blue from aqueous solution onto carbon prepared from pine cone". The 42nd National Convention of the South African Chemical Institute held at the Southern Sun Elangeni Hotel in Durban, South Africa from 29th November 2015 – 4th December 2015. Oral presentation

- "Degradation of methylene blue by heterogeneous Fenton oxidation process using pine cone carbon supported iron oxide catalyst" Centre of Renewable Energy and Water (CREW):held at VUT Southern Gauteng Science & Technology Park, Sebokeng on the 26 February 2016. Oral presentation

- Effect of microwave power on the methylene blue number (MBN) and iodine number (IN) on the production of activated carbon via microwave pyrolysis" 2016 International Conference of Pure and Applied Chemistry held in Mauritius from 18-22 July 2016. Oral presentation

- " Influence of the microwave power during catalyst preparation for heterogeneous catalytic Fenton's degradation of methylene blue" Catalysis Society of South Africa held at Champagne Sports Resort, Central Drakensberg, South Africa from 6 – 9 November 2016-Poster.

ABSTRACT

Fenton oxidation is classified into two processes, homogeneous and heterogeneous. Homogeneous Fenton oxidation process, have been shown to be efficient in the degradation of organic pollutants. However, it was shown to have limitations which can be addressed by the heterogeneous Fenton oxidation. Despite the high efficiency of the heterogeneous Fenton oxidation process in the degradation of recalcitrant organic pollutants, the currents synthesis trends of the heterogeneous Fenton catalyst have been proven to be time and energy constraining, since it involves the multi-step were the activated carbon have to be prepared first then co-precipitate the iron oxide on the activated carbon. However, as much as the heterogeneous Fenton catalyst has been proven to have high catalytic activity towards degradation of organic pollutants, these catalysts have some limitations, such limitations include metal ions being leached from the catalyst support into the treated water causing catalyst deactivation and a secondary pollution to the treated water.

In this thesis, these catalysts have been applied in the degradation of recalcitrant organic pollutants such as methylene blue and phenols. This study focuses on the single step synthesis of iron oxide nanoparticles supported on activated carbon, were carbonaceous material is impregnated with iron salt then pyrolysed via microwave heating. Microwave power and the amount of iron salt were optimized. The prepared activated carbon-iron oxide composites were applied to the degradation of 2-nitrophenol (2-NP) and methylene blue (MB). Methylene blue was used as a model compound due to the fact that it is easier to monitor the degradation process with UV-Vis as compared to 2-nitrophenol . 2-nitrophenol the additional step for the adjustment of pH is required since nitrophenols are colorless in color at lower pH.

The characterization showed that the microwave power and the amount of the iron precursor have an influence on the porosity and surface functional groups of the activated carbon. Further it was

observed that microwave power and iron precursor influnces the amount of iron oxide formed on the surface of the support. It was also observed that the activated carbon-iron oxide composite have the catalytic effects on the Fenton oxidation process of MB and 2-NP. The parameters such as H_2O_2, pH, catalyst dose, initial concentration, temperature affect the degradation of both MB and 2-NP.

Kinetics studies showed that Fenton is a surface driven reaction since the results fitted the pseudo first order model. The thermodynamics parameters also showed that the reaction is endothermic, spontaneous and is randomized. This implies that the reaction of the degradation of MB and 2-NP is feasible and the catalysts prepared have high catalytic activity. MB and 2-NP were degraded to smaller organic molecules (carboxylic acids). The stability of the catalyst observed to decrease as the number of cycles increased, this is due to the leaching of iron ions from the support material. Hence it was concluded that the activated carbon-iron oxide composite was successfully synthesized and had the high catalytic activity for the degradation of MB and 2-NP.

OUTLINE

The study is divided into nine chapters

Chapter 1:

The chapter covers the introduction, problem statement, aim, objectives and hypothesis of the research

Chapter 2:

The literature review of the pollutants in industrial wastewater and methods of their removal is dealt with in this chapter. The heterogeneous Fenton oxidation process is introduced as an alternative technique for the degradation of the pollutants. An in-depth review on the activated carbon-iron oxide composites as heterogeneous Fenton catalyst, its merits and limitations are also discussed together with their synthesis methods.

Chapter 3:

The experimental procedures for the synthesis, characterization, and application of the activated carbon iron oxide composite as catalyst for the Fenton oxidation of 2-nitrophenol and methylene blue

Chapter 4:

This chapter describes the first part of the results and discussion. The chapter focuses on the characterization of the synthesized PCP-AC-Iron oxide composites using various techniques.

Chapter 5:

The chapter describes the second part of the results. It focuses on the effect of experimental conditions for the degradation of methylene blue and 2-nitrophenol by Fenton oxidation process. It reports the following details: effect of H_2O_2, the effect of pH, catalyst dose, stirring speed, the effect of initial concentration of the pollutant, and effect of temperature.

Chapter 6:

This chapter discusses part three of the results. It focuses on fitting the data to the pseudo-first-order, pseudo-second-order model, and Langmuir-Hinshelwood model and it is presented together with the error functions.

Chapter 7:

It describes and discusses the fourth part of the results and discussion. It focuses on the discussion of the thermodynamic parameters of the degradation process of 2-NP. The temperatures were varied during the degradation of 2-NP so that rate constants and activation energies were calculated. The thermodynamics parameters such as Gibbs free energy (ΔG), change in enthalpy (ΔH), and change in entropy (ΔS) were also determined.

Chapter 8:

This chapter presents and discusses the fifth part of the results. It presents and discusses the degradation mechanism, catalyst stability and degradation products of MB and 2-NP by Fenton oxidation process. It reports on the effect of radical scavenging on the degradation, the amount of iron oxide leached during catalyst reuse.

Chapter 9

This chapter presents conclusion and recommendations of the study

TABLE OF CONTENTS

LIST OF ABBREVIATIONS AND SYMBOLS

2-NP	2-nitrophenol
MB	Methylene blue
LMB	Leuco-methylene blue
PCP	Pine cone powder
PCP-AC	Pine cone powder-activated carbon
MBN	Methylene blue number
IN	Iodine number
XRD	X-ray diffraction
FTIR	Fourier-transform infrared spectroscopy
TGA	Thermogravimetric analysis
SEM	Scanning electron microscopy
EDX	Electron dispersive spectroscopy
GC-MS	Gas chromatography-mass spectroscopy
XPS	X-ray photoelectron spectroscopy
PZC	Point of zero charge
r	Rate of degradation
C	Initial concentration
C_t	Concentration at any time
k_1	Pseudo first-order rate constant
k_2	Pseudo second order rate constant

θ_L	Fraction of surface sites covered
ΔG	Gibbs free energy
ΔH	Change in enthalpy
ΔS	Change in entropy
Ea	Activation energy

LIST OF FIGURES

LIST OF TABLES

CHAPTER 1: INTRODUCTION

1.1 Background

The interest will be shown to water due to the fact that it is one of the essential elements on which all forms of life depends on. In the 21st century, the major problem humanity is facing is water quality. Water researchers have approximated that by the year 2025 the world will be facing water crisis (KULSHRESHTHA, 1998, RIJSBERMAN, 2006). More than one-third of earth's freshwater is utilized for domestic, agricultural and industrial purposes. Consequently, these activities lead to enormous water pollution with different synthetic and geogenic natural chemicals at different concentrations (COSGROVE and RIJSBERMAN, 2000). Chemical pollution of natural water has become one of the major problem in all parts of the world. Due to an increase in urbanization and industrialization as the results of population growth, resulting putting on the depletion of freshwater in many parts of the world.

Traces organic pollutants such as pharmaceutical and personal care products (PPCPs) and other effluents have been reported in wastewater and aquatic system (RIJSBERMAN, 2006, SCHWARZENBACH et al., 2006). These compounds are usually introduced to water bodies through a number of ways but primarily from untreated wastewater and inadequately treated sewage (KUMAR et al., 2007). Due to the increasing environmental and health concerns, these organic pollutants of have been of particular interest due to the fact that a long-term exposure, even at low levels could have serious effects on both aquatic and terrestrial ecosystems including human health (UNESCO, 2009).

The occurrence of these organic pollutants results in two major problems in water management, which are a source of water protection and the potential reuse of industrial and municipal

wastewater. The long term of water sustainability solely depends on the management of water resources, protection of water sources and the efficiency of the wastewater treatment techniques for various pollutants (FATTA-KASSINOS et al., 2015). However, the traditional method of wastewater treatment cannot completely remove many of these contaminants of emerging concerns. An alternative process for wastewater treatment in order to degrade these contaminants has been of interest recently (TIZAOUI and GRIMA, 2011). Advanced oxidation processes (AOPs) are the extensively studied processes. They employ the use hydroxyl radical to oxidize contaminants to smaller and less polluting molecules or mineralize them to carbon dioxide, water and inorganic ions (NOGUEIRA et al., 2014).

1.2 Problem statement

Rapid increase in industrialization has led to the disposal of toxic chemicals into water bodies,the effectsare considered harmful to both plants and animals. Treatment of contaminated wastewater is a challenge since they contains a variety of pollutants such as heavy metals and organic compounds, at different concentrations. There have been efforts by researchers from all over the world to produce several efficient and cost effective treatment techniques to combat the issue of an ever-increasing disposal of contaminated effluents into water bodies.

Heterogeneous Fenton's degradation has been proven to be effective for the removal of recalcitrant organic compounds in wastewater by many researchers but this process has some limitations, such as, the current synthesis trends demand high energy. The synthesis trends are also time consuming due to the fact that it requires multiple steps. Activated carbon is used as a support but commercially activated carbon is usually expensive. The conventional heating when preparing activated carbon is not favorable because is time-consuming and demands high temperatures which leads to high cost due to the consumption of high energy.

As much as heterogeneous Fenton catalyst have shown to be efficient in the degradation of recalcitrant organic pollutants, the catalysts faces some chagellenges such as, some metal ions being leached from the support into the treated water causing another secondary pollution problem in the water and also causing catalyst deactivation, due to their multi steps synthesis process.

1.3 Aim and objectives

The aim of the study is to prepare low-cost and non-toxic heterogeneous Fenton catalyst from an iron oxide nanoparticle supported on activated carbon that is produced from an agricultural waste material for 2-nitrophenol (2-NP) and methyelene blue degradation (MB).

The research aim was achieved through the following objectives:

a. To prepare activated carbon-iron oxide composite from agricultural waste by microwave pyrolysis

b. To utilize iron chloride hexahydrate as a chemical activator and source of iron oxide

c. Catalyst characterization

d. To study the influence of microwave power and iron loading on the degradation of MB and 2-NP by Fenton-like oxidation process

e. To study the influence of iron loading and microwave power on the amount of leached iron

f. To study the degradation mechanism and kinetics

g. To study the degradation products

1.4 Hypothesis

There has been efficient catalyst before but some catalysts were experiencing catalytic leaching, which caused contamination to the treated water and the catalytic degradation. This affected the activity of the catalyst. It can be hypothesized by adding iron during the activated carbon formation would yield a catalyst which has a greater metal oxide support interaction leading to a decrease in the leaching of the iron oxide.

1.5 References

COSGROVE, W. J. & RIJSBERMAN, F. R. 2000. *World Water Vision: Making Water Everybody's Business,* London:World Water Council, Earthscan.

FATTA-KASSINOS, D., MANAIA, C., BERENDOK, T. U., CYTRYN, E., BAYONA, J., CHEFETZ, B., SLOBONDNIK, J., KREUZINGER, N., RIZZO, L., MALATO, S., LUNDY, L. & LEDIN, A. 2015. COST Action ES1403: New and Emerging challenges and opportunities in wastewater REUse (NEREUS). *Environmental Science and Pollution Research International,* 22**,** 7183-7186.

KULSHRESHTHA S, N. 1998. A global outlook for water resources to the year 2025. *Water Research Management,* 12, 167-184.

KUMAR, A., KUMAR, S., KUMAR, S. & GUPTA, D. V. 2007. Adsorption of phenol and 4-nitrophenol on granular activated carbon in basal salt medium: Equilibrium and kinetics. *Journal of Hazardous Materials.,* 147, 155-166.

NOGUEIRA, A. E., CASTRO, I. A., GIROTO, A. S. & MAGRIOTIS, Z. M. 2014. Fenton-Like Catalytic Removal of Methylene Blue Dye in Water Using Magnetic Nanocomposite (MCM-41/Magnetite). *Journal of Catalysts***,** 6.

RIJSBERMAN, F. R. 2006. Water scarcity: Fact or fiction? *Agricultural Water Management,* 80, 5-22.

SCHWARZENBACH, R. P., ESCHER, B. I., FENNER, K., HOFSTETTER, T. B. & JOHNSON, C. 2006. The challenge of micropollutants in aquatic systems. *Science,* 313, 1072-1077.

TIZAOUI, C. & GRIMA, N. 2011. Kinetics of the ozone oxidation of Reactive Orange 16 azo dye in aqueous solution. *Chemical Engineering Journal*, 173**,** 463-473.

UNESCO 2009. The United Nations World Water Development Report 3: Water in a Changing World. Paris: United Nations Education, Scientific and Cultural Organisation/Berghahn Books.

CHAPTER 2: LITERATURE REVIEW

2.1 Wastewater

Water is essential to all living creatures. There is approximately over 1×10^9 km^3 of water on earth. Although the majority of the planet is covered by water, the vast majority is unavailable to the terrestrial and freshwater system. Less than 3% water is fresh enough to drink or irrigate crops and of that total, more than two-thirds are locked away in glaciers and ice caps. Freshwater lakes and rivers hold 100 000 km^3 globally, which is less than 0.01% of water on earth (JACKSON et al., 2001). The consumption of fresh water has increased globally by 1 % since the 1980s. The demand for potable water has increased due to the increasing urbanization and rising living standards. Kulshreshtha and Rijsberman projected that by 2025 the world will be facing water crisis(KULSHRESHTHA, 1998, RIJSBERMAN, 2006).

Wastewater is any water that has been contaminated by organic/inorganic chemicals, microorganisms, or any substance that deteriorates its quality. Effluent containing pollutants like heavy metals, pharmaceuticals, pesticides, dyes are a major threats to our water quality (OLLER et al., 2011). These pollutants enter the water bodies either directly (effluents from industries to water streams) or indirectly (when pollutants are released into the air or land) (DEBLONDE et al., 2011). Some of these pollutants found in the wastewater especially industrial wastewaters are synthetic dyes and phenols.

2.1.1 Synthetic dyes

Synthetic dyes are a group of organic pollutants found in industrial wastewaters. They are used in textile, paper, plastic, pharmaceutical, leather, paint, food packaging, and other industries to color products. These organic molecules, when released into the aquatic systems, cause coloration of the

water and the view of the public on water quality is greatly influenced by color (CHOY et al., 2004). There are more than 100 000 commercial dyes with more than 7×10^8 kg being produced annually (PEARCE et al., 2003, RAMAN and KANMANI, 2016). Wastewater containing dyes is very difficult to treat since they are highly soluble, recalcitrant organic molecules, resistant to aerobic digestion and are stable to light, heat and oxidizing agents (SUN and YANG, 2003). This is due to their complex chemical structure, xenobiotic nature and synthetic organic origin (CRINI, 2006). Disposal of wastewater containing dyes without proper treatment causes myriad of problems to the aquatic environment, such as reducing gas solubility, light penetration, and photosynthesis. Dyes may also be toxic to some aquatic life due to the presence of aromatics, metals, chlorides and other elements (FU and VIRARAGHAVAN, 2001). Traditional biological wastewater treatment techniques based on aerobic and anaerobic digestion are not efficient at dye removal from wastewater since dyes are toxic to the organisms being used (KUSIC and BOZOIC, 2007). According to Greluk and Hubicki (2010), dyes can be classified into three categories: (1) Anionic- (Methyl Orange), (2) Non-ionic (Eriochrome Black T), (3) Cationic (Methylene Blue) dyes.

2.1.1.1 Methylene Blue

Methylene blue is an inexpensive and common dye used in textile industries (OLEJNIK et al., 2016). It is a cationic dye with chemical structure (Figure 2.1):

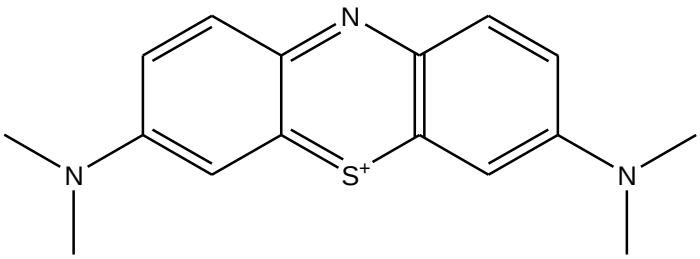

Figure 2. 1: Structure of Methylene Blue (MB)

Methylene Blue is known to cause irritation to gastrointestinal tract with symptoms of nausea, vomiting, diarrhea if swallowed and also methemoglobinemia, cyanosis, convulsion and etc. (RAMAN and KANMANI, 2016).

Physical and chemical techniques such as coagulation, adsorption, ultrafiltration and reverse osmosis are usually used to remove these dyes efficiently from wastewater. However, these processes may transfer the dyes from liquid phase to solid waste. As a result, the technique for the degradation of dyes and many other organic molecules in wastewater is essential.

2.1.2 Phenols

One of the organic contaminants that have attracted interest is phenols and substituted phenols. Phenols and substituted compounds have been put as the priority of pollutants (KUMAR et al., 2007). Phenolic compounds are major pollutants that are produced from industries like petrochemical, pharmaceuticals, petroleum, and food processing industries. These phenol and derivatives are usually detected in the surface water, agricultural and industrial water due to their low biodegradability, high solubility, low vaporization pressure and weak ionization capacity. According to World Health Organization (WHO)(UNESCO, 2009), the allowed limit of detection for the phenolic compounds in tap water is 1 ppb.

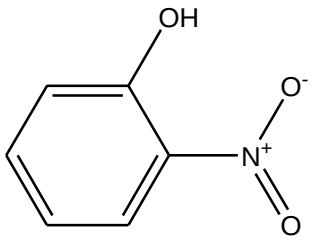

2-nitrophenol

Figure 2. 2: Structure of 2-nitrophenol

2-nitrophenol which is a phenol derivative is highly toxic to organisms even at low concentration, hence it has been classified by the United State Environmental Protection Agency (USEPA) as a priority hazardous pollutant. Clean Water Act (CWA), has listed 2-nitrophenol within the 126 priority of organic pollutants under the permissible limit of 20 ppb in the environment (TEH and MOHAMED, 2011). This pollutant is biorecalcitrant, meaning it cannot be biodegraded easily. Stronger chemical degradation processes are thus required to degrade these pollutants to smaller molecules that can be removed easily (BELTRAN et al., 2005).

Due to the toxic and carcinogenic properties of this organic pollutant, it is necessary to treat polluted water before releasing into the environment. Despite its presence at low concentrations, this pollutant poses serious threats to freshwater supply, living organisms, and public health (BREZONIK and ARNOLD, 2012). This pollutant is produced in large quantities especially in developed countries therefore, good reliable methods are necessary to treat effluents before discharge. Hence it has been selected as the targeted organic pollutant.

2.2 Wastewater Treatment Technologies

There are several methods available to decompose organic pollutants in water. These methods include adosption, fltrattion, advanced oxidation processes (AOPs). AOPs are defined as a process that involves the production of highly reactive radicals required for the oxidation of organic

pollutants present in wastewater (ANASTASIOU et al., 2009). These treatment processes have shown to be very promising in the treatment of wastewater that has bio-recalcitrant pollutants. These AOPs are shown to be better alternatives for the degradation of the toxic organic pollutants which are based on the production of hydroxyl radicals. The hydroxyl radicals are non-selective and powerful oxidizing agent which reacts faster than ozone and hydrogen peroxide (MARTÍNEZ-HUITLE and BRILLAS, 2009).

Table 2. 1: oxidizing agent potential

OXIDIZING AGENT	OXIDATION POTENTIAL (V)
Hydroxyl radicals	2.80
Oxygen (atomic)	2.42
Ozone	2.08
Hydrogen peroxide	1.78
Oxygen (molecule)	1.23

(HABER and WEISS, 1934)

AOPs have the ability to completely degrade an organic pollutant to CO_2, H_2O and mineral salts(GUO et al., 2017). AOPs are suitable for effective degradation of dissolved organic contaminants such as halogenated hydrocarbons, aromatics, phenols, pesticides, and several toxic pollutants. Therefore, AOPs are promising technologies for the degradation of toxic organic pollutants in water. AOPs are attracting attention due to their potential as a successful solution to water pollution and friendliness to the environment. Among the AOPs, Fenton oxidation process has been recognized as a low-cost technology, since it operates at mild conditions and requires simple installations.

2.2.1 Catalytic wet peroxide oxidation/ Fenton oxidation process

Catalytic wet peroxide oxidation (CWPO) is also known as Fenton oxidation process. It is the process whereby hydrogen peroxide decomposes in the presence of a catalyst to produce hydroxyl radicals that are a strong oxidant that is further used for the oxidation and the degradation of organic pollutants (SUN et al., 2007). The first published work on the oxidation of organic molecules using Fe^{2+} and H_2O_2 was done by the British researcher H.J Fenton in 1894, where he reported on the oxidation of tartaric acid based on the mixture of H_2O_2 and Fe^{2+} (FENTON, 1894). The Fenton process is efficient when the optimum pH of the aqueous solution is around 2.8-3.0. Typical conditions are room temperature and atmospheric pressure (ZAZO et al., 2006). The use of Fenton's process has been widely employed because iron is low in cost, less toxic and the easy handling of the hydrogen peroxide due to the fact that it decomposes into molecules that are friendly to the environment. Some advantages of Fenton's process compared to other oxidation techniques are that it needs simple installation and it has mild operating conditions (PEREZ et al., 2002).

2.2.1.1 Homogeneous Fenton's reaction

Several industries use the homogeneous Fenton's reaction in wastewater purification processes. Homogeneous CWPO is the process where the mixture of iron (II) salt and H_2O_2 know as Fenton reagent is used for oxidation of organic pollutants. Reseachers proposed a reaction mechanism where Fe^{2+} decomposes H_2O_2 in an acidic and dark condition in the absence of the organic compound that consists of a sequence of reactions. According to the study, the combination of Fe^{2+} and H_2O_2 induces series of chain reactions initiated by the consumption of hydrogen peroxide to hydroxyl radicals, the reaction can be summarized as follows(Equations 1 – 6) (SUN et al., 2009):

$Fe^{2+} + H_2O_2 \longrightarrow Fe^{3+} + OH^- + OH^\cdot$ 1

$Fe^{3+} + H_2O_2 \longrightarrow Fe^{2+} + H^+ + HOO^\cdot$ 2

$H_2O_2 + OH^\cdot \longrightarrow HOO^\cdot + H_2O$ 3

$Fe^{2+} + HO^\cdot \longrightarrow Fe^{3+} + HO^-$ 4

$HOO^\cdot + H_2O_2 \longrightarrow H_2O + HO^\cdot + O_2$ 5

$HOO^\cdot + HOO^\cdot \longrightarrow H_2O_2 + O_2$ 6

The Fenton process has been efficient in the degradation and oxidation of various organic pollutants. It has also been applied in the wastewater treatment, industrial dyes discoloration (GOGATE and PANDIT, 2004) and also degrading toxic and recalcitrant organic compounds (HOU et al., 2016b, WAN et al., 2017, YANG et al., 2016). The efficiency of the Fenton process depends on factors such as temperature, H_2O_2, pH, and catalyst concentration. However some drawback can be attributed to the homogeneous Fenton reaction, which includes high cost and risk due to the transportation and storage of hydrogen peroxide, the need for significant chemicals for acidifying the effluent at the pH before degradation, accumulation of iron sludge that has to be also treated at the end of the reaction leading to additional treatment step and increasing treatment cost (GUO et al., 2017). Nevertheless, this drawback can be overcome by the heterogeneous process, which most of them are operated in close to neutral pH range and also precipitation of Fe^{3+} in the form of sludge can be avoided by using a solid iron-containing catalyst.

2.2.1.2 Heterogeneous Fenton reaction

Heterogeneous Fenton reaction is a process whereby a mixture of a solid iron-containing catalyst and H_2O_2 are applied for the oxidation and degradation of organic pollutants. Several iron-based

materials such as alumina, zeolites, activated carbon, clays, silica and ion exchange resins have been studied in the heterogeneous Fenton reaction for the removal of recalcitrant organic pollutants (OTURAN and AARON, 2014). Heterogeneous Fenton-type of a catalyst has been used based on porous supports such as activated carbon, silica, alumina, and clays in the degradation of organic compounds such phenols and other organic pollutants. The oxidation of phenols using ion-exchange medium pore zsm-5 was studied and also the effect of pH and iron leaching was explored (FAJERWERG and DEBELLEFONTAINE, 1996). Ovejero et al studied the different iron-containing zeolite and they found out that the amount of iron leaching depended on the synthesis route, concentration and strength of the acids sites present and the iron environment in the zeolites (OVEJERO et al., 2001). Most of the iron oxides which are formed are inherently in the Nano size, this fact makes iron hydroxides suitable catalyst that is why they have been applied mostly in catalysis. The application of natural and synthetic iron oxide/hydroxide as a catalyst in waste water treatment like the Fenton-like process has been studied (PEREIRA et al., 2012). Guimaraes et al degraded quinoline in an aqueous solution using modified goethite surface by thermal treatment with hydrogen to produce the active Fenton-like catalyst. The controlled thermal treatment resulted in the reduction of Fe^{3+} to Fe^{2+} thus increased the catalyst efficiency (GUIMARAES et al., 2008). Nevertheless, the perfect solid Fenton catalyst should not be vulnerable to iron leaching but most of the Fenton-like heterogeneous catalyst developed still suffer this problem up until now. Iron ions are leached from the surface of the catalyst during the reaction thus reducing the catalytic activity and also causes iron pollution to the treated water, this is still why the development of heterogeneous Fenton-like catalyst with high activity and not vulnerable to leaching is still a challenging approach.

2.3 Catalytic leaching

Catalytic leaching is when the catalyst from the support material is released due to the dissolution of minerals and complexation processes (Pio and Luca 1999). The process itself is universal, any material exposed to contact with water will leach its components from its surface or interior depending on the porosity of the material considered (PIO and LUCA, 1999). The concept of leaching is important for four reasons (a) since homogeneous catalyst are known to be effective catalyst for the liquid phase oxidation, dissolved metal ions must be responsible for homogeneously catalysed reactions and homogeneous-heterogeneous reaction (b) an implementation of additional step such as membrane separation be needed to remove the leached metal (c) continuous leaching of catalyst would result in the degradation of the catalyst which will affect the catalyst activity and stability (d) pollute the environment (PIO and LUCA, 1999).

2.3.1 Chemical, physical and kinetic aspects of catalyst deactivation

The knowledge of the chemical and physical aspects of catalyst deactivation is of pivotal importance for the design of deactivation-resistant catalysts, the operation of industrial chemical reactors, and the study of specific reactivating procedures. Deactivation can occur by a number of different mechanisms, both chemical and physical in nature. Other mechanisms of deactivation include masking and loss of the active elements via volatilization, erosion, and attrition (GAYA and ABDULLAH, 2008, MOULIJN et al., 2001).

2.3.2 Poisoning

Chemical aspects of poisoning. Poisoning is the loss of activity due to the strong chemisorption on the active sites of impurities present in the feed stream. The adsorption of a basic compound onto an acid catalyst (e.g isomerization catalyst) is an example of poisoning. A poison may act simply by blocking an active site (geometric effect) or may alter the adsorptivity of other species

essentially by an electronic effect. Poisons can also modify the chemical nature of the active sites or result in the formation of new compounds (reconstruction) so that the catalyst performance is definitively altered (MOULIJN et al., 2001).

As the result, it is important to develop a highly efficient heterogeneous catalyst, where the adverse impact of metal leaching in aqueous environments is minimized and the catalyst can be recovered after its application (ANIPSITAKIS et al., 2005). The solid iron catalyst in the advanced oxidation technologies may undergo some degradation that is caused by the deposition and strong adsorption of a polymeric carbon layer and from leaching of the active species of the catalyst (FAJERWERG and DEBELLEFONTAINE, 1996, GUO and AL-DAHHAN, 2006, LIOU et al., 2005, ZAZO et al., 2006).

If the problem of the catalyst leaching can be solved, the advanced oxidation technologies would be widely applied. Many studies have revealed that iron oxides clusters, which are held to the support by the weak Van der Waals bonds, are easily leached out into the liquid phase during reaction, whereas the iron cations that are incorporated into the support, which is bonded by the covalent bonds are stable towards leaching (CROWTHER and LARACHI, 2003, FAJERWERG and DEBELLEFONTAINE, 1996, WANG et al., 2002).

The use of iron precursor salts as chemical activators during the production of activated carbon may lead to good iron oxide support interaction leading to minimized leaching. Therefore this option will be investigated as an alternative to impregnation of the iron salt after the production of activated carbon.

2.4 Types of catalyst

The application of Nano-sized particles as a catalyst materials has drawn the attention of the scientific community due to their intrinsic properties, which makes them better as compared to their microscopic counterparts. These materials exhibit a different behavior as compared to the bulk materials, owing to their high surface area, enhanced chemical, mechanical, magnetic, optical, and electrical properties (POURAN et al., 2014). Various nano-sized catalyst has been widely applied in the AOPs, such as TiO_2, Ag/AgCl, ZnO and iron oxides. Hence iron oxides has shown interest in the degradation of organic pollutant due to their low toxicity.

2.4.1 Iron oxide nanoparticles

Several types of iron magnetic particles such as Fe_2O_3 (HOU et al., 2016b), maghemite (EL-QANNI et al., 2016), Fe_3O_4 (HOU et al., 2016a) and FeOOH (MESQUITA et al., 2016) have been explored for potential catalyst for degradation of organic pollutants from water. Iron magnetic particles have gained popularity in recent years for numerous applications (Jiang *et al*., 2011). According to Rakhshaee and Panahandeh (2011), these magnetic particles contain zerovalent iron Fe^0 nano-iron material (Fe^0 NPs) which are active for remediating contaminants that are susceptible to reductive transformation like dyes, and halogenated organics (YANG and LEE, 2005). Nanomagnetic materials have the advantage of being easily synthesized, environmentally friendly, and manipulated through coating and functionalization (GUPTA and NAYAK, 2012).

One major issue in the use of nanoparticles is agglomeration which occurs primarily by direct interparticle interactions via Van der Waals forces and magnetic interaction (CUSHING et al., 2004). This phenomenon of agglomeration causes a reduction of specific surface area, interfacial

free energy and ultimately particle reactivity (RAKHSHAEE and PANAHANDEH, 2011). Iron magnetic nanoparticles especially, Fe_3O_4, are also known to show poor stability under acid conditions (LIU et al., 2012). Surface modification using a stabilizer is therefore of great importance in determining the nanoparticle stability under physiochemical conditions. These stabilizers are capable of increasing dispersion of the nanoparticles by electrostatic repulsion and steric hindrance (YANG and LEE, 2005). Hence activated carbon has been widely used as a catalyst support.

2.5 Activated carbon as catalytic support

Both the catalyst and the support play important roles in catalysis (ZHAO et al., 2009). The use of carbonaceous materials as a catalytic supports continues to increase because of the high versatility of this material (FUENTE et al., 2001). The most important carbon support material is activated carbon followed by carbon black and graphite materials (AUER et al., 1998). Based on its porous structure and surface functional groups, activated carbon exhibits the most favorable physical and chemical characteristics (SYCH et al., 2012).

Among many carbonaceous materials activated carbon have been widely used in catalytic ozonation because of its favorable properties, which are:

- Large surface area, (BELTRÁN et al., 2002, RIVERA-UTRILLA and SÁNCHEZ-POLO, 2002) (Beltran *et al*., 2002; Utrilla *et al*., 2002)
- Good adsorption capacity (BELTRÁN et al., 2002, RIVERA-UTRILLA and SÁNCHEZ-POLO, 2002)(Beltran *et al*., 2002; Utrilla *et al*., 2002)
- It is stable under acidic and basic conditions, (RODRIGUEZ-REINOSO, 1998).
- Its surface chemistry can be modified to provide controlled metal loading sites,

- It is stable at high temperatures (RODRIGUEZ-REINOSO, 1998).
- It can be combusted to recover spent catalysts (RODRIGUEZ-REINOSO, 1998).
- Very good microwave absorbents, allowing it to be modified by microwave pyrolysis (MENENDEZ et al., 2010).
- It also can act as an adsorbent, a reactive support and radical initiator (MENENDEZ et al., 2010).

Disadvantages of carbon supports include combustion in the presence of oxygen and a potential loss of selectivity from metal impurities in ash (RODRIGUEZ-REINOSO, 1998). An ideal support is highly influenced by carbon material properties such as metal impurities, acidic oxygenated groups, basic active sites and, textural and structural features.

2.6 The influence of carbon material properties on the efficiency of the Fenton oxidation process

2.6.1 Metal impurities

In the carbonaceous materials, the presence of metal impurities such as iron as a consequence to their origin or synthesis origin or synthesis procedures has shown to improve the catalytic activity. Hence it is natural to consider ash content as one of the most important factors on the carbonaceous materials that affect the CWPO activity. Dominguez et al investigated on the carbonaceous materials that have different structural, textural and surface chemical properties and reported that the presence of metal impurities particularly iron increases the catalytic activity. However it should be noted that the high decomposition of H_2O_2 does not mean the high generation of hydroxyl radicals which leads to high degradation of organic pollutants by CWPO. In some cases, H_2O_2 decomposes to water and oxygen which are not as efficient as the hydroxyl radical.

2.6.2 Surface chemistry

Another factor that plays an important role in the catalytic activity is the availability of the active sites on the surface of the carbonaceous material. Furthermore, the catalytic activity has been linked to the surface chemistry of the catalyst.

2.6.2.1 Acidic oxygenated groups

In CWPO oxidation process, H_2O_2 decomposes to form hydroxyl radicals with the help of the active sites on its surface. However for this process to happen. The electron has to move from the active sites to the H_2O_2 molecule. Nevertheless, the acid oxygenated groups on the surface of the carbonaceous materials limit the catalytic activity of the CWPO process due to the fact that they have electron withdrawing capacity (RIBEIRO et al., 2016, SERP and FIGUEIREDO, 2009).

2.6.2.2 Basic active sites

As it is reported in literature the basicity of the carbonaceous material is mainly made up by the presence of the oxygen containing functional groups such as chromene, pyrone, quinones and non-heteroatomic Lewis base site characterized by regions of π-electron density on the carbon basal planes. However, it should be clearly stated that the overall basicity of the carbonaceous material has not been clearly explained. In contrast with the acidic oxygenated groups, the basic groups are electron donating species, which is a necessary condition to improve the hydroxyl radical generation (PAPIRER et al., 1987, RIBEIRO et al., 2013).

2.6.3 Textural and Structural features

Any ideal carbonaceous material suitable for catalysis should exhibit adequate properties in order to guarantee diffusion limitations and the deactivation or leaching is reduced. Factors that affect the catalytic activity are mainly nature, accessibility of active sites.

2.6.3.1 Surface area and Porosity

The porous and texture of the most heterogeneous solid catalyst are determined by the preparation method. The area of the catalyst is expected to strongly influence the catalytic activity due to the fact that the catalytic reactions occur on the surface of the catalyst. Furthermore, in order to reach the active sites, the reactants must diffuse into the pores of the carbon material, then the products desorb from the catalyst. For example, the catalyst active sites will be well dispersed in the carbonaceous material with a high surface area, in that way it will improve the decomposition rate of H_2O_2. Therefore the balance between the chemical and structural properties is of importance in the synthesis of highly efficient catalyst for CWPO (LEOFANTI et al., 1998). Activated carbon have been widely prepared from two primary sources such as coal and wood. However, due to the environmental constraints, there has been a need to look for locally, readily available and inexpensive alternative source of activated carbon.

2.7 Pine as source of activated carbon

Pinecone is an agricultural by-product from the pine plantations grown for the timber, wood, pulp and paper industries. Pines are softwood trees in the genus *Pinus*, in the family Pinaceae, order Pinales, class Pinopsida, division Pinophyta and kingdom Plantae (RYAN, 1999). The pine tree is mostly monoecious; having the male (microsporangium) and female (megasporangium) cones on the same trees, though few species are sub-dioecious with individuals predominantly, not wholly

single sex. At maturity, the cones open to release seeds depending on their dispersal mechanism. The scales of the mature cone are composed of epidermal and sclerenchyma cells which contains cellulose, hemicelluloses, lignin, rosin (mixture of resin acids) and tannins in their cell wall which contain polar functional groups such as alcohols, aldehydes, ketones, carboxylic acids, phenolic and ether groups (ROBBINS et al., 1957, SAKGAMI et al., 1992). Their use as the carbonaceous material might reduce the problem of environment disposal, and produce an alternative precursor for the activated carbon.

Commercial activated carbons that are prepared from coal, coconut shells and wood are usually costly (ABDULLAH et al., 2011). But the need for low cost, readily available and renewable materials as a potential precursor in the production of activated carbon has initiated an interest of many researchers. Pinecone, a well-known agricultural waste, has been studied for its potential application as a biosorbent in its raw form, modified form and as a source of activated carbon. Pine cones compose of mostly lignin and resins that contain most organic compounds (MOMČILOVIĆ et al., 2011).

The proximate and the ultimate analysis of raw pine on a percentage dry-ash-free basis as determined by Haykiri-Acma and Yaman (2007) are shown in Tables 1 and 2. Table 1 shows the pine cone had a moisture content of about 9.4% and a high volatile matter content of 69 %. The wt. % fixed carbon content on pine cone is as high as 20.9 % and ash content of pine cone is 0.7 % (HAYKIRI-ACMA and YAMAN, 2007). The ultimate analysis presented in Table 2 shows a low value of nitrogen indication that the protein content of pine cone is low. The carbon content is as high as 44.1 % confirming the high percentage of fixed carbon. The oxygen content is 50 % indicating a lot of oxygenated groups on the pine cone. Table 3 shows that pine cone is mainly

composed of lignin, hemicelluloses, cellulose. The extractives include resin acids, tannins, simple sugars, and other soluble organic substances. Some of the extractives have been found to have medicinal effects (HAYKIRI-ACMA and YAMAN, 2007)

Table 2.2. Proximate analysis of and gross calorific value for pine cone (on original basis)

Moisture	**volatile matter**	**fixed carbon**	**Ash**	**gross calorific value**
9.4 wt. %	69.0 wt.%	20.9 wt.%	0.7 wt.%	18.6 MJ k/g

Table 2.3. Ultimate analysis results for pine cone (% on dry ash basis)

Carbon	**Hydrogen**	**Nitrogen**	**Oxygen**
44.1	5.9	0.01	48.8

Table 2. 2: Main constituents of pine cone (% on a dry weight basis)

Lignin	**Hemicelluloses**	**Cellulose**	**Extractives**
24.9	37.6	32.7	4.8

2.7.1. Lignin

Lignin is a branched, three dimensional, complex polymer that occurs in the plant cell walls. The molecule has apparent infinite molecular weight and is covalently linked with xylans in the case of hardwood and galactoglocomannans in softwoods (DEMIRBAS, 2008). It consists of both aliphatic and aromatics constituents, built mainly with the *p*-hydroxycinnamoyl alcohols with different degrees of methoxylation (CHUAQUI et al., 1993). The structure of lignin is not known

completely but various molecular models have been proposed (FAULON and HATCHER, 1994). Lignin offers structural and mechanical support to plant cells.

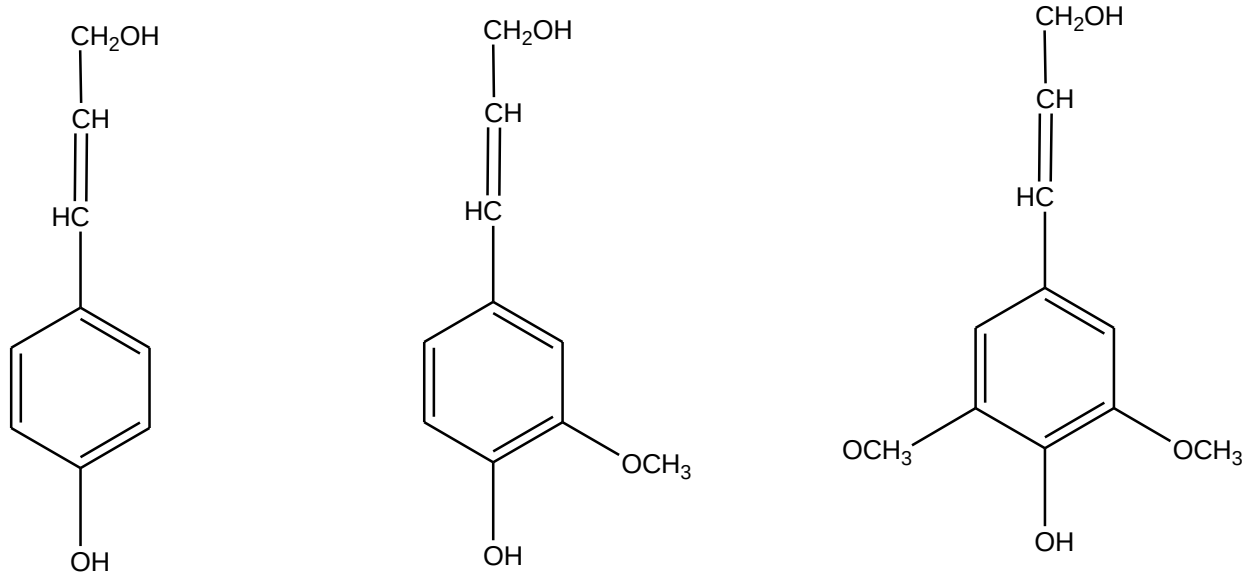

p-cumaril alcohol coniferil alcohol sinapil alcohol

Figure 2. 3: Structure of Phenylpropane

Figure 2.3 shows the main phenylpropane units which are linked together by ring-ring, side-chain-side and ring-side chain bonds forming a complex three-dimensional structure of lignin. This makes lignin to be highly insoluble and unreactive towards common chemical reagents. The sequence of the repeating monomer units is not homogeneous a lignin lacks a primary structure.

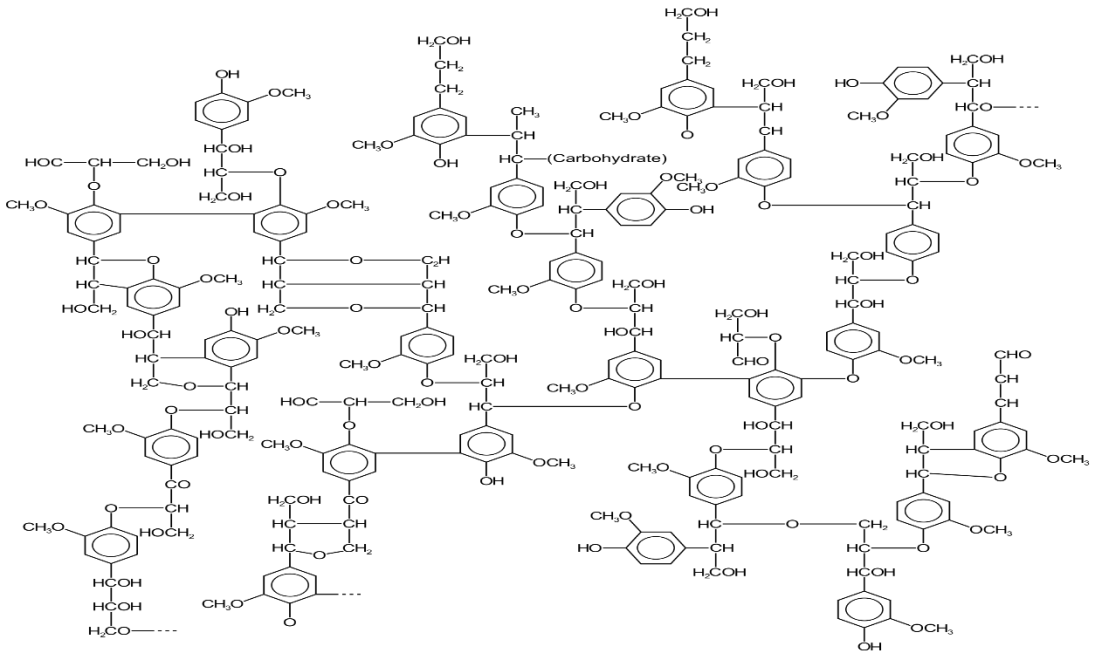

Figure 2. 4: Structure of Lignin

2.7.2. Cellulose

Cellulose is a carbohydrate homopolymer consisting of β-D-glucopyranose (anhydroglucose) monomer units joined together by β-1.4-glycosidic linkages forming a cellobiose dimmer units (GURGEL et al., 2008, QIN et al., 2008). Unlike starch, the glucose units in the cellulose are oriented with $–CH_2OH$ groups alternating above and below the plane of rings, thus producing long and unbranched chains. The absence of side chains allows cellulose molecules to form organized stacked structure. The linear cellulose chains are linked to by inter and intra-chain hydrogen bonds making it highly crystalline and insoluble. Cellulose chains can be orientated in parallel and in antiparallel conformation: the two forms are called cellulose I and II respectively (TAKACS et al., 2000).

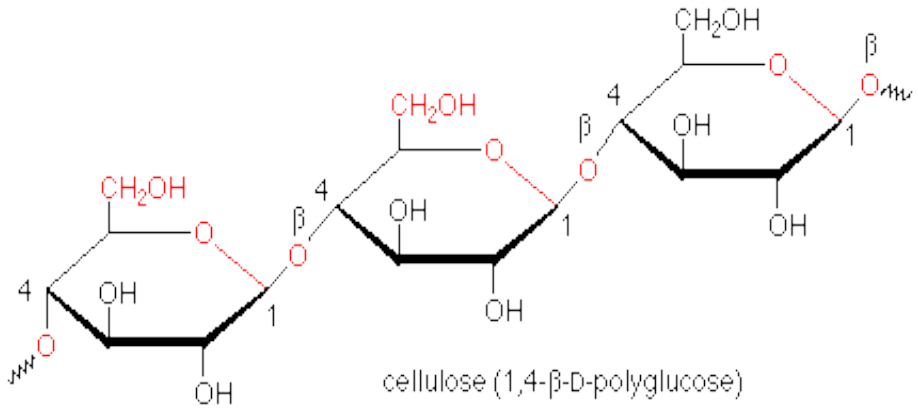

Figure 2. 5: Structure of Cellulose

2.7.3. Hemicelluloses

Hemicelluloses are a group of plant-derived heteropolysaccharides with much lower polymerization degree as compared to cellulose. They possess five and six-membered rings. They contain side chains which prohibit the formation of intermolecular hydrogen bonds and the stacking conformation making them amorphous and thus reactive and soluble in dilute acids, in comparison to cellulose. Hemicelluloses have different sugar monomers but all have two structural features in common which bear importantly on their biological function: (1) they have straight flat β-1.4-linked backbones. Any side chains attached to their backbone are short, usually, just one sugar long and stick out to the side of the backbone. (2) All some features which prevent the chains from extended self-aggregation of the type which exists between the β-1.4-linked glucan chains of cellulose. Most common hemicellulose are xylan, glucuronoxylan, arabinoxylan, glucomannan, galactoglucomannan, and xyloglucan.

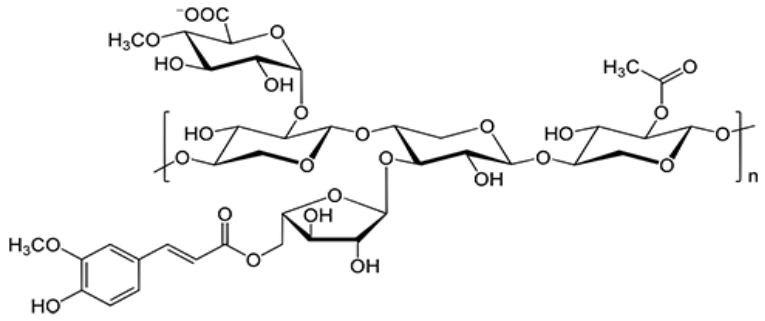

Figure 2. 6: Structure of Xylan

2.8 Synthesis of activated carbons via microwave heating

Lately, microwave pyrolysis has been a point of interest for many researchers for the preparation of activated carbon (YUEN and HAMEED, 2009). Microwave use electromagnetic radiation of a wavelength that ranges from 0.001 m to 1 m, and it can be used to heat dielectric materials. Microwave pyrolysis offers that are different from the furnace heating, because the heat is generated directly in the interior of the sample via the interaction of the molecules of the sample with the electromagnetic field (THOSTENSO and CHOU, 1999). The application of microwave pyrolysis has few advantages as compared to the furnace heating, which are:

- The temperature rises quickly (FOO and HAMEED, 2012b).
- The temperature is distributed uniformly, (FOO and HAMEED, 2012b).
- Less consumption of time and energy (FOO and HAMEED, 2012a).
- Modifies the surface chemistry and pores (YAHMUR et al., 2008).
- Preserves pore structure (ANIA et al., 2005).
- Doubles the yield (DUAN et al., 2011).

Although microwave heating in the preparation of activated carbon is being used at the laboratory scale level, it shows a great potential for industrial production because of its number of advantages over the conventional heating method.

2.9 Parameters influencing the physical, chemical properties and percentage yield of activated carbon

Table 2. 3 shows the effects of each parameter on the chemical, physical properties and percentage yield of activated carbon. According to literature at optimum, those properties shown in Table 2.3 are most desirable. It is shown that power below the optimum level there could be incomplete charring due to the no reaction between the biomass the activating agent (FOO and HAMEED, 2011a). However, at the power above the optimum level, the carbon burns and the pores get destroyed leading to a lower percentage yield due to the greater gasification (FOO and HAMEED, 2011a). When time increases, the activation stage also increases but up to a certain point beyond that point, radiation time destroyed the pore leading to a lower adsorption capacity (DENG et al., 2009). The impregnation ratio also affects the physical and chemical properties of the activated carbon. The excess of the activating agent could lead to blockage of the pores and lead to less adsorption capacity due to the less accessible area (FOO and HAMEED, 2011b).

Table 2. 3 :optimum condition of the preparation of activated carbon by chemical activation from agricultural waste and their adsorption capacity

Biomass	Activating agent	Power (W)	Activating time (min)	IR	iodine number (mg/g)	MB number (mg/g)	Reference
Pomelo skin	NaOH	500	5	1:1,25	444.45	501.10	(FOO and HAMEED, 2011a)
Cotton stalk	$ZnCl_2$	560	9	1.6:1	972.92	193.50	(DENG et al., 2009)
	H_3PO_4	600	8	-	-	245.70	(MENENDEZ et al., 2010)
Pine wood	$ZnCl_2$	700	10	2.5:1	1100	200	(TONGHUA and LIANG, 2009)
Rice husk	KOH	600	7	1:1.075	-	444.52	(FOO and HAMEED, 2011b)
Orange peels	K_2CO_3	600	6	1.25:1	-	382.75	(FOO and HAMEED, 2012c)

2.10 $FeCl_3$ as a chemical activating agent to synthesis of activated carbon

Sahira *et al,* (2013) researched the effects of activating agents on activated carbon prepared from Lapsi seed and reported that the activated carbon using ferric chloride activating agent has a lower adsorption capacity of iodine and methylene blue as compared to frequently used activating agent

like zinc chloride and phosphoric acid as shown in Table 2.4. However ferric chloride does not show a poor adsorption capacity, hence in the study ferric chloride will be used as an activating agent and it will also be used as an iron precursor for catalysis.

Oliveria *et al.* (2009) reported that activated carbon prepared ferric chloride as an activating agent had a large surface area of 965 m^2/g and very small pores. The activated carbon that was found in this study it showed a high adsorption capacity for dyes and phenols (OLIVERIA et al., 2009). However in this study different iron salt as activating agents will be investigated. Activated carbon is hydrophobic, the different iron salt might modify the hydrophobic character of the activated carbon and might lead to the catalyst with different properties (Rey *et al.*, 2009).

Table 2. 4: Iodine and Methylene blue numbers of activated carbons

Activated carbon	**Activating agent**	**Iodine number (mg/gm)**	**Methylene blue number (mg/gm)**
LAC2	KOH	510	158
LAC3	$FeCl_3$	502	108
LAC7	H_3PO_4	845	277

2.11 Conclusions

Substantial research has been done to investigate the degradation capability of activated iron oxide composite prepared using microwave. The literature search showed that there are various factors affecting an ideal heterogeneous Fenton catalyst, were catalytic leaching is minimized in the Fenton oxidation process. Furthermore, it can be hypothesized adding the iron during the activated

carbon formation would yield a catalyst which has a greater metal oxide support interaction leading to a decrease in the leaching of the metal oxide.

2.12 References

ABDULLAH, M. O., TAN, I., A, W & LIM, L., S 2011. Automobile adsorption air-conditioning system using oil palm biomass-based activated carbon: A review. *Renewable and Sustainable Energy Reviews,* 15**,** 2061-2072.

ANASTASIOU, N., MONOU, M., MANTZAVINOS, D. & KASSINOS, D. 2009. Monitoring of the quality of winery influents/effluents and polishing of partially treated winery flows by homogeneous Fe(II) photo-oxidation. *Desalination,* 248**,** 836-842.

ANIA, C. O., PARRA, J. B., MENDEZ, J. A. & PIS, J. J. 2005. Effect of microwave and conventional regeneration on the microporous and mesoporous network and on the adsorptive capacity of activated carbon. *Microporous and Mesoporous Materials,* 85**,** 7-15.

ANIPSITAKIS, G. P., STATHATOS, E. & DIONYSIOU, D. D. 2005. Heterogeneous activation of oxone using Co_3O_4. *Journal of Physical Chemistry B.,* 109**,** 13052-13055.

AUER, E., FREUND, A., PIETSCH, J. & TACKE, T. 1998. Carbons as supports for industrial precious metal catalysts. *Applied Catalysis A: General,* 173**,** 259-271.

BELTRAN, F. J., RIVAS, F. J. & MONTERO-DE-ESPINOSA, R. 2005. Iron type catalysts for the ozonation of oxalic acid in water. *Water Research Management,* 39**,** 3553-3564.

BELTRÁN, F. J., RIVAS, J., ÁLVAREZ, P. & MONTERO-DE-ESPINOSA, R. 2002. Kinetics of Heterogeneous Catalytic Ozone Decomposition in Water on an Activated Carbon. *The Journal of the International Ozone Association,* 24**,** 227-237.

BREZONIK, P. L. & ARNOLD, W. A. 2012. Water chemistry: Fifty years of change and progress. *Environ. Sci. Technol,* 46**,** 5650-5657.

CHOY, K. K. H., PORTER, J. F. & MCKAY, G. 2004. Intraparticle diffusion in single and multi component acid dye adsorption from wastewater onto carbon. *Chemical Engineering Journal,* 103**,** 135-145.

CHUAQUI, C. A., RAJAGOPAL, S., KOCACS, A., STEPANIK, T., MERRIT, J., GYOGY, I., WHITEHOUSE, R. & EWING, D. 1993. Radiation-induced effects in lignin model compounds: a pulse and steady-state radiolysis study *Tetrahedron,* 49**,** 9689-9698.

CRINI, G. 2006. Recent development in polysaccharide based material used as adsorbents in wastewater treatment *Progress in Polymer Science,* 30**,** 778-783.

CROWTHER, N. & LARACHI, F. 2003. Iron containing silicates for phenol catalytic wet peroxidation. *Applied Catalysis B: Environment,* 46**,** 293.

CUSHING, B. L., KOLESNICHENKO, V. L. & O'CONNOR, C. J. 2004. Recent Advances in the Liquid-Phase Syntheses of Inorganic Nanoparticles. *Chemical Review,* 104**,** 3893–3946.

DEBLONDE, T., COSSU-LEGUILLE, C. & HARTEMANN, P. 2011. Emerging pollutants in wastewater: A review of the literature. *Int. J. Hyg. Environ. Health,* 214**,** 442-448.

DEMIRBAS, A. 2008. Heavy metal adsorption onto agro-based waste materials: A review. *Journal of Hazardous Materials,* 157**,** 220-229.

DENG, H., YANG, L., TAO, G. & DAI, J. 2009. Preparation and characterization of activated carbon from cotton stalk by microwave assisted chemical activation: application in methylene blue adsorption from aqueous solution. *Journal of Hazardous Materials,* 166**,** 1514-1521.

DUAN, X., SRINIVASAKANNAN, C., PENG, J. H., ZHANG, L. B. & ZHANG, Z. Y. 2011. Preparation of activated carbon from Jatropha hull with microwave heating: Optimization using response surface methodology. *Fuel Processing Technology,* 92**,** 394-400.

EL-QANNI, A., NASSAR, N. N., VITALE, G. & HASSAN, A. 2016. Maghemite nanosorbcats for methylene blue adsorption and subsequent catalytic thermo-oxidative decomposition: Computational modeling and thermodynamics studies. *Journal of Colloid and Interface Science,* 461**,** 396-408.

FAJERWERG, K. & DEBELLEFONTAINE, H. 1996. Wet oxidation of phenol by hydrogen peroxide using a heterogeneous catalysis Fe-ZSM a promising catalyst. *Applied Catalysis B: Environment,* 10**,** 229.

FAULON, J. & HATCHER, P. G. 1994. Is there any order in the structure of lignin. *Energy & Fuel,* 8**,** 402-407.

FENTON, H. J. H. 1894. Oxidation of tartaric acid in presence of iron. *Journal of the Chemical Society* 65**,** 899-910.

FOO, K. Y. & HAMEED, B. H. 2011a. Microwave-assisted preparation of activated carbon from pomelo skin for the removal of anionic and cationic dyes. *Chemical Engineering Journal,* 173**,** 385-390.

FOO, K. Y. & HAMEED, B. H. 2011b. Utilization of rice husks as a feedstock for preparation of activated carbon by microwave induced KOH and K_2CO_3 activation. *Bioresource Technology,* 102**,** 9814-9817.

FOO, K. Y. & HAMEED, B. H. 2012a. Factors affecting the carbon yield and adsorption capability of the mangosteen peel activated carbon prepared by microwave assisted K_2CO_3 activation. *Chemical Engineering Journal,* 180**,** 66-74.

FOO, K. Y. & HAMEED, B. H. 2012b. Preparation of activated carbon by microwave heating of langsat empty fruit waste. *Bioresource Technology,* 116**,** 522-525.

FOO, K. Y. & HAMEED, B. H. 2012c. Preparation, characterization, and evaluation of adsorptive properties of orange peel based activated carbon via microwave induced K_2CO_3 activation. *Bioresource Technology,* 104**,** 679-686.

FU, Y. & VIRARAGHAVAN, T. 2001. Fungal decolorization of wastewater: a review. *Bioresource Technology,* 79**,** 251-262.

FUENTE, A. M., PULGAR, G., GONZÁLEZ, F., PESQUERA, C. & BLANCO, C. 2001. Activated carbon supported Pt catalysts: effect of support texture and metal precursor on activity of acetone hydrogenation. *Applied Catalysis A: General,* 208**,** 35-46.

GAYA, U. I. & ABDULLAH, A. H. 2008. Heterogeneous photocatalytic degradation of organic contaminants over titanium dioxide: A review of fundamentals, progress and problems. *Journal of Photochemistry and Photobiology C: Photochemistry Reviews,* 9**,** 1-12.

GOGATE, P. R. & PANDIT, A. B. 2004. A review of imperative technologies for wastewater treatment I: oxidation technologies at ambient conditions. *Advances in Environmental Research,* 8**,** 501-551.

GUIMARAES, I. R., OLIVEIRA, L. C. A., QUEIROZ, P. F., RAMALHO, T. C., PEREIRA, M., FABRIS, J. D. & ARDISSON , J. D. 2008. Modified goethites as catalyst for oxidation of quinoline: Evidence of heterogeneous Fenton process. *Applied Catalysis A: General,* 374**,** 89-93.

GUO, J. & AL-DAHHAN, M. 2006. Activity and stability of iron containing pillared clay catalyst for wet oxidation of phenol. *Applied Catalysis A: General,* 299**,** 175.

GUO, S., YUAN, N., ZHANG, G. & YU, J. C. 2017. Graphene modified iron sludge derived from homogeneous Fenton process as an efficient heterogeneous Fenton catalyst for degradation of organic pollutants. *Microporous and Mesoporous Materials,* 238**,** 62-68.

GUPTA, V. K. & NAYAK, A. 2012. Cadmium removal and recovery from aqueous solutions by novel adsorbents prepared from orange peel and Fe_2O_3 nanoparticles. *Chemical Engineering Journal,* 180**,** 81-90.

GURGEL, L. V. A., JUNIOR, O. K., GIL, R. P. F. & GIL, L. F. 2008. Adsorption of Cu (II), Cd (II), Pb (II) from aqueous single metal solution by cellulose and mercerized cellulose chemically modified with succinic anhydride. *Bioresource Technology,* 99**,** 3077-3083.

HABER, F. & WEISS, J. 1934. The catalytic decomposition of hydrogen peroxide by iron salts. *Proceedings of the Royal Society of London. Series A, Mathematical and Physical Sciences Coverage,* 147**,** 332-351.

HAYKIRI-ACMA, H. & YAMAN, S. 2007. Interpretation of biomass gasification yields regarding temperature intervals under nitrogen–steam atmosphere. *Fuel Processing Technology,* 88**,** 417-425.

HOU, L., WANG, L., ROYER, S. & ZHANG, H. 2016a. Ultrasound-assisted heterogeneous Fenton-like degradation of tetracycline over a magnetite catalyst. *Journal of Hazardous Materials,* 302**,** 458-467.

HOU, X., HUANG, X., AI, Z., ZHAO, J. & ZHANG, L. 2016b. Ascorbic acid/Fe@Fe_2O_3: A highly efficient combined Fenton reagent to remove organic contaminants. *Journal of Hazardous Materials,* 310**,** 170-178.

JACKSON, R. B., CARPENTER, S. R., DAHM, C. N. & MCKNIGHT, D. M. 2001. Water in changing world. *Ecological Society of America,* 11**,** 1027-1045.

KULSHRESHTHA, S. N. 1998. A global outlook for water resources to the year 2025. *Water Research Management,* 12**,** 167-184.

KUMAR, R., KNICK, V. B., RUDOLPH, S. K., JOHNSON, J. H., CROSBY, R. M., CROUTHAMEL, M. C., HOPPER, T. M., MILLER, C. G., HARRINGTON, L. E., ONORI, J. A. & MULLIN, R. J. 2007. Pharmacokinetic-pharmacodynamic correlation from mouse to human with pazopanib, a multikinase angiogenesis inhibitor with potent antitumor and antiangiogenic activity. *American Association for Cancer Research Journal,* 6.

KUSIC, H. & BOZOIC, A. L. 2007. Fenton type process for minimization of organic content in colored wastewater: Part 1: Process optimization. *Dyes & Pigments,* 74**,** 380-387.

LEOFANTI, G., PADOVAN, M., TOZZOLA, G. & VENTURELLI, B. 1998. Surface area and pore texture of catalysts. *Catalysis Today,* 41**,** 207-219.

LIOU, R. M., CHEN, S. H., HUNG, M. Y., HU, C. S. & LAI, J. Y. 2005. Fe(III) supported on resins as effective catalyst for the heterogeneous of phenol in aqueous solution. *Chemosphere,* 59**,** 117.

LIU, X., BI, T. X., LIU, C. & LIU, Y. 2012. Performance of Fe/AC catalyst prepared from demineralized pine bark particles in a microwave reactor. *Chemical Engineering Journal,* 193-194**,** 187-195.

MARTÍNEZ-HUITLE, C. A. & BRILLAS, E. 2009. Decontamination of wastewaters containing synthetic organic dyes by electrochemical methods: A general review. *Applied Catalysis B: Environmental,* 87**,** 105-145.

MENENDEZ, J. A., ARENILLAS, A., FIDALGO, B., Y, F., ZUBIZARRETA, L., CALVO, E. G. & BERMUDEZ, J. M. 2010. Microwave heating processes involving carbon materials. *Fuel Processing Technology* 91**,** 1-8.

MESQUITA, A. M., GUIMARÃES, I. R., CASTRO, G. M. M., GONÇALVES, M. A., RAMALHO, T. C. & GUERREIRO, M. C. 2016. Boron as a promoter in the goethite (α-FeOOH) phase: Organic compound degradation by Fenton reaction. *Applied Catalysis B: Environmental,* 192**,** 286-295.

MOMČILOVIĆ, M., PURENOVIĆ, M., BOJIĆ, A., ZARUBICA, A. & RANĐELOVIĆ, M. 2011. Removal of lead(II) ions from aqueous solutions by adsorption onto pine cone activated carbon. *Desalination,* 276**,** 53-59.

MOULIJN, J. A., VAN DIEPEN, A. E. & KAPTEIJN, F. 2001. Catalyst deactivation: is it predictable?: What to do? *Applied Catalysis A: General,* 212**,** 3-16.

OLEJNIK, T., PASIECZNA-PATKOWSKA, S., LESIUK, A. & RYCZKOWSKI, J. 2016. Phenol and methylene blue photodegradation over Ti/SBA-15 materials under UV light. *Polish Journal of Chemical Technology,* 18**,** 30-38.

OLIVERIA, L. C. A., PEREIRA, E., GUIMARAES, I. R., VALLONE, V., PEREIRA, M., MESQUITA, P. M. & SAPAG, K. 2009. Preparation of activated carbon from coffee husk utilizing $FeCl_3$ and $ZnCl_2$ as activating agent. *Journal of Hazardous Materials,* 165**,** 87-94.

OLLER, I., MALATO, S. & SÁNCHEZ-PÉREZ, J. A. 2011. Combination of Advanced Oxidation Processes and biological treatments for wastewater decontamination- A review. *Sci. Total. Environ,* 409**,** 4141-4166.

OTURAN, M. A. & AARON, J. J. 2014. Advanced Oxidation Processes in Water/Wastewater Treatment: Principles and Applications. A Review. *Critical Reviews in Environmental Science and Technology,* 44**,** 2577-2641.

OVEJERO, G., SOTELO, J. L., MARTINEZ, F., MELERO, J. A. & GORDO, K. 2001. Wet Peroxide Oxidation of Phenolic Solutions over Different Iron-Containing Zeolitic Materials. *Industrial & Engineering Chemistry Research,* 40**,** 3921-3928.

PAPIRER, E., LI, S. & DONNET, J. B. 1987. Contribution to the study of basic surface groups on carbons. *Carbon,* 25**,** 243-247.

PEARCE, C. I., LLOYD, J. R. & GUTRHIE, J. T. 2003. The removal of color from textile wastewater using whole bacterial cells:a review. *Dyes & Pigments,* 58**,** 179-196.

PEREIRA, M. C., OLIVEIRA, C. A. & MURAD, E. 2012. Iron oxide catalysts: Fenton and Fenton-like reactions- a review. *Clay Minerals,* 47**,** 285-302.

PEREZ, M., TORRADES, F., GARCIA-HORTAL, J. A., DOMENECH, X. & PERAL, J. 2002. Removal of organic contaminants in paper pulp treatment effluents under Fenton and photo-Fenton conditions. *Applied Catalysis B: Environmental,* 36**,** 63-74.

PIO, F. & LUCA, L. 1999. Catalyst deactivation. *Catalysis Today,* 52**,** 165-181.

POURAN , S. R., RAMAN*, A. A. A. & DAUD, W. M. A. W. 2014. Review on the application of modified iron oxides as heterogeneous catalysts in Fenton reactions. *Journal of Cleaner Production* 64**,** 24-35.

QIN, C., SOYKEABKAEW, N., XIUYUAN, N. & PEJIS, T. 2008. The effect of fibre volume fraction and mercerization on the properties of all-cellulose composite *Carbohydrates Polymers,* 71**,** 458-467.

RAKHSHAEE, R. & PANAHANDEH, M. 2011. Stabilization of a magnetic nano-adsorbent by extracted pectin to remove methylene blue from aqueous solution: A comparative studying between two kinds of cross-likened pectin. *Journal of Hazardous Materials,* 189**,** 158-166.

RAMAN, C. D. & KANMANI, S. 2016. Textile dye degradation using nano zero valent iron: A review. *Journal of Environmental Management,* 177**,** 341-355.

RIBEIRO, R. S., SILVA, A. M. T., FIGUEIREDO, J. L., FARIA, J. L. & GOMES, H. T. 2013. The influence of structure and surface chemistry of carbon materials on the decomposition of hydrogen peroxide. *Carbon,* 62**,** 97-108.

RIBEIRO, R. S., SILVA, A. M. T., FIGUEIREDO, J. L., FARIA, J. L. & GOMES, H. T. 2016. Catalytic wet peroxide oxidation: a route towards the application of hybrid magnetic carbon nanocomposites for the degradation of organic pollutants. A review. *Applied Catalysis B: Environmental,* 187**,** 428-460.

RIJSBERMAN, F. R. 2006. Water scarcity: Fact or fiction? *Agricultural Water Management,* 80**,** 5-22.

RIVERA-UTRILLA, J. & SÁNCHEZ-POLO, M. 2002. Ozonation of 1,3,6-naphthalenetrisulphonic acid catalysed by activated carbon in aqueous phase. *Applied Catalysis B: Environmental,* 39**,** 319-329.

ROBBINS, W. W., WEIER, T. E. & STOCKING, C. R. 1957. Botany-An introduction to Plant Science. *Soil Science* 84**,** 180.

RODRIGUEZ-REINOSO, F. 1998. The role of carbon materials in heterogeneous catalysis. *Carbon,* 36**,** 159-175.

RYAN, M. G. 1999. The complete Pine *BioScience,* 49**,** 1023-1024.

SAKGAMI, H., TAKEDA, M., KAWAZOE, Y., NAGATA, K., ISHIHAMA, A., UEDA, M. & YAMAKAZI, S. 1992. Anti-influenza virus activity of a lignin fraction from pine cone of *Pinus parviflora* Sieb. et Zucc. *In Vivo,* 6**,** 491-495.

SERP, P. & FIGUEIREDO, J. L. 2009. *Carbon Materials for Catalysis,* Hoboken, New Jersey, John Wiley and Sons, Inc.

SUN, J. H., SUN, S. P., WANG, G. L. & QIAO, L. P. 2007. Degradation of azo dye Amido black 10B in aqueous solution by Fenton oxidation process. *Dyes and Pigments,* 74**,** 647-652.

SUN, Q. & YANG, L. 2003. The adsorption of base dyes from aqueous solution on modified peat-resin particles. *Water Research,* 37**,** 1535-1544.

SUN, S., P, LI, C., J, SUN, J., H, SHI, S., H, FAN, M., H & ZHOU, Q. 2009. Decolorization of an azo dye Orange G in aqueous solution by Fenton oxidation process: Effect of system parameters and kinetic study. *Journal of Hazardous Materials,* 161**,** 1052-1057.

SYCH, N. V., TROFYMENKO, S. I., PODDUBNAYA, O. I., TSYBA, M. M., SAPSAY, V. I., KLYMCHUK, D. O. & PUZIY, A. M. 2012. Porous structure and surface chemistry of phosphoric acid activated carbon from corncob. *Applied Surface Science,* 261**,** 75-82.

TAKACS, E., WOJNAROVITS, L., FOLDVARY, C. S., HARGITTAI, P., BORSA, J. & SAJO, I. 2000. The effect of combined gamma-irradiation and alkali treatment on cotton cellulose *Radiation Physics & Chemistry,* 57**,** 399-403.

TEH, C. M. & MOHAMED, A. R. 2011. Roles of titanium dioxide and ion-doped titanium dioxide on photocatalytic degradation of organic pollutants (phenolic compounds and dyes) in aqueous solutions: A review. *Journal of Alloys and Compounds,* 509**,** 1648-1660.

THOSTENSO, E. T. & CHOU, T. W. 1999. Microwave processing: fundamentals and applications. *Composites Part A: Applied Science and Manufacturing,* 30**,** 1055-1071.

TONGHUA, W. S. T. & LIANG, C. 2009. Preparation and characterization of activated carbon from wood via microwave-induced ZnCl2 activation. *Carbon,* 47**,** 1880-1883.

UNESCO 2009. The United Nations World Water Development Report 3: Water in a Changing World. Paris: United Nations Education, Scientific and Cultural Organisation/Berghahn Books.

WAN, D., LI, W., WANG, G., LU, L. & WEI, X. 2017. Degradation of p-Nitrophenol using magnetic Fe0/Fe3O4/Coke composite as a heterogeneous Fenton-like catalyst. *Science of The Total Environment,* 574**,** 1326-1334.

WANG, Y., ZHANG, Q., SHISHIDO, T. & TAIKEHIRA, K. 2002. Characterization of iron containing MCM-41 and its catalytic properties in epoxidation of styrene with hydrogen peroxide. *Journal of Catalysts,* 209**,** 186.

YAHMUR, E., OZMAK, M. & AKTAS, Z. 2008. A novel method for production of activated carbon from waste tea by chemical activation with microwave energy. *Fuel Processing Technology*.

YANG, G. C. C. & LEE, H. L. 2005. Chemical reduction of nitrate by nanosized iron: kinetics and pathways. *Water Research,* 39**,** 884-894.

YANG, X., HE, J., SUN, Z., HOLMGREN, A. & WANG, D. 2016. Effect of phosphate on heterogeneous Fenton oxidation of catechol by nano-Fe3O4: Inhibitor or stabilizer? *Journal of Environmental Sciences,* 39**,** 69-76.

YUEN, F. K. & HAMEED, B. H. 2009. Recent developments in the preparation and regeneration of activated carbons by microwave. *Advances in Colloid and Interface Science,* 149**,** 19-27.

ZAZO, J. A., CASAS, J. A., MOHEDANO, A. F. & RODRIGUEZ, J. J. 2006. Catalytic wet peroxide oxidation of phenols with Fe/active carbon catalyst. *Applied Catalysis B: Environment,* 65**,** 261.

ZHAO, L., MA, J., SUN, Z. & LIU, H. 2009. Mechanism of heterogeneous catalytic ozonation of nitrobenzene in aqueous solution with modified ceramic honeycomb. *Applied Catalysis B: Environmental,* 89**,** 326-334.

CHAPTER 3: METHODOLOGY

3.1 Apparatus

- Oven
- 100 mL stoppered glass bottle
- Thermostatic bath
- Analytical balance
- Weighing boat
- pH meter
- Microwave

3.2 Chemicals

- $FeCl_3$. $6H_2O$
- 2-nitrophenol
- nitrogen gas
- Potassium iodide
- Methylene blue
- Iodine
- H_2SO_4
- $Na_2S_2O_3$
- Na_2CO_3
- Isopropanol
- Benzoquinone

- Oxalic acid
- Ethanol

3.3 Method

Liu et al., 2012 reported that catalysts prepared by preloading the metal precursor to the biomass before carbonization and activation had a higher activity as compared to the catalysts prepared by loading the metal precursor after carbonization and activation of the biomass (LIU et al., 2012).

3.3.1 Synthesis of pine cone activated carbon impregnated with $FeCl_3$ by microwave heating technique

Pine cone was collected from Vaal universityof technology, Vanderbijlpark campus, washed and dried for 48 hours in an oven at 90 ^{0}C. The scales of pine cone was peeled off and crushed. The pine cone powder was sieved into a particle size of less than 150µm and used as the source of activated carbon (OFOMAJA et al., 2010). Microwave heating was conducted in a domestic Kelvinator Microwave oven with suitable modifications. The impregnation ratio (IR) of ferric chloride hexahydrate ranging from 0.01 g to 0.5g to the biomass of 5 g samples was prepared and stirred for 3hrs. The slurry was subjected to a vacuum drying at 100^{o}C overnight. The impregnated biomass was purged with nitrogen and pyrolyzed at a different power level ranging from 600 W-1200 W for 20 minutes (MUBARAK et al., 2014). After pyrolysis, the sample was cooled down to room temperature. The produced activated carbon was weighed to determine the percentage yield of the products. Finally, the sample was stored in closed bottles.

3.3.2 Characterization of pince cone powder activated carbon-iron oxide composites.

The support material and the pine cone powder activated carbon iron oxide (PCP-AC-iron oxide) catalyst was characterized by the following analytical instruments

Fourier Transform Infrared (FTIR)

The FTIR spectra of the Pine cone powder-activated carbon (PCP-AC) and pine cone powder activated carbon iron oxide (PCP-AC-iron oxide) were recorded on a Perkin-Elmer (USA) FTIR Spectra 400 spectrometer in the range 650-4000 cm^{-1} to elucidate the functional groups present

Thermogravimetric Analysis (TGA)

A TGA was used to measure the changes in the weight loss of the sample as a function of temperature in an inert environment. The PCP-AC and PCP-AC-iron oxide compared to the activated carbon with $FeCl_3$ as the activating agent. To check the metal oxide support interaction. The activated carbon was subjected to heat ranging from 30 – 700 ^{O}C in an inert environment at a heating rate of 10 $^{o}C.min^{-1}$ using Perkin Elmer (USA) Simultaneous Thermal Analyzer 600 instrument.

X-ray Diffraction (XRD)

X-ray diffraction (XRD) was conducted to identify the chemical composition and crystallographic structure of the prepared materials. A X'Pert PRO X-ray diffractometer (PANalytical, PW3040/60 XRD; CuKα anode; $\lambda = 0.154$ nm) was used to obtain the XRD patterns. The samples were placed in an aluminum holder and scanned at 45 kV and 40 mA from 10 ° to 70 ° 2θ, the exposure time for each sample was 20 minutes and a step size of 0.02 °.

X-ray Fluorescence (XRF)

X-Ray Fluorescence was used to determine the amount of iron oxide on the catalyst. XRF Regaku NEX QC was used for the analysis

Scanning Electron Microscope (SEM)

SEM was used to obtain the image of the surface morphology of PCP-AC-Iron oxide and the dispersion of iron oxide on the support. Cerl-Zeiss-Sigma instrument (Germany) was used for the analysis

Transmission Electron Microscopy (TEM) Measurement

A transmission electron microscopy (TEM) was used for the size measurement and size distribution of the iron oxide nanoparticles on the activated carbon support on a JEOL 2010 FET TEM (Japan).

Gas Chromatography-Mass Spectroscopy (GC-MS)

GC-MS was performed on the treated samples to determine the degradation products. Claurus 500: PE Auto system with built in the autosampler was used for the analysis.

Determination of surface area and pore volumes by iodine number

The iodine number was determined according to the ASTM d4607-94 method. The experiment consisted of treating 0.1g of activated carbon with 10mL of 5% HCl. The mixture was then boiled for the 30s and cooled. Soon afterwards, 100 mL of 0.1 mol/L iodine solution was added to the mixture and was stirred for 30 s. The resulting solution was filtered and 50 mL of the filtrate was titrated with 0.1 mol/L of sodium thiosulfate, using starch as indicator. The iodine amount adsorbed per gram of carbon was plotted against the mass dosage of the $FeCl_3$ and microwave power to obtain monolayer (ASTM, 2006).

***Determination of surface area and pore volumes by methylene blue* numbers**

In this experiment, 10 mg of activated carbon was placed in contact with 10 mL of methylene blue solution at different concentrations (10, 25, 100, 250, 500 and 1000 mg/L) for 24h at room temperature. The remaining concentration of methylene blue was analyzed using a UV-Vis

spectrophotometer at 645 nm. The amount of methylene blue adsorbed from each solution was calculated by the equation

$$q_{eq} = \frac{(C_0 - C_e)V}{M} \quad (1)$$

Where C_0(mg/L) is the initial concentration of the methylene blue solution, C_e is the concentration of the methylene blue at equilibrium, V(L) is the volume of the treated solution and M(g) is the mass of the adsorbent. To determine the methylene blue number for the Langmuir model, an q_{eq} plot is made in function of C_e.

Determination of point of zero charge

The pH at point zero charge (pH_{PZC}) of the PCP-AC and PCP-AC-Iron oxide was determined by the solid addition method (Mall et al., 2006). To a series of 100 cm^3 conical flasks, 22.5 cm^3 of 0.01 $mol.dm^{-3}$ KNO_3 solution of known concentration was transferred. The pH values of the solution was adjusted to within the range of pH 2 to 12 adding either 0.10 $mol.dm^{-3}$ HCl or NaOH. The total volume of the solution in each flask was made up to 25 cm^3 by adding KNO_3 of the same strength. The pH_i values of the solution were accurately noted, and 0.05g of PCP was added to the flask, which was securely capped immediately. The suspension was manually shaken and allowed to equilibrate for 48 hr with intermittent manual shaking. The pH value of the supplements liquids was noted. The difference between the initial and the final pH values ($\Delta pH = pH_i - pH_f$) was plotted against the pH_i. The point of intersection of the resulting curve at which $\Delta pH = 0$ gave the pH_{pzc}.

3.3.3 Degradation of methylene blue by Fenton-like reaction using commercial hydrogen peroxide

Methylene blue aqueous solution was chosen as the model dye for treatment. A stock solution of 1000 mg/l at neutral pH was prepared. In each degradation study, 10 ml of the 1000 mg/l was mixed with 20 ml of H_2O_2 (30%), 70 ml of distilled water and 0.2g of PCP-AC-Iron oxide. The experiment was performed in 250 ml beaker at 500 rpm stirring speed. At a certain time, 1 ml of samples was pipetted, filtered and the concentration was determined at 660 nm wavelength for methylene blue using UV-Vis spectrophotometer. Effects of various parameters were investigated as shown in Table 3.1.

Table 3. 1: Experimental conditions for the degradation of methylene blue

Variables	Experimental conditions
Volume of H_2O_2 (ml)	0,5, 20, 30, 40, 60, 80
Catalyst dose (g)	0.01, 0.10, 0.15, 0.20, 0.30
Concentration of iron loaded (g)	0, 0.01, 0.05, 0.10, 0.20, 0.30
Microwave power (W)	600, 720, 840, 960,1200
MB concentration (mg/l)	100, 150, 200, 250
Stirring rate (rpm)	250, 375, 500, 750, 800, 950,1000
Temperature ($^{\circ}$C)	27, 30, 35, 40, 50
pH	3, 5, 7, 8, 10
Time (min)	1, 5, 10, 15, 20, 30, 45, 60

3.3.4 Degradation of 2-Nitrophenol by Fenton-like reaction using commercial hydrogen peroxide

At high pH (11-12), the phenolic proton dissociates giving a phenolate anion with an intense yellow color that can be easily measured by UV/Vis spectrometer (OFOMAJA and

UNUABONAH, 2011). The procedure for the determination of the final concentrations of 2-nitrophenol after degradation involves adding equal volumes of the 2-nitrophenol and 0.5 M of Na_2CO_3 solution of pH of about 11-12 before analyzing with Perkin-Elmer (USA) Lambda 25 UV-Visible spectrometer. The absorption of the resulting mixture was analyzed at a wavelength of 400 nm using distilled water as a blank.

The 2-nitrophenol aqueous solution was chosen as the simulation wastewater. A stock solution of 1000 mg/l at neutral pH was prepared. In each degradation study, 10 ml of the 1000 mg/l was mixed with 20 ml of H_2O_2 (30%), 70 ml of distilled water and 0.2g of PCP-AC-Iron oxide. The experiment was performed in 250 ml beaker at 500 rpm stirring speed. At a certain time, 1 ml of samples was pipetted, filtered and mixed with 1 ml of 0.5 M Na_2CO_2. The mixture was analyzed at 400 nm for the determination of 2-nitrophenol using UV-Vis spectrophotometry.

Table 3. 2: Experimental conditions for the degradation of phenol

Variables	**Experimental conditions**
Volume of H_2O_2 (ml)	0,20, 30, 40, 50
Catalyst dose (g)	0.15, 0.20, 0.25
Concentration of iron loaded (g)	0, 0.01, 0.05, 0.10, 0.20, 0.30
Microwave power (W)	600, 720, 840, 960, 1200
MB concentration (mg/l)	100, 150, 200, 250
Temperature ($^{\circ}$C)	27, 37, 47, 57
pH	5, 7, 9
Sampling time (min)	1,5,10, 15, 20, 30, 45, 60, 45, 90, 120

3.3.5 Catalyst reusability and stability

To confirm the stability of the catalyst in the heterogeneous Fenton oxidation of methylene blue and 2-nitro phenol, 100ppm of methylene blue at pH 7 was degraded and the catalyst was

recovered. The recovered catalyst was recycled three times for use in the degradation of methylene blue and 2-nitrophenol solution. At the end of each cycle, the catalyst was washed with ethanol to remove adsorbed methylene blue and 2-nitrophenol, then washed with distilled water three times followed by drying in the vacuum oven.

3.3.6 Determination of the mechanism

To confirm the degradation mechanism, the degradation was measured in the absence and presence of radical scavenger, for example with 10 ml of 1 mM isopropanol which acts as scavenger for hydroxyl radicals $\left(\cdot OH\cdot\right)$ and 10 ml of 1 mM of Benzoquinone that acts as radical scavenger for superoxide radicals (O_2^{-}) were added at the beginning of the Fenton oxidation of MB and 2NP. The degradation of MB without and with isopropanol and benzoquinone using catalyst prepared with different masses of the iron precursor at 600 W and those prepared with 0.20 g iron precursor at different microwave power were measured and compared.

3.3.7 Determination of intermediation products by Gas chromatography-mass spectrometry (GC-MS) Analysis

The control 2NP and MB sample along with the Fenton treated samples extracted with chloroform were applied to the GC-MS analysis. Claurus 500: PE Auto system with built in the autosampler, column: Elite 5 – ms, GC-capillary: 30 m, Diameter: 0.25 mm, Carrier gas: Helium, flow rate: 1.0 mL/min, temperature program for 2-NP: oven temperature 40^{o}C was raised to 270 °C at 8 °C/min. Temperature program for MB: oven temperature of 40 ^{o}C was held for 2 min and was raised to 200 at 2 ^{o}C/min and was held for 10 min. Injection volume 1 μL. Spectra system is Flame ionization detector and Electron capture detector

3.4. Kinetics modeling of data

Researchers often determine the potential of the catalyst by kinetics models. The experimental data is analyzed using kinetic models to establish the mechanism and efficiency of the catalytic degradation process. Degradation reaction orders were studied using pseudo-first-order, pseudo-second order, and Langmuir-Hinshelwood models.

3.5. Thermodynamics analysis

Values for thermodynamic parameters such as Gibbs free energy change, entropy change, and enthalpy change were calculated. These parameters are of importance as they show the spontaneity, feasibility, and nature of the Fenton oxidation process.

3.6. Conclusions

A study has been carried out to investigate the ability of the pine cone as an alternative source of carbonaceous material. Also the ability for to synthesize activated carbon-iron oxide composite, to apply as a catalyst for the Fenton oxidation process by single step synthesis.

3.7 References

2006. Standard Test Method for Determination of Iodine Number of Activated Carbon. *D4607-94.* United States of America: American Society for Testing Materials (ASTM).

LIU, X., BI, X. T., LIU, C. & LIU, Y. 2012. The performance of Fe/AC catalyst prepared from demineralized pine bark particles in a microwave reactor. *Chemical Engineering Journal,* 193-194**,** 187-195.

MUBARAK, N. M., KUNDU, A., SAHU, J. N., ABDULLAH, E. C. & JAYAKUMAR, N. S. 2014. Synthesis of palm oil empty fruit bunch magnetic pyrolytic char impregnation with FeCl3 by microwave heating technique. *Biomass and Bioenergy,* 61**,** 265-275.

OFOMAJA, A. E., NAIDOO, E. B. & MODISE, S. J. 2010. Dynamic studies and pseudo-second order modeling of copper(II) biosorption onto pine cone powder. *Desalination,* 251**,** 112-122.

OFOMAJA, A. E. & UNUABONAH, E. I. 2011. Adsorption kinetics of 4-nitrophenol onto a cellulosic material, mansonia wood sawdust and multistage batch adsorption process optimization. *Carbohydrates Polymers,* 83**,** 1192-1200.

CHAPTER 4: CATALYST CHARACTERIZATION

The chapter presents and discusses the characterization of the pine cone powder activated carbon-iron oxide (PCP-AC-Iron oxide) and pine cone-activated carbon (PCP-AC). It reports on the following characterization: iodine and methylene blue number, FTIR, XRD, TGA, the point of zero charge, SEM, Elemental mapping, EDX, XPS, and XRF.

4.1 Iodine and Methylene blue number

Methylene Blue and Iodine number are widely used methods for the characterization of pore properties of activated carbon. Mesoporous and microporous structures of activated carbon are largely responsible for their adsorption/catalytic behavior. The mesopores are pores of diameter between 20 and 500 Å which can be accessed by large molecules such as methylene blue molecules(AHMED, 2016), while the micropores are within the size range of $\geq$ 20 Å and can be assessed easily by small molecules such as the iodine molecules (BOTA et al., 1997). In the preparation of activated carbon using activating agents containing metallic spicies such as K^+, Na^+, Zn^{2+} and Fe^{2+} or Fe^{3+}, migration of the metal ion spicies at the boiling points or above boiling point through the carbon precursor is majorly responsible for well-developed pore structure (KHEZAMI et al., 2007, OLIVEIRA et al., 2009, SALMAN, 2014). In the preparation of activated carbon for environmental application, it is necessary to select process parameters that produces high volumes of micropores of various sizes that can adsorb a wide variety of molecules as well as substantial amounts of meso- and macropores that will provide access into the micropores (MOLINA-SABIO and RODRIGUEZ-REINOSO, 2004). Therefore, in optimizing the preparation of PAP-AC-iron oxide composite for use as Fenton catalyst via microwave method using pine cone biomass as a

carbon source and $FeCl_3$ as an iron precursor, the effect of iron precursor and microwave power on the pore structure of the composite was examined.

The effect of the amount of iron precursor used for catalyst preparation on the methylene blue number and iodine number of the composite produced at different microwave power are shown in Figure 4. 1. 1a and b. The results in Figure 4. 1. 1a showed that there was an increase in methylene blue number when the iron precursor amount was increased from 0.01 to 0.10 g for all microwave power treatment. The methylene blue number then reduced with a further increase in the amount of iron precursor added. The increase in methylene blue number with increasing iron precursor amount has been attributed to increased iron species migrating through the matrix of the pine biomass during activation (OLIVEIRA et al., 2009). This increase in larger pore formation was observed to reach its optimum with the addition of 0.10 g of iron precursor and above this amount led to lower methylene blue capacities due to increased gasification which leads to widening and destruction of pores (FOO and HAMEED, 2011, MUBARAK et al., 2014, WARTELLE et al., 2000). The methylene blue number was also observed to increase with increasing microwave power of 600 to 840 W and then reduce as the microwave power was increased from 920 to 1200 W. Higher microwave power has been reported to be associated with higher rate of reaction between the activating agent and iron precursor (HESAS et al., 2013b). Therefore, as the microwave power is increased from 600 to 840 W the reaction between the iron precursor ($FeCl_3$) and carbon precursor increases rapidly and above microwave power of 840 W, gasification reactions which lead to widening and destruction of pores occurs. The optimum amount of large pores was obtained with 0.10 g of the iron precursor at 840 W.

Figure 4. 1. 1b shows the effect of increasing iron precursor content from 0.01 to 0.30 g at different microwave power (600 to 1200 W) on iodine number. The plot shows that there was a steady

increase in iodine number as the iron precursor amount was increased from 0.01 to 0.20 g at all microwave power applied. As the iron precursor amount was increased to 0.30 g, the iodine number was observed to reduce for all microwave power applied. As explained earlier, increase in microwave power is accompanied by increased reaction rate between the iron precursor and pine biomass. Comparing the plots in Figure 4.1.1a and 4.1.1b, it was observed that the rate of increase in iodine number as the amount of iron precursor increased was higher as compared to the rate of increase in methylene blue number. This result, therefore, suggests that smaller pores (micropores) were initially formed at higher rates than larger pores (macropores) and the amounts small and large pores increased with microwave power (LI et al., 2008). Rapid formation of small pores with an increase in the amount of iron precursor and microwave power eventually results in the combining of small pores (coalescence) to form larger pores (ZHANG and CHEN, 2015). A rapid increase in the rate of formation of large pores may then increase the rate of ablation of the outside of the carbon particles producing burn-off which reduces the amounts of large pores (RODRIGUEZ-REINOSO and MOLINA-SABIO, 1994). The 600 W microwave treatment using 0.20 g of the iron precursor was observed to produce the optmum amount of small pores.

The effect of microwave power used for catalyst preparation on the methylene blue number and iodine number of the composite produced at different microwave are shown in Figures 4. 1. 2a and b. The results in Figure 4. 1. 2a shows that when microwave power was increased from 600 to 840 W the methylene blue number (formation of large pores) increased rapidly and the increase was higher when 0.10 g of the iron precursor was applied. Further increase in microwave power was observed to decrease the methylene blue number (larger pores) due to the complete destruction of pores. On the other hand, Fig. 2b showed that the iodine number which is a measure of a number of small pores was higher at 600 W for all amounts of iron precursor applied and reduced with an

increase in microwave power. Comparing the plots in Figures 4. 1. 2a and b, it was observed that the rate of decrease in iodine number at the initial stage of microwave power increase was higher than that for methylene blue number. These results again suggest that the rate of small pore formation is more influenced by microwave power and that the small pores influence the formation of larger pores. Since it was observed higher iodine number at lower microwave power of 600 W and the smaller pores widen to lager pores as microwave power increases form 600 to 1200 W

The Fenton reaction is known to take place by the decomposition of H_2O_2 by Fe^{2+} to produce the active hydroxyl radical species $(HO^{\cdot})$ which carries out the pollutant decomposition (LIMA et al., 2013). For this reason, the H_2O_2 molecules need to be adsorbed onto sites having Fe^{2+}, thus making the surface area of the composite important. It is well known that micropores contribute largely to the total surface area, therefore the PCP-AC-iron oxide with optimal amounts of small pores was chosen for this study. Samples with the highest amounts of small pores were those prepared at 600 W and with iron precursor content from 0.01 to 0.30 g.

.

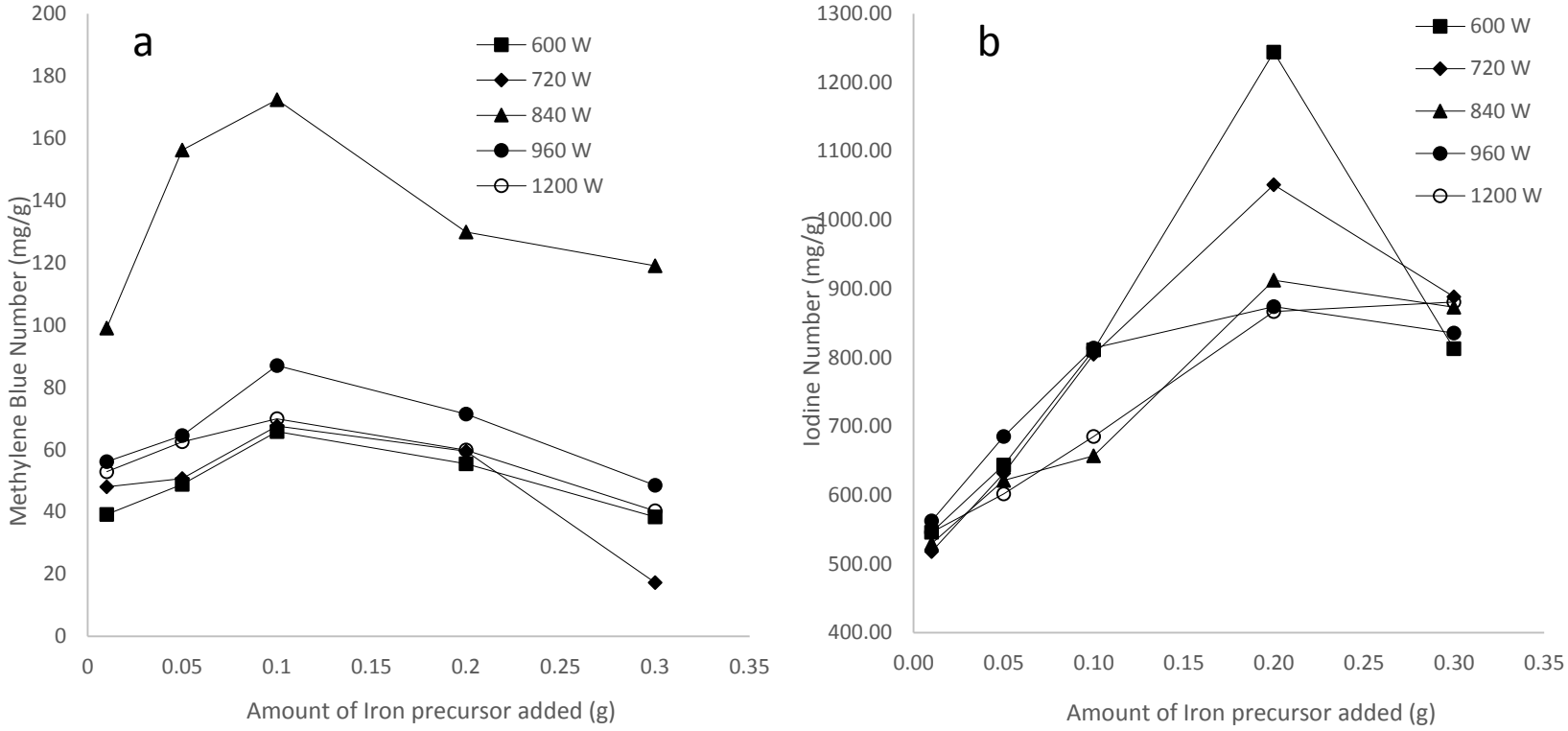

Figure 4. 1. 1: Effect of iron precursorr on (a) methylene blue number and (b) iodine number

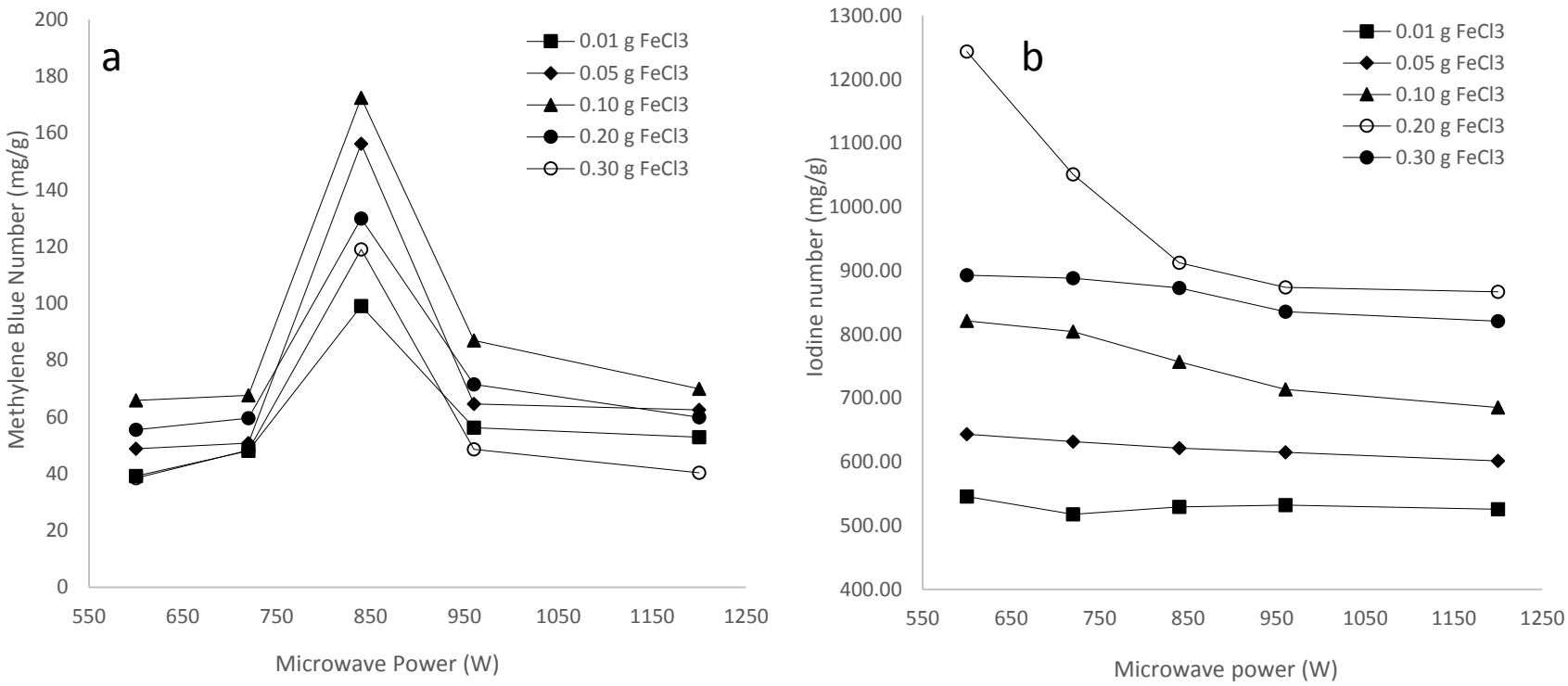

Figure 4. 1. 2: Effect of microwave power on (a) methylene blue number and (b) iodine number

4.2 FTIR Analysis

The results of FTIR analysis of activated carbon produced from pine cone biomass without $FeCl_3$ at 600 W (PCP-AC) is shown Figure 4. 2. 1. The spectrum revealed the presence of several functional groups on the carbon produced which includes a broadband at 3357 cm^{-1} which is associated with the O–H stretching vibration mode of hydroxyl functional groups (AHMED and THEYDAN, 2013). The peak at 2937 cm^{-1} is assigned to C-H of aliphatic compounds (KARTHIKEYAN et al., 2014), while the peaks at 1704 and 1598 cm^{-1} corresponds to C=O stretching vibration in ketones, aldehydes, lactones and carboxyl groups and C--O stretching in carboxylic groups, and carboxylate moieties (SADIQ et al., 2015). The band at 1512 cm^{-1} is assigned to C=C vibrations in the aromatic ring (WANG et al., 2014), while those at 1450, 1368, 1265, 1213 cm^{-1} represents conjugated C=O stretching and C-O stretching in carboxylic, carboxylate moieties or basic groups (TSONCHEVA et al., 2015). The peak at 1000 cm^{-1} is characteristic of C–OH vibrations corresponding to tertiary and secondary alcohols while those at 861 and 855 cm^{-1} corresponds to the flexion of out-of-plane C–H of aromatic compounds (LU et al., 2012). The peaks at 671and 627 cm^{-1} can be attributed to alkenes and aromatics out of plane bend (ALMAZÁN-SÁNCHEZ et al., 2015).

The FTIR spectra of the PCP-AC-iron oxide prepared at 600 W using varying amounts of $FeCl_3$ salt (0.01 to 0.30 g) are shown in Figure 4. 2. 2a. The sample treated with 0.01 g iron precursor showed similar peaks to the PCP-AC except that the peak intensities for the majority of the groups containing atoms with lone pairs of electrons such as oxygen and groups containing π-electrons such as C=C in the PCP-AC-iron oxide were reduced. The appearance of a new peak appeared at 540 cm^{-1} was also observed. The peaks representing O–H stretching vibration mode of hydroxyl groups (3357 cm^{-1}), C=O stretching (1704 and 1598 cm^{-1}), C=C vibrations in the aromatic ring

(1512 cm^{-1}) and the C–OH vibrations corresponding to tertiary and secondary alcohols were all observed to reduce in intensity when PCP was modified with 0.01 g of iron precursor before activation. Several authors (LU et al., 2012, WANG et al., 2014, MOHAMMED et al., 2015) have shown that the interaction between iron oxide and functional groups on AC occurs during the synthesis of AC-Iron oxide composites. The peak appearing at 540 cm^{-1} was attributed to the formation of iron oxide (Fe-O-H) in the PCP-AC-Iron oxide composite (CASTRO et al., 2009a, KRISHNAN and HARIDAS, 2008, TANG et al., 2014).

As the mass of $FeCl_3$ added to PCP prior microwave treatment was increased from 0.01 to 0.30 g (Figure 4. 2. 2a), the above-mentioned peaks were all observed to reduce further. The further reduction in peak intensities may be attributed to increased interaction between iron oxide particles and functional groups on the activated carbon and also to the fact that since $FeCl_3$ acts as a dehydrating agent during the carbonization of lignocellulosic materials (CHI et al., 2012), a reduction in the peaks of the oxygenated groups is expected.

As the microwave power was increased from 600 to 1200 W, the peaks in the spectra remained the same but differed in their intensities. With increased in microwave power, the intensities of the oxygenated functional groups were observed to decrease suggesting that higher microwave power which corresponds to higher temperature led to decomposition of the surface functional groups. Zhang et al. observed an increase in carbon content and a decrease in the content of heteroatoms with increasing microwave power during the production of activated carbon from coconut shell (ZHANG et al., 2013). At 1200 W, a drastic reduction in functional groups having heteroatoms can be seen in Fig. 4. 2. 2b. Furthermore, a disappearance of the peak at 543 cm^{-1} and an appearance to two new peaks was observed at microwave heating power of 960W and 1200 W. The disappearance of the peak at 543 cm^{-1} and appearance of two new peaks at 573 and 558 cm^{-1} may

be attributed the increase in size of the iron oxide particles due to sintering effect occurring at higher microwave power (NASRAZADANI and NAMDURI, 2006).

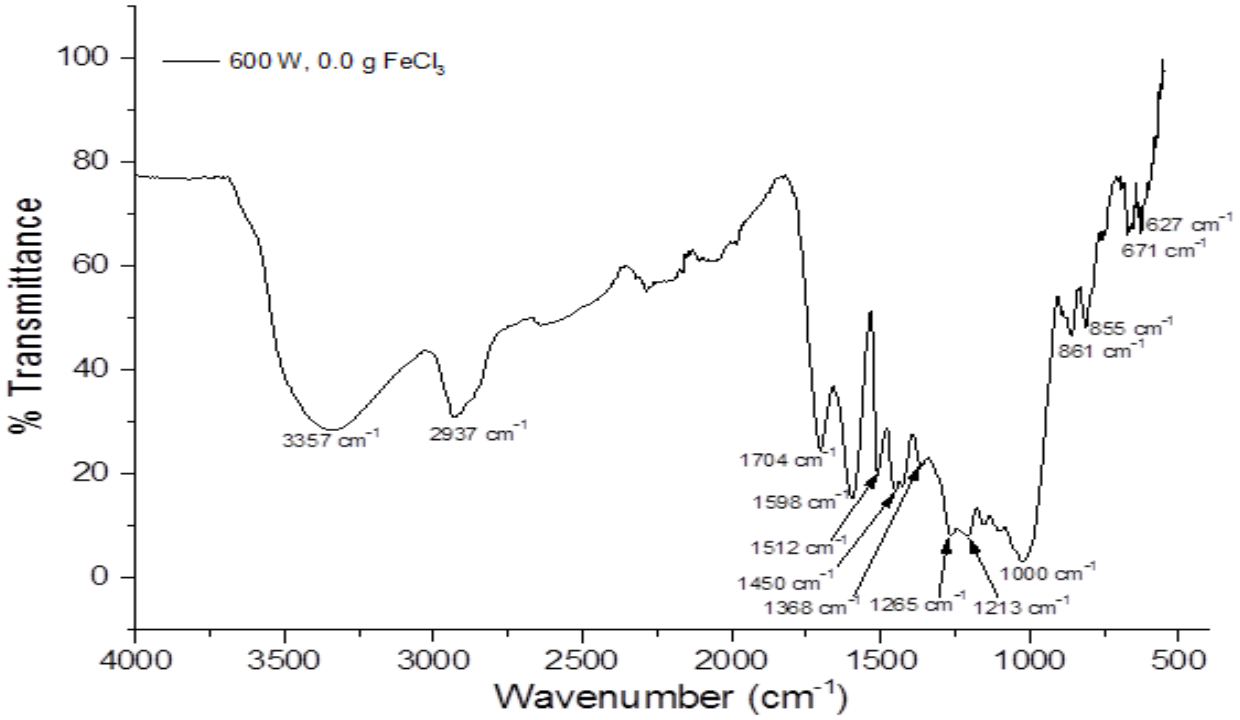

Figure 4. 2. 1: FTIR spectrum of activated carbon produced from pine cone biomass at microwave power 600 W.

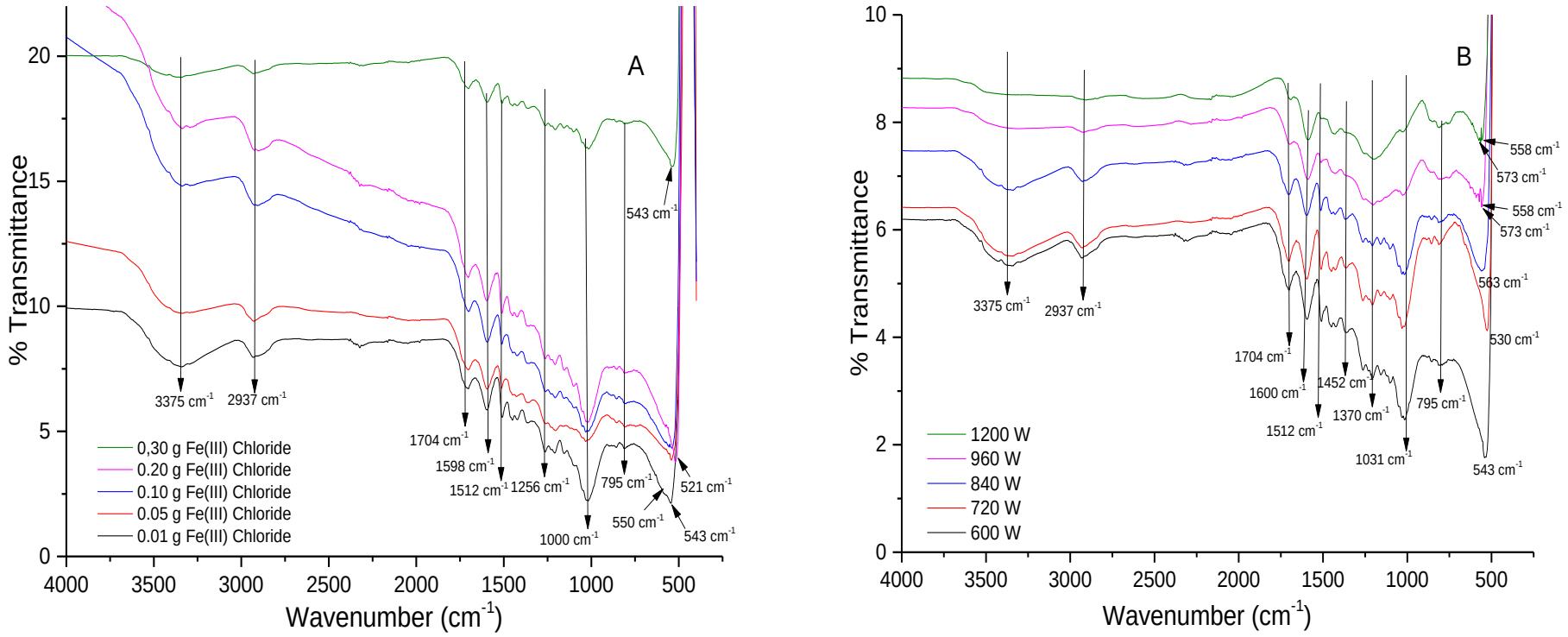

Figure 4. 2. 2: FTIR spectra of (a) PCP-AC-iron oxide prepared using different amounts of $FeCl_3$ at 600 W and (b) PCPAC-iron oxide prepared at different microwave power using a constant mass of $FeCl_3$ = 0.2

4.3 XRD Analysis

The X-ray diffractograms for PCP-AC and PCP-AC-iron oxide were recorded at room temperature and displayed in Figure 4. 3. 1a. The XRD pattern of the pure PCP-AC revealed that there was no detectable crystalline phase. Broad reflections of typically amorphous materials were observed at 2θ = 15.29°, 21.14°, 26.66° (0 0 4) and 35.74° which corresponds to micrographitic structure characteristic of activated carbons (CASTRO et al., 2009b)which is in line with the PDF card JCPDS 026-1080. When incremental amounts of $FeCl_3$ was added to the carbon source prior to microwave treatment, it was observed that the new peaks at 2θ = 45.01° (3 1 1) and 60.11° (3 4 1) which is in line with the PDF card JCPDS 074-4121. The reduction of the peak at 2θ = 35.74° (2 3 0) are characteristic of low iron oxide concentration and/or formation of small particle size iron oxide dispersed over the carbon matrix (GONÇALVES et al., 2015, SCHWARTMAN and CORNELL).

The X-ray diffractograms for PCP-AC-iron oxide prepared with the constant amount of $FeCl_3$ and irradiated with increasing microwave power is shown in Figure 4. 3. 1b. Two observations could be made from this XRD pattern in Fig. 4b. Firstly, the amorphous material peaks of carbon at 2θ = 15.29° and 21.14° were found to reduce in intensity as microwave power was increased from 600 to 1200 W and a new peak at 45.01° representing iron oxide was also observed. Hesas et al. reported that higher microwave power produces higher rates of reaction between activating agent and precursor which promote the carbonization process and loss of carbon (HESAS et al., 2013a). This may account for the reduction of the amorphous peaks of carbon. However, the crystal size could not be, calculated due to the fact that the iron and carbon overlap at the same peak at 2θ = 35.71°.

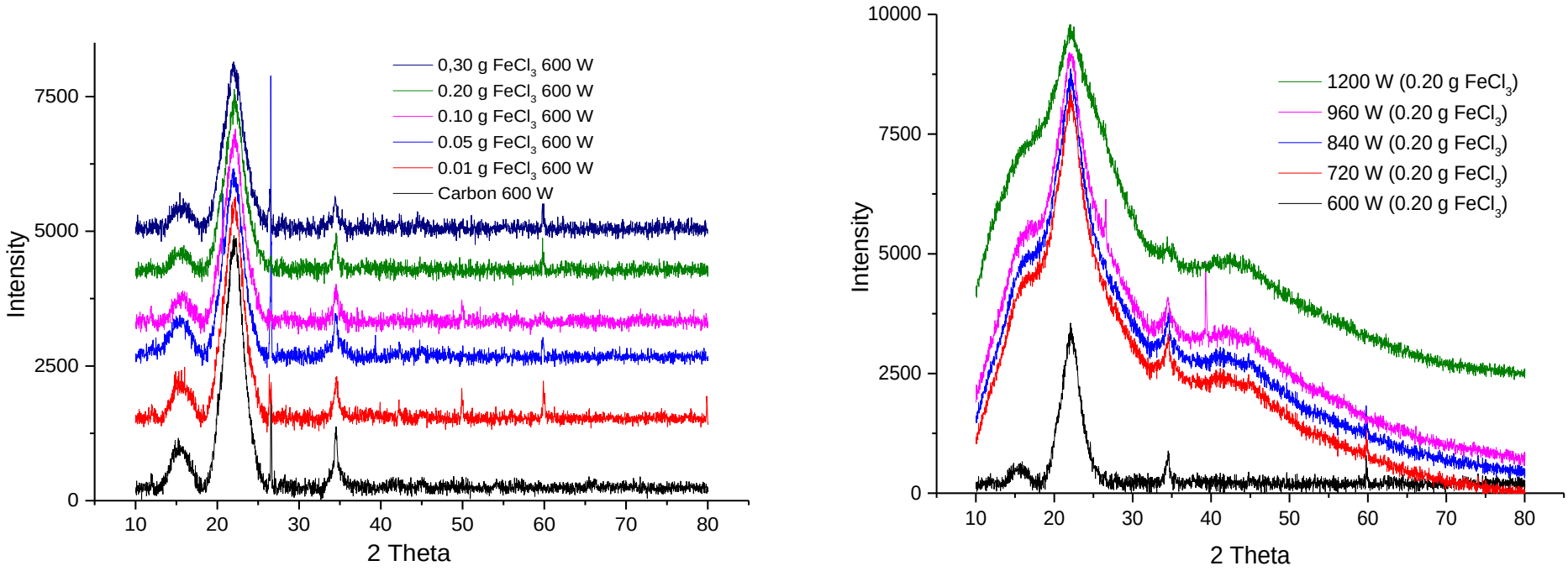

Figure 4. 3. 1: XRD spectra of (a) PCP-AC-iron oxide prepared using different amounts of $FeCl_3$ at 600 W and (b) PCP-AC-iron oxide prepared at different microwave power using a constant mass of $FeCl_3$ = 0.20 g.

4.4 Thermogravimetric Analysis

The thermal behavior of PCP-AC AND PCP-AC-Iron oxide was observed in an inert environment to confirm the composition of the PCP-AC-Iron oxide. The analysis was performed from 30 ^{o}C to 900 ^{o}C at a heating rate of 10 ^{o}C/min. As shown in the Figures 4. 4. 1a and b, it was observed that at 0 ^{o}C to 100 ^{o}C there was a weight loss which is attributed to the loss of adsorbed water on the surface of the catalyst (SHRESTHA et al., 2012). From 200 ^{o}C to 400 ^{o}C the weight percentage decreased steeply, this major weight loss is attributed to the decomposition of polymeric cellulose network and hemicellulose. The gradual weight loss observed at 400 ^{o}C to 900 ^{o}C is due to the decomposition of lignin molecule (RAZIA et al., 2014). However, Figure 4. 4. 1a shows the effect of iron content on the thermal analysis of the catalysts. The weight retention of PCP-AC was less than 40 %, while as the iron content increases from 0.01g to 0.30g during activation, the weight retention also increases (OH et al., 2015a, OH et al., 2015b). This is due to the fact that when the iron content during activation increases, the formation of iron oxide increase. Ruoff et al and Baykal et al reported that Fe_3O_4 and Fe_2O_3 retained almost 100 % of its weight (RUOFF et al., 2011, BAYKAL et al., 2010). Hence there is an increase in weight retention as the amount of iron oxide increases. Figure 4.4.1b shows the effect of microwave power during activation on the thermal behavior of the catalyst prepared at different microwave power. As the microwave power increases the amount of weight retention also increases, this is attributed to the increase in iron oxide, as the microwave power increases during catalyst synthesis.

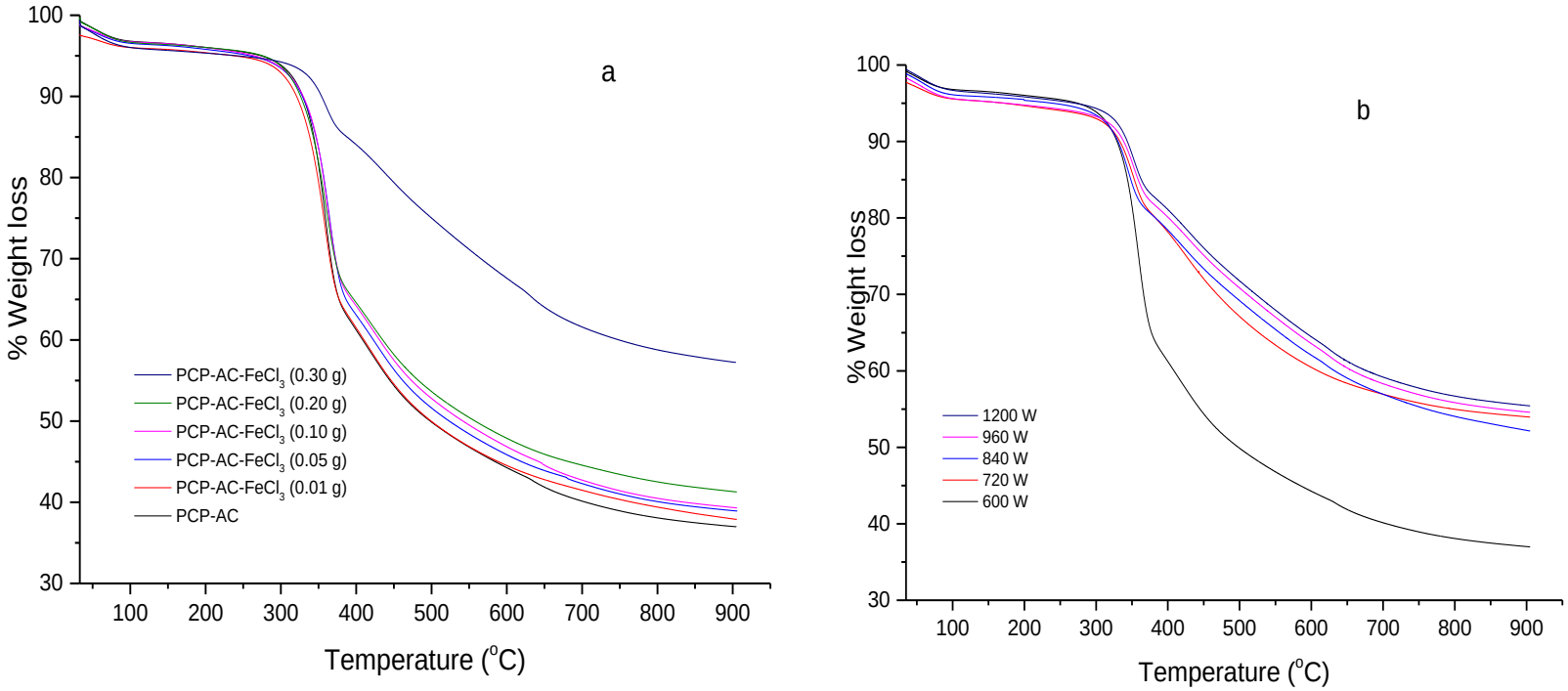

Figure 4. 4. 1: TGA spectra of (a) PCP-AC-iron oxide prepared using different amounts of $FeCl_3$ at 600 W and (b) PCP-AC-iron oxide prepared at different microwave power using a constant mass of $FeCl_3$ = 0.20 g.

4.5 Point of Zero Charge

The point of zero charge analysis was performed to observe where the net charge of the catalyst equals to zero. At a pH solution lower than the $pH_{PZC,}$ the catalyst will react as a positive surface and at pH solution higher than the $pH_{PZC,}$ the catalyst will react as a negative surface. Therefore for the higher pH solution than $pH_{PZC,}$ will increase the surface negative charge, hence it will promote the degradation activity of the cationic dye due to charge attraction. Figure 1a shows the effect of iron content on the pH_{PZC} of the composite. It is observed that as the iron content increases from 0 g to 0.01 g there was an increase in the pH_{PZC} from 6.37 to 6.77. However, when the iron content further increases from 0.01 g to 0.30 g there was a decrease in the pH_{PZC} from 6.77 to 6.25. This indicates that as the iron content increases there is a greater amount of oxygenated groups, mainly carboxylic acid, lactones, and phenols. The presence of this surface acidic groups will limit the Fenton oxidation process (RIBEIRO et al., 2016, SERP and FIGUEIREDO, 2009). However, the high iron content is also preferable in the Fenton oxidation, hence the 0.20g iron content was preferred as the optimum due to the fact that it has the high amount of iron content and a reasonable amount of pH_{PZC} of 6.55. Figure 4. 5. 1b shows the effect of microwave power on the pH_{PZC} of the composite. It can be observed that as microwave power increases from 600 to 1200 W the pH_{PZC} decreases from 6.55 to 6.25. This indicates that the composite becomes more acidic as the microwave power increases. In Fenton oxidation process, the active sites on the surface of the composite assist in the decomposition of the H_2O_2 to form hydroxyl radicals. The electron moves from the active site to the H_2O_2. The oxygenated groups have electron withdrawing capacity, hence this phenomenon limits the Fenton oxidation process (RIBEIRO et al., 2013, REY et al., 2011, RIBEIRO et al., 2016).

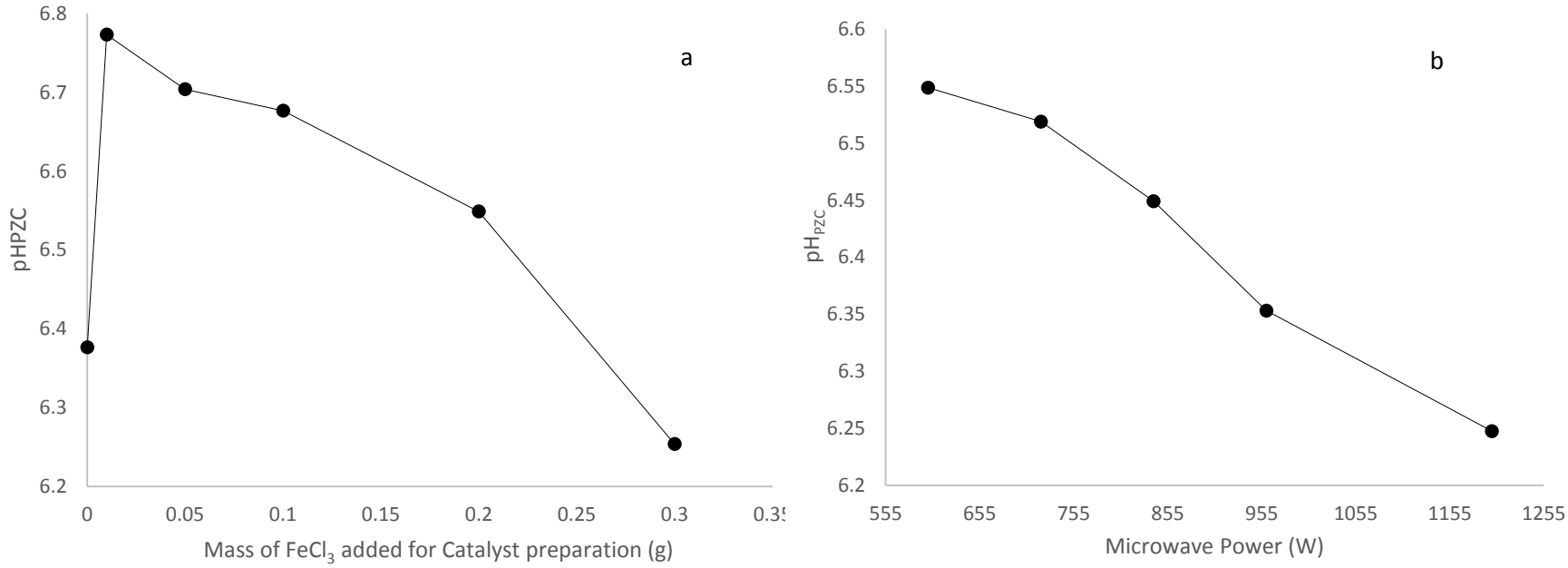

Figure 4. 5. 1: Point of zero charge of (a) PCP-AC-iron oxide prepared using different amounts of $FeCl_3$ at 600 W and (b) PCPAC-iron oxide prepared at different microwave power using a constant mass of $FeCl_3$ = 0.20 g.

4.6 (a) Scanning electron microscopy (SEM) analysis

SEM was performed on the catalyst to explore the surface characteristics of the catalyst. Figure 4.6.1 (a-f) shows SEM micrographs of activated carbon particles. They revealed cavities, pores and rough surfaces of the prepared activated carbon. It also revealed that the activating agent and activation microwave power affect the surface characteristics of the carbon surface and show that the pores are non-uniform. Figure 4.6.1a shows carbon prepared without the iron precursor, it barely shows pores, however when the iron precursor is introduced from 0.01 g to 0.10 g, there is a partial development of pores, this is due to the fact that metal chlorides promote extraction of water molecules in the lignocellulosic materials resulting in the development of pores (MARSH and RODRÍGUEZ –REINOSO, 2006). When the mass iron precursor was increased further to 0.20 g, well developed and distributed pores was observed, but further increase of the activating agent to 0.30 g resulted in the widening and destruction of pores When increasing the amount of the activating agent the micropores opened and widened with a shift to more of mesopores as the exterior of the particles is extremely burned-off due the more gasification, leading to the destruction of the carbon structure(RODRIGUEZ-REINOSO and MOLINA-SABIO, 1994, SAHIRA et al., 2013). This was also confirmed by the iodine and methylene blue number.

Figure 4.6.4 (a-e) shows the SEM images of the effect of microwave power on the pores and structural texture on the catalyst prepared at different microwave power. Figure 4.6.2a shows the activated carbon prepared at 600W has a well-developed porosity, this is attributed to the migration of the metal iron through the carbon precursor for well-developed pore structures. However, when the microwave power increases from 600W to 1200W micropores tends to widen, shifting to mesopores and macropores which ultimately leads to the destruction of pores completely. This is as a result of the increased in hydration, volatilization and also migration of the metal ion spicies

above boiling point through the carbon precursor (SALMAN, 2014, OLIVEIRA et al., 2009). Hence 0.20g iron content was chosen as the optimum mass of the iron precursor due to its high micropores and a considerable amount of mesopores (DENGA et al., 2010)

4.6 (b) Elemental mapping and Energy Dispersive X-Ray (EDX) analysis

Figure 4.6.3 (a-f) shows the elemental mapping of the dispersed of iron oxide on the activated carbon. Figure 4.6.3a displays the carbon prepared without the iron precursor and no traces of iron was observed. However, as the mass of the iron precursor increases from 0.01 g to 0.10 g of the activating agent, the PCP-AC-Iron oxides composite showed the presence of iron, with a well dispersed and moderate amount of iron oxide. When the mass of the iron precursor further increases to 0.20 g, the iron oxide increases and a highly dispersed iron oxide on the surface of the carbon was observed, which is a desirable characteristic of an ideal catalyst. As the iron content further increases to 0.30g, there was an increase in iron content, also the contrast of the particles becomes brighter and it was also observed increased space between particles suggesting the increase in particle size of the iron oxide. Figure 4.6.6 (a-e) shows the mapping images of the effect of microwave power on the surface and pore structure on the activated carbon. As the microwave power increases the amount of iron oxide increases, however when the microwave power increases from 600W- 1200W space between the particles increase, indicating sintering of particles leading to the formation of big particles due to higher irradiation on the microwave.

EDX analysis was performed to summarize the elemental composition of the catalysts. Figure 4.6.2 (a-f) and 4.6.5 (a-e) show that all of the samples contained carbon and oxygen which can be attributed to the activated carbon support. However, the sample impregnated with ferric chloride hexahydrate showed traces of iron due to the formation of the iron oxide during pyrolysis, it also showed no impurities such as chloride ions. Figure 4.6.2a show the carbon prepared without the

iron precursor and it shows no traces of iron. The elemental analysis showed as the iron content increase 0g, 0.01g, 0.05g, 0.10g, 0.20g, and 0.30g, the percentage of iron increase from 0%, 0.70%, 0.95%, 1.55%, 1.92%, and 2.80% respectively as shown in Table 4.6.1. The icrease in the percentage of iron could be attributed to the increase in the mass of the iron precursor. Table 4.6.2 shows the catalyst prepared at constant iron content and different microwave power. The increase in microwave power from 600W, 720W, 840W, 960W, and 1200W which leads to increase in the iron from 1.92%, 2.30%, 2.95%, 3.08% and 3.06% respectively as shown in Table 4.6.2. This trend can be attributed to the increase in energy which may cause an in cresase in the formation of iron oxide.

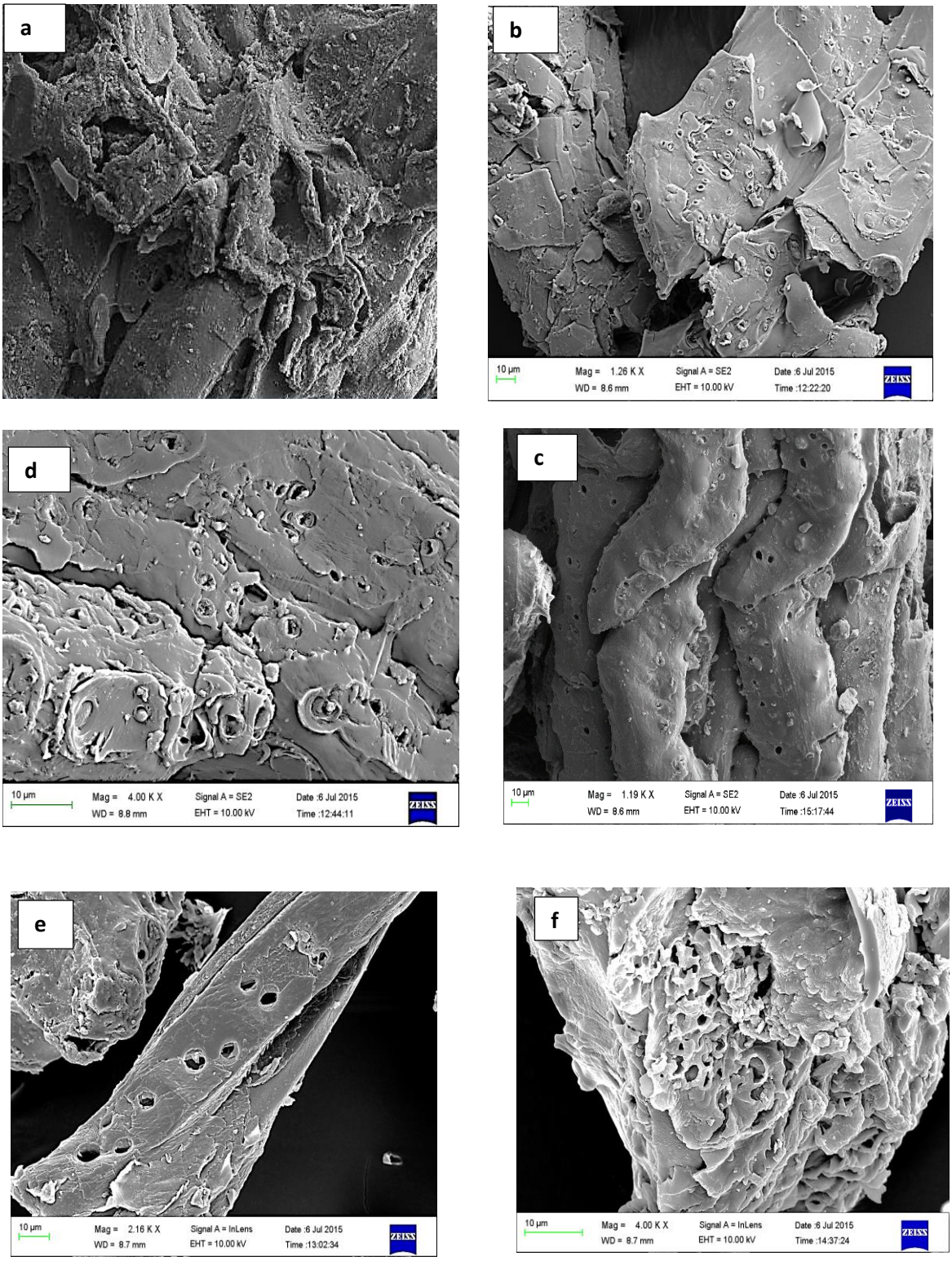

Figure 4. 6. 1: SEM images of PCP-AC-iron oxide prepared using different amounts of $FeCl_3$ at 600 W (a) 0g (b) 0.01g (c) 0.05 (d) 0.10g (e) 0.20g (f) 0.30g

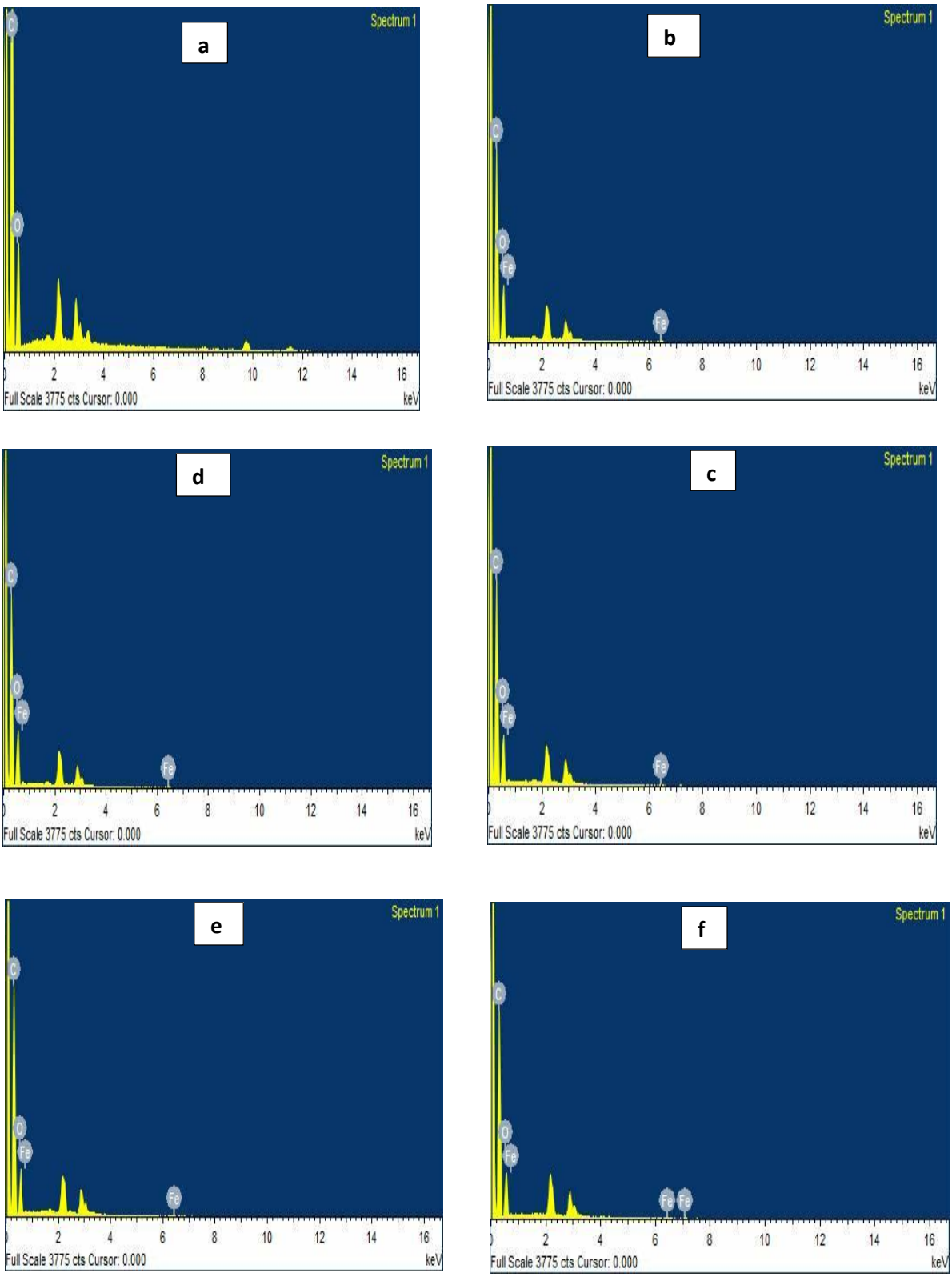

Figure 4. 6. 2: EDX spectra of PCP-AC-iron oxide prepared using different amounts of $FeCl_3$ at 600 W (a) 0g (b) 0.01g (c) 0.05 (d) 0.10g (e) 0.20g (f) 0.30g

Table 4. 6. 1: The effect of $FeCl_3$ amount on the chemical composition

	Weight %		
	C	O	Fe
0g $FeCl_3.6H_2O$	66.63	37.37	0
0.01g $FeCl_3.6H_2O$	65.03	34.27	0.7
0.05g $FeCl_3.6H_2O$	71.99	27.60	0.95
0.10g $FeCl_3.6H_2O$	61.00	31.44	1.55
0.20g $FeCl_3.6H_2O$	74.98	23.10	1.92
0.30g $FeCl_3.6H_2O$	67.18	30.02	2.80

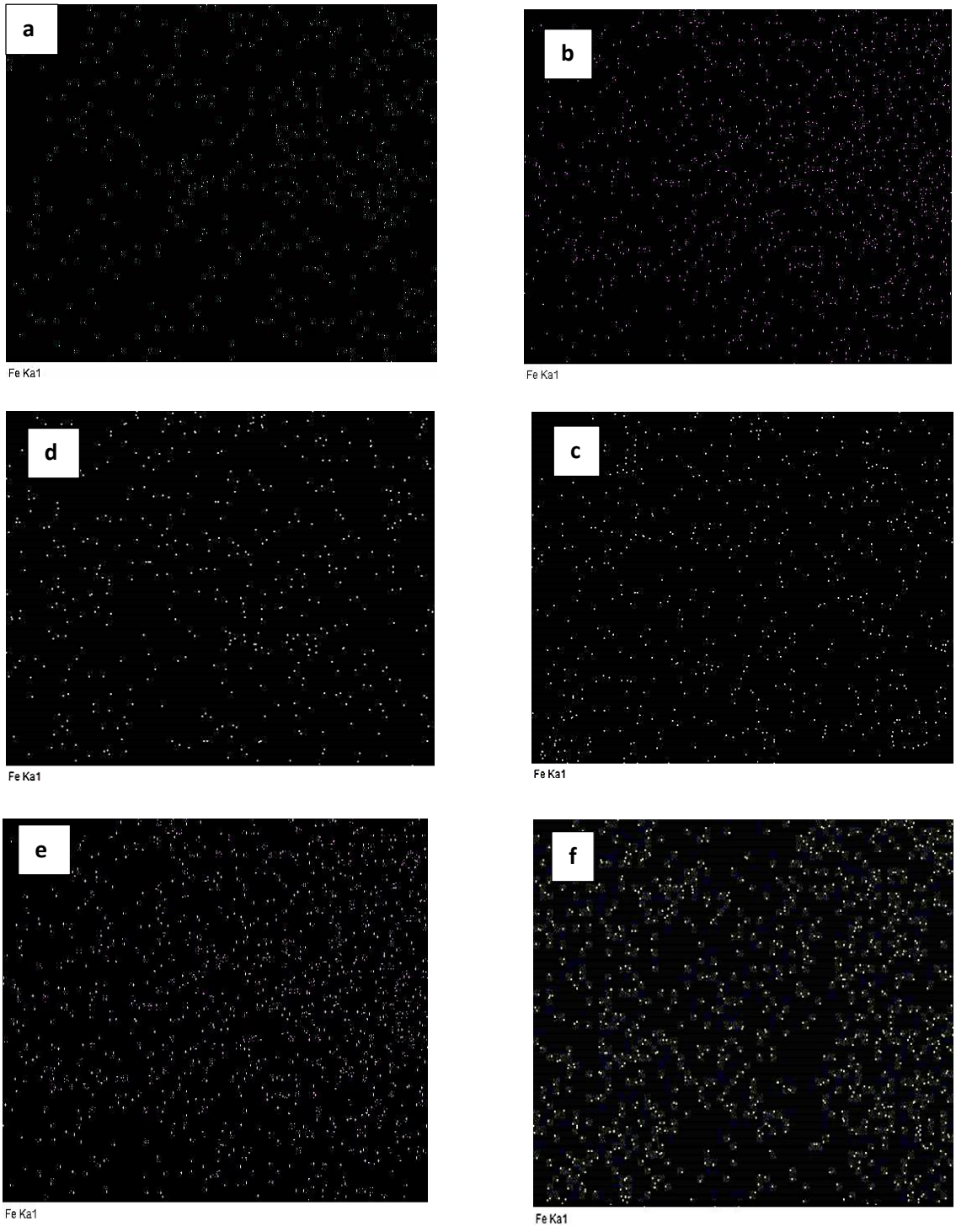

Figure 4. 6. 3: Elemental mapping of PCP-AC-iron oxide prepared using different amounts of $FeCl_3$ at 600 W (a) 0 g (b) 0.01 g (c) 0.05 g (d) 0.10 g (e) 0.20 g (f) 0.30 g

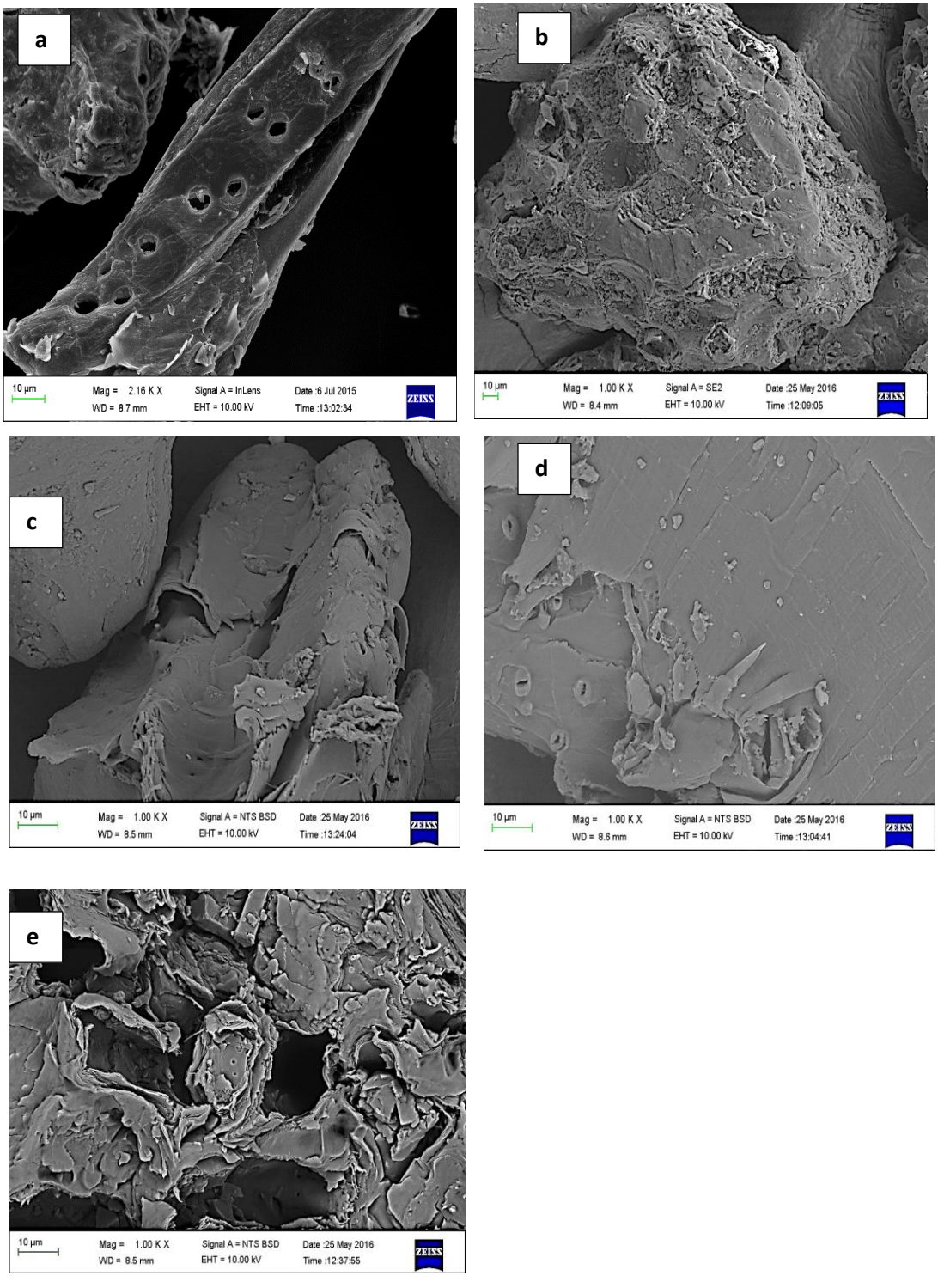

Figure 4. 6. 4: SEM images of PCPAC-iron oxide prepared at different microwave power using a constant mass of $FeCl_3$ = 0.20 g, (a) 600 W (b) 720 W (c) 840 W (d) 960 W (e) 1200 W

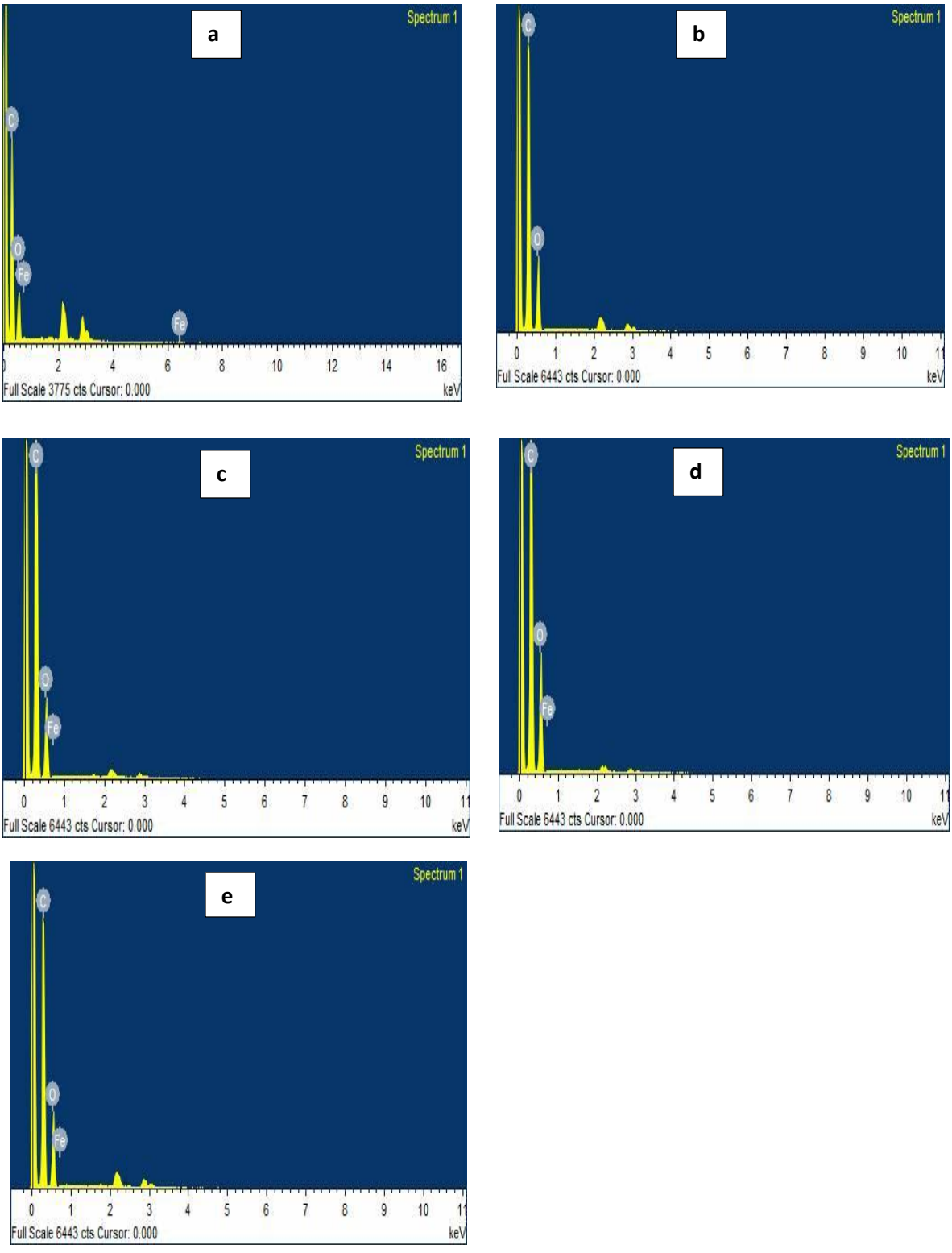

Figure 4. 6. 5: EDX spectra of PCPAC-iron oxide prepared at different microwave power using a constant mass of $FeCl_3$ = 0.20 g, (a) 600 W (b) 720 W (c) 840 W (d) 960 W (e) 1200 W

Table 4. 6. 2: The effect of microwave power on the chemical composition

	Weight %		
	C	O	Fe
0.20g $FeCl_3.6H_2O$ 600W	74.98	23.10	1.92
0.20g $FeCl_3.6H_2O$ 720W	63.80	33.81	2.38
0.20g $FeCl_3.6H_2O$ 840W	70.09	26.96	2.95
0.20g $FeCl_3.6H_2O$ 960W	68.14	29.78	3.08
0.20g $FeCl_3.6H_2O$ 1200W	70.27	26.67	3.06

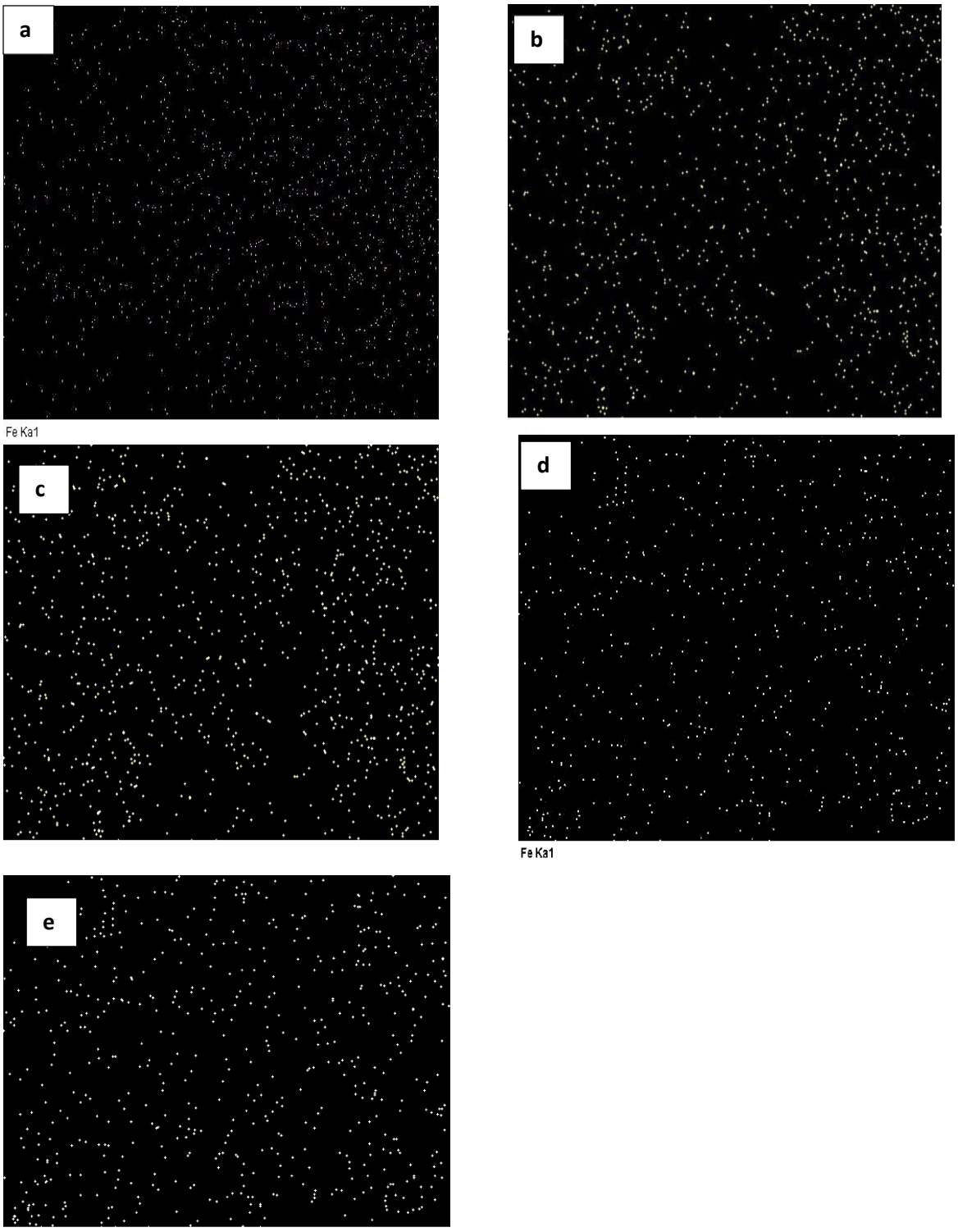

Figure 4. 6. 6: Elemental mapping of PCPAC-iron oxide prepared at different microwave power using a constant mass of $FeCl_3$ = 0.20 g, (a) 600 W (b) 720 W (c) 840 W (d) 960 W (e) 1200 W

4.7 X-ray Fluorescence (XRF) Analysis

XRF analysis of PCP-AC and PCP-AC-iron oxide prepared with different $FeCl_3$ amounts and at different microwave power are displayed in Figs. 5a and b. The results show that the PCP-AC prepared without iron precursor had an iron content of 0.02 % (Fig. 5a) indicating that the original PCP had a very low iron content. When 0.01 g of iron precursor was added into the carbon precursor before heating at 600 W, the iron content of the PCP-AC-iron oxide increased to 0.3 %, and further increase in the amounts of iron precursor to 0.05 g, 0.10 g, 0.20 g and 0.30 g led to an increase in the iron oxide content to 1.6 %, 2.1 %, 2.7 and 2.6 % respectively. The result, therefore, indicates that increasing the amount of iron precursor on the carbon precursor led to an increase in the iron oxide content of the catalyst.

When 0.02 g of $FeCl_3$ of added to the carbon precursor and the sample heated at different microwave powers (600 to 120 W), the iron content of the samples was found to increase with microwave power. The iron oxide contents were found to 2.7, 3.2, 3.4, 3.5 and 3.7 % as microwave power increased from 600 to 1200 W. Increase in iron content with microwave power at the addition of a constant amount of iron precursor can be attributed sintering of iron particles at high temperatures. An increase in microwave power produces higher temperatures that cause iron particles to sinter or aggregate and be retained in the carbon matrix

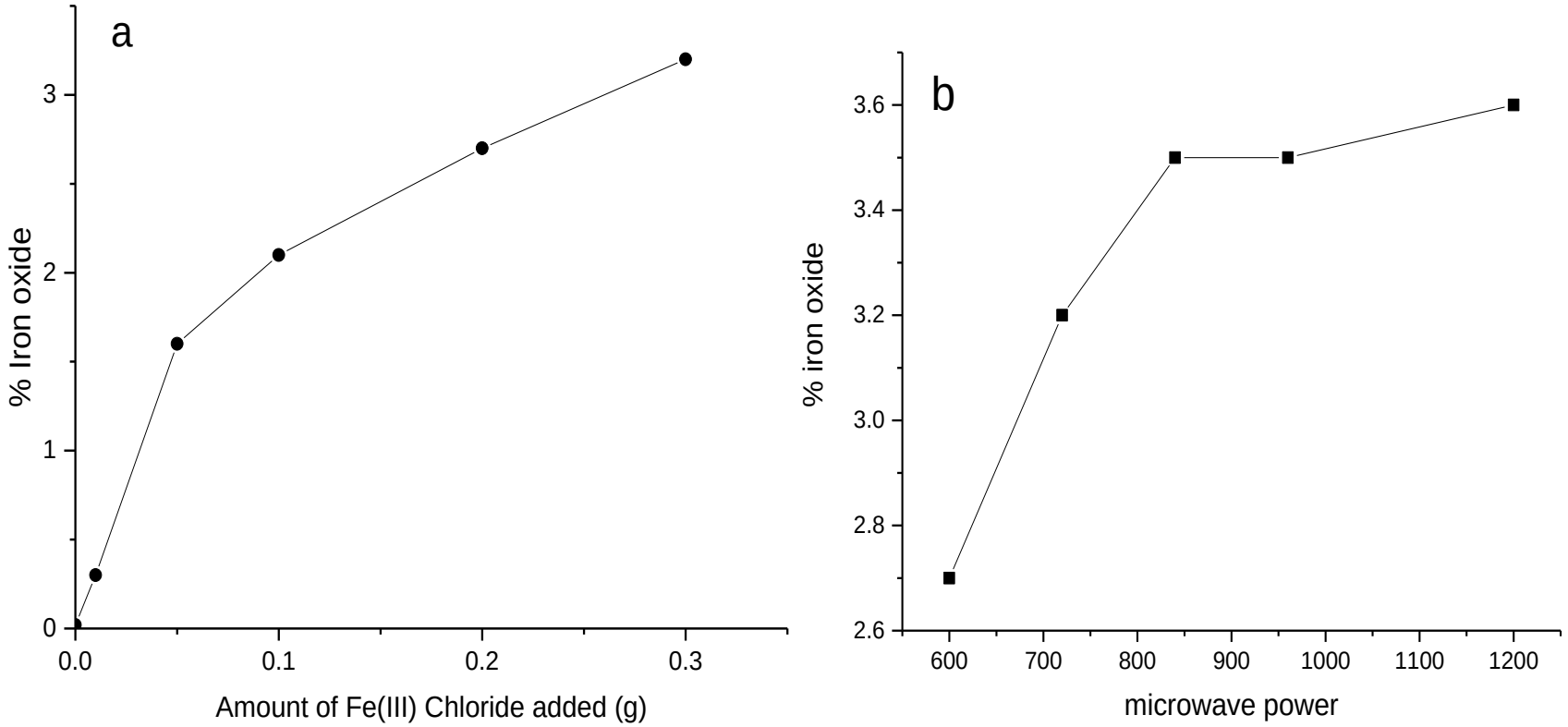

Figure 4. 7. 1: XRF plot of (a) PCP-AC-iron oxide prepared using different amounts of $FeCl_3$ at 600 W and (b) PCPAC-iron oxide prepared at different microwave power using a constant mass of $FeCl_3$ = 0.2

4.8 X-ray photoelectron spectroscopy (XPS) Analysis

XPS was used to examine the chemical composition of the surface of the PCAC-Iron oxide. XPS analysis was performed for the sample with the highest amount of iron precursor. In Figure 4.8.1a full scanned spectrum was measured in the energy range of 0-1400 eV. There are strong peaks located at 296 and 544 due to C1s and O1s binding energies of the composite. The substantial changes in the nature of the carbon due to the changes in the surface chemistry such as oxidation state can be identified through examination of the C1s core region (HUANG et al., 2015). The C1s spectra have been resolved in three individual components peaks as shown in Figure 4. 8. 1b. The spectra indicate the presence of C-C or C-H (hydrocarbons), C-O (Hydroxyl or ether), O-C=O (Carboxylic or esters) at binding energies of 284.81, 286.36, 289.02 eV respectively (SHAFEEYAN et al., 2010, BINIAK et al., 1997). The high-resolution spectrum of O1s is shown in Figure 4. 8. 1c. It showed a peak at 532.72, which is attributed to the C-O-C (ether). The high-resolution spectrum for 2p is shown in figure 4.8.1b. The Fe2p levels with binding energies of 700.60 and 726 are assigned to $Fe2p_{3/2}$ and $Fe2p_{1/2}$ respectively. This is the characteristics of trivalent iron, suggesting that the iron oxide formed on the surface exist as Fe_2O_3 (CHEN and HASHISHO, 2012, MU et al., 2011, ZHANG et al., 2011).

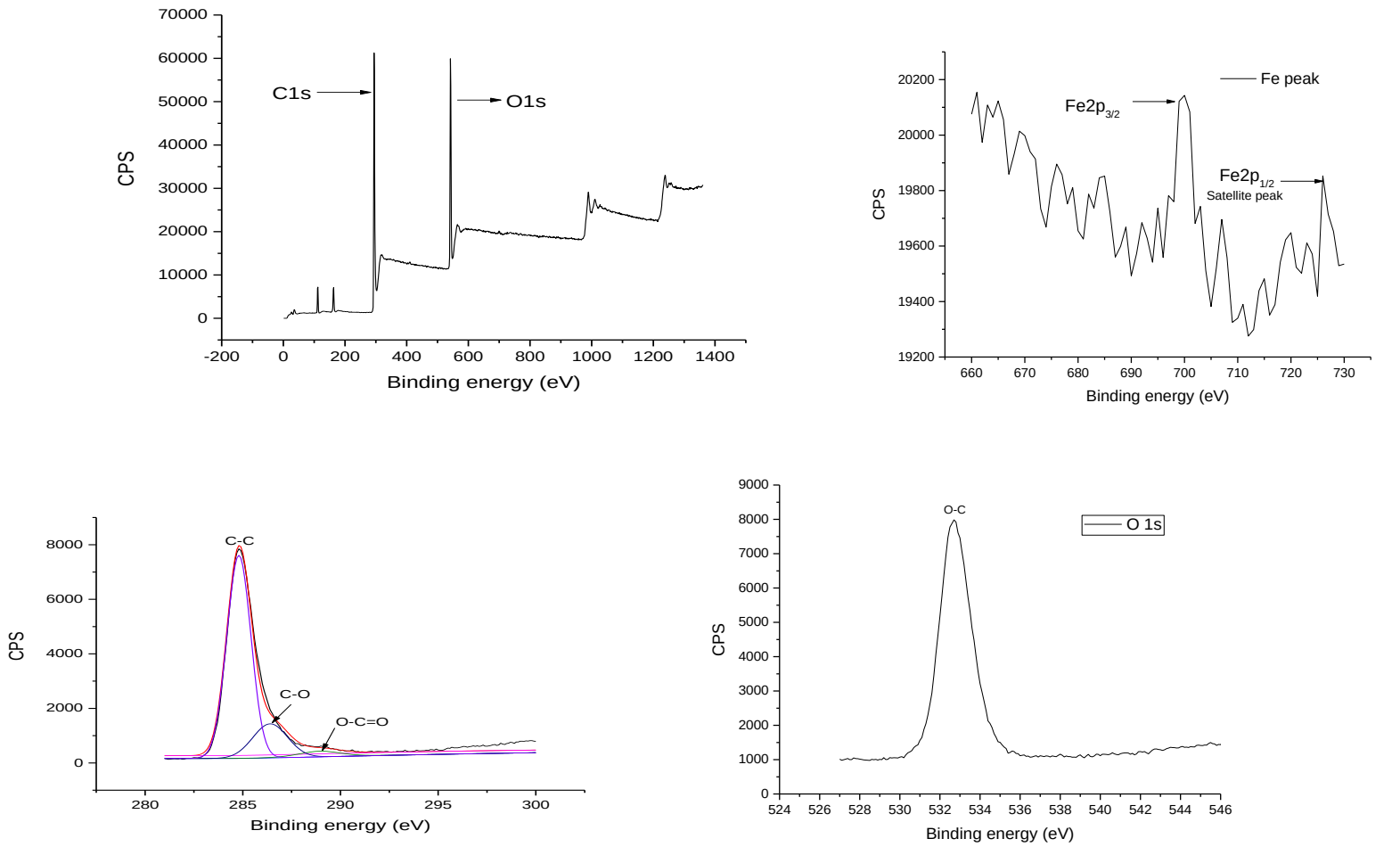

Figure 4. 8. 1: XPS Spectra PCPAC-iron oxide (a) Full spectrum (b) Zoomed iron peak (c) C1s resolved spectra (d) O1s resolved spectrum

4.9 TEM analysis

TEM was performed on the catalyst to observe the morphology and the size of the iron oxide. It showed that the particles of iron oxide on the surface of the support have an irregular shape as shown in figure 4.9.1 The iron oxide particles are well dispersed on the surface of the support material. Figure 4.9.1 shows an average size distribution of a range between 0.5 to 4.5 nm. It can be concluded that the iron oxide formed on the surface of the activated are in a nano size with the average size of 1.72 nm and also they are embedded on the surface of the activated carbon support, resulting in the formation of activated carbon-iron oxide composite

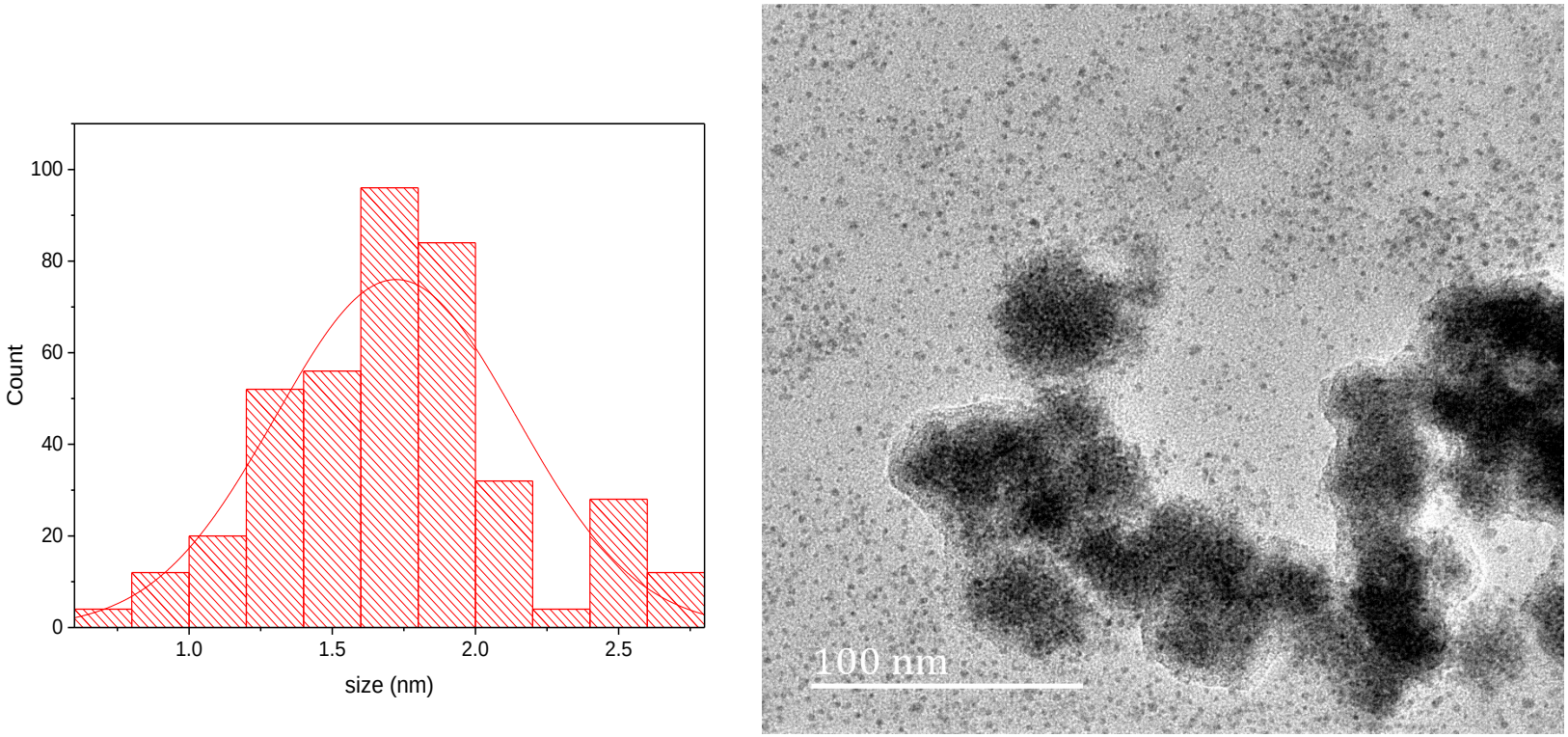

Figure 4. 9. 1:(a) average size distribution and (b) TEM image

4.10 Conclusion

The results showed a successful synthesis on the PCP-AC-Iron oxide catalyst by microwave single step synthesis, as it was shown by FTIR, XRD, EDX, XPS and TEM. This characterization shown that microwave power and the mass of the precursor influence the chemical compositon and surface chemistry. of PCP-AC-Iron oxide The synthesized catalysts were also characterized by iodine and methylene blue number, hence the optimum synthesis conditions were found to be at 600 W microwave treatment using 0.20 g of iron precursor since it was observed to produce the considerable amount of micropores and mesopores. The elemental mapping also showed the high dispersion of iron oxide on the surface of the support.

4.11 References

AHMED, M. J. 2016. Application of agricultural based activated carbons by microwave and conventional activations for basic dye adsorption: Review. *Journal of Environmental Chemical Engineering,* 4**,** 89-99.

AHMED, M. J. & THEYDAN, S. K. 2013. Microwave assisted preparation of microporous activated carbon from Siris seed pods for adsorption of metronidazole antibiotic. *Chemical Engineering Journal,* 214**,** 310-318.

ALMAZÁN-SÁNCHEZ, P. T., CASTAÑEDA-JUÁREZ, M., MARTÍNEZ-MIRANDA, V., SOLACHE-RÍOS, M. J., LUGO-LUGO, V. & LINARES-HERNÁNDEZ, I. 2015. Behavior of TOC and Color in the Presence of Iron-Modified Activated Carbon in Methyl Methacrylate Wastewater in Batch and Column Systems. *Water Air Soil Pollution,* 72**,** 226-238.

BAYKAL, A., UNAL, B., TOPRAK, M. S., DURMUS, Z. & SOZERI, H. 2010. Synthesis, structural and conductivity characterization of alginic acid Fe3O4 nanocomposite. *Journal of Nanoparticles Research,* 12**,** 3039-3048.

BINIAK, S., SZYMANSKI, G., SIEDLEWSKI, J. & SWIATKOWSKI, A. 1997. The characterization of activated carbons with oxygen and nitrogen surface groups. *Carbon,* 35**,** 1799-1810.

BOTA, A., LASZLO, A., NAGY, L., SUBKLEW, G., SCHLIMPER, H. & SCHWUGER, M. J. 1997. Adsorbents from Waste materials. *Adsorption,* 3**,** 81-91.

CASTRO, C. S., GUERREIRO, M. C., GONCALVES, M., OLIVEIRA, L. C. A. & ANASTÁCIO, A. S. 2009a. Activated carbon/iron oxide composites for the removal of atrazine from aqueous medium. *Journal of Hazardous Materials,* 164**,** 609-614.

CASTRO, C. S., GUERREIRO, M. C., OLIVEIRA, L. C. A., GONÇALVES, M., ANASTAÇIO, A. S. & NAZZARRO, M. 2009b. Iron oxide dispersed over activated carbon: Support influence on the oxidation of the model molecule methylene blue. *Applied Catalysis A: General,* 367**,** 53-58.

CHEN, H. & HASHISHO, Z. 2012. preparation of activated carbon from oil sands coke using microwave-assisted activation. *Fuel,* 95**,** 178-182.

CHI, Y., GENG, W., ZHAO, L., YAN, X., YUAN, Q., LI, N. & LI, X. 2012. Comprehensive study of mesoporous carbon functionalized with carboxylate groups and magnetic nanoparticles as a promising adsorbent. *Journal of Colloids and Interface Science,* 369**,** 366-372.

DENGA, H., LI, G., YANGA, H., TANGA, J. & TANGA, J. 2010. Preparation of activated carbons from cotton stalk by microwave assisted KOH and K_2CO_3 activation. *Chemical Engineering Journal,* 163**,** 373-381.

FOO, K. Y. & HAMEED, B. H. 2011. Utilization of rice husks as a feedstock for preparation of activated carbon by microwave induced KOH and K_2CO_3 activation. *Bioresource Technology,* 102**,** 9814-9817.

GONÇALVES, G. R., SCHETTINO JR., M. A., MORIGAKI, M. K., E, N., CUNHA, A. G., EMMERICH, F. G., PASSAMANI, E. C., BAGGIO-SAITOVITCH, E. & FREITAS, J. C. C. 2015. Synthesis of nanostructured iron oxides dispersed in carbon materials and in situ XRD study of the changes caused by thermal treatment. *Journal of Nanoparticle Research,* 17.

HESAS, R. H., DAUD, W. M. A. W., SAHU, J. N. & ARAMI-NIYA, A. 2013a. The effect of a microwave heating on the production of activated carbon from agricultural wastes: A review. . *Journal of Analytical Applied Pyrolysis,* 100**,** 1-11.

HESAS, R. H., DAUD, W. M. A. W., SAHU, J. N. & ARAMI-NIYA, A. 2013b. The effects of a microwave heating method on the production of activated carbon from agricultural waste: A review. *Journal of Analytical and Applied Pyrolysis,* 100**,** 1-11.

HUANG, Y., CUI, C., ZHANG, D., LI, L. & DING, P. 2015. Heterogeneous catalytic ozonation of dibutyl phthalate in aqueous solution in the presence of iron-loaded activated carbon. *Chemosphere,* 119**,** 295-301.

KARTHIKEYAN, S., JUDIA MAGTHALIN, C., MANDAL, A. B. & SEKARAN, G. 2014. Controlled synthesis and characterization of electron rich iron(III) oxide doped nanoporous activated carbon for the catalytic oxidation of aqueous ortho phenylene diamine. *Royal Society of Chemistry Advances,* 4.

KHEZAMI, L., OULD-DRIS, A. & CAPRT, R. 2007. Activated carbon from thermo-compressed wood and other lignocellulosic precursors. *Bioresource Technology,* 2.

KRISHNAN, K. A. & HARIDAS, A. 2008. Removal of phosphate from aqueous solutions and sewage using natural and surface modified coir pith. *Journal of Hazardous Materials,* 152**,** 527-535.

LI, W., ZHANG, L. B., PENG, J. H., LI, N. & ZHU, X. Y. 2008. Preparation of high surface area activated carbons from tobacco stems with K_2CO_3 activation using microwave radiation. *Journal of Industrial Crops and Production,* 27**,** 341-347.

LIMA, S. B., BORGES, S. M. S., RANGEL, M. D. & MARCHETTI, S. G. 2013. Effect of iron content on the catalytic properties of activated carbon-supported magnetite derived from biomass. *Journal of Brazillian Chemical Society,* 24**,** 344-354.

LU, X., JIANG, J., SUN, K., XIE, X. & HU, Y. 2012. Surface modification, characterization and adsorptive properties of a coconut activated carbon. *Applied Surface Sciences,* 258**,** 8147-8252.

MARSH, H. & RODRÍGUEZ –REINOSO, F. 2006. *Activated Carbon,* Amsterdam, Elsevier.

MOHAMMED, J., NASRI, N. S., ZAINI, M. A. A., HAMZA, U. D. & ANI, F. N. 2015. Adsorption of benzene and toluene onto KOH activated coconut shell based carbon treated with NH_3. *International Biodeterioration & Biodegradation,* 102**,** 245-255.

MOLINA-SABIO, M. & RODRIGUEZ-REINOSO, F. 2004. Proceedings of the Third International TRI/Princeton Workshop "Characterization of Porous Materials: from Angstroms to Millimeters. *Colloids and Surfaces A: Physicochemical and Engineering Aspects,* 241**,** 15-25.

MU, J., CHEN, B., GUO, Z., ZHANG, M., ZHANG, Z. & ZHANG, P. 2011. Highly dispersed Fe_3O_4 nanosheets on one-dimensional carbon nanofibers: synthesis, formation mechanism, and electrochemical performance as supercapacitor electrode materials. *Nanoscale,* 3**,** 5034-5040.

MUBARAK, N. M., KUNDU, A., SAHU, J. N. & ABDULLAH, E. C. 2014. Synthesis of palm oil empty fruit magnetic pyrolytic char impregnating with $FeCl_3$ by microwave heating technique. *Biomass and Bioenergy,* 61**,** 265-275.

NASRAZADANI, S. & NAMDURI, H. 2006. Study of phase transformation in iron oxides using Laser Induced Breakdown Spectroscopy. *Spectrochimica Acta Part B: Atomic Spectroscopy,* 61**,** 565-571.

OH, I., KIM, M. & KIM, J. 2015a. Controlling hydrazine reduction to deposit iron oxides on oxidized activated carbon for supercapacitor application. *Energy,* 86**,** 292-299.

OH, I., KIM, M. & KIM, J. 2015b. Deposition of Fe_3O_4 on oxidized activated carbon by hydrazine reducing method for high performance supercapacitor. *Microelectronics Reliability,* 55**,** 114-122.

OLIVEIRA, L. C. A., PEREIRA, E., GUIMARAES, I. R., VALLONE, A., PEREIRA, M., MESQUITA, J. & SAPAG, K. 2009. Preparation of activated carbon from coffee husk utilizing $FeCl_3$ and $ZnCl_2$ as activating agents. *Journal of Hazardous Materials,* 165**,** 87-94.

RAZIA, S. M., HUSSAIN, S. & ZAMIN, G. 2014. Efficiency of Iron Supported on Porous Material (Prepared from Peanut Shell) for Liquid Phase Aerobic Oxidation of Alcohols. *Modern Research in Catalysis,* 3**,** 35-48.

REY, A., ZAZO, J. A., CASAS, J. A., BAHAMONDE, A. & RODRIGUEZ, J. J. 2011. Influence of the structural and surface characteristics of activated carbon on the catalytic decomposition of hydrogen peroxide. *Applied Catalysis A: General,* 402**,** 146-155.

RIBEIRO, R. S., SILVA, A. M. T., FIGUEIREDO, J. L., FARIA, J. L. & GOMES, H. T. 2013. The influence of structure and surface chemistry of carbon materials on the decomposition of hydrogen peroxide. *Carbon,* 62**,** 97-108.

RIBEIRO, R. S., SILVA, A. M. T., FIGUEIREDO, J. L., FARIA, J. L. & GOMES, H. T. 2016. Catalytic wet peroxide oxidation: a route towards the application of hybrid magnetic

carbon nanocomposites for the degradation of organic pollutants. A review. *Applied Catalysis B: Environmental,* 187**,** 428-460.

RODRIGUEZ-REINOSO, F. & MOLINA-SABIO, M. 1994. Activated carbons from lignocellulosic materials by chemical and/or physical activation: an overview. *Carbon,* 30**,** 1111-1118.

RUOFF, R. S., ZHU, X., ZHU, Y., MURALI, S. & STOLLER , M. D. 2011. Nanostructured reduced graphene oxide/Fe_2O_3 composite as a high-performance anode material for lithium ion batteries. *ACS Nano,* 5**,** 3333-3335.

SADIQ, M., AMAN, R., HUSSAIN, S., ZIA, M. A., RAHMAN, N. U. & SAEED, M. 2015. Green and Efficient Oxidation of Octanol by Iron Oxide Nanoparticles Supported on Activated Carbon. *Modern Research on Catalysis,* 4**,** 28-35.

SAHIRA, J., MANDIRA, A., BHADRA PRASAD, P. B. & RAJA RAM, P. R. 2013. Effects of activating agents on the activated carbons prepared from lapsi seed stone. *Research Journal of Chemical Sciences,* 3**,** 19-24.

SALMAN, J. M. 2014. Optimization of preparation conditions for activated carbon from palm oil fronds using response surface methodology on removal of pesticides from aqueous solution. *Arabian Journal of Chemistry,* 7**,** 101-108.

SCHWARTMAN, U. & CORNELL, R. M. Iron oxide in the laboratory: Preparation and Characterisation. *WileyVCH Verlag GmBH, Weinheim, Germany.*

SERP, P. & FIGUEIREDO, J. L. 2009. *Carbon Materials for Catalysis,* Hoboken, New Jersey, John Wiley and Sons, Inc.

SHAFEEYAN, M. S., DAUD, W. M. A. W., HOUSHMAND, A. & SHAMIRI, A. 2010. A review on surface modification of activated carbon for carbon dioxide adsorption. *Journal of Analytical and Applied Pyrolysis,* 89**,** 143-151.

SHRESTHA, R. M., YADAV, A. P., POKHAREL, B. P. & PRADHANANGA, R. R. 2012. Preparation and Characterization of Activated Carbon from Lapsi (Choerospondias axillaris) Seed Stone by Chemical Activation with Phosphoric acid. *Research Journal of Chemical Sciences,* 2**,** 80-86.

TANG, L., YANG, G. D., ZENG, G. M., CAI, Y., LI, S. S., ZHOU, Y. Y., PANG, Y., LIU, Y. Y., ZHANG, Y. & LUNA, B. 2014. Synergistic effect of iron doped ordered mesoporous carbon on adsorption-coupled reduction of hexavalent chromium and the relative mechanism study. *chemical Engineering Journal,* 239**,** 114-122.

TSONCHEVA, T., VELINOV, N., IVANOVA, R., STOYCHEVA, I., TSYNTSARSKI, B., SPASSOVA, I., PANEVA, D., ISSA, G., KOVACHEVA, D., GENOVA, I., MITOV, I. & PETROV, N. 2015. Formation of catalytic active sites in iron modified activated carbons from agriculture residues. *Microporous and Mesoporous Materials,* 217**,** 87-95.

WANG, Z., SHI, M., LI, J. & ZHENG, Z. 2014. Influence of moderate pre-oxidation treatment on the physical, chemical and phosphate adsorption properties of iron-containing activated carbon. *Journal of Environmental Science,* 26**,** 519-528.

WARTELLE, L. H., MARSHALL, W. E., TOLES, C. A. & JOHNS, M. M. 2000. Comparison of nutshell granular activated carbons to commercial adsorbents for the purge-and-trap gas chromatographic analysis of volatile organic compounds. *Journal of Chromatography A,* 879**,** 169-175.

ZHANG, L., MI, M., LI, B. & DONG, Y. 2013. Modification of Activated Carbon by Means of Microwave Heating and its Effects on the Pore Texture and Surface Chemistry. *Research Journal of Applied Sciences Engineering and Technology,* 5**,** 1836-1840.

ZHANG, W., LIANG, F., LI, C., QIU, L., YUAN, L., PENG, F., JIANG, X., XIE, A., SHEN, Y. & ZHU, J. 2011. Microwave-enhanced synthesis of magnetic porous covalent triazine-based framework composites for fast separation of organic dye from aqueous solution. *Journal of Hazardous Materials,* 186**,** 984-990.

ZHANG, X. & CHEN, W. 2015. Mechanisms of pore formation on multi-wall carbon nanotubes by KOH activation. *Microporous and Mesoporous Materials,* 206**,** 194-201.

CHAPTER 5: EFFECT OF EXPERIMENTAL CONDITIONS ON METHYLENE BLUE AND 2-NITROPHENOL DEGRADATION

The chapter presents and discusses the effect of experimental conditions for methylene blue and 2-nitrophenol of the Fenton-like degradation. It reports the following details: effect of H_2O_2, the effect of pH, catalyst dose, stirring speed, the effect of initial concentration of the pollutant, and effect of temperature Fenton-like degradation of methyelene blue and 2-nitrophenol.

5.1 Effect of H_2O_2 volume added

The effect of increasing H_2O_2 volume added to PCP-AC-iron oxide on the degradation of MB and 2-NP when 10, 20, 30 and 40 ml of 30 % H_2O_2 was added to the reaction while holding catalyst mass at 0.2 g, pH of the MB and 2-NP solution at 3, initial concentration of MB and 2-NP at 100 mg/dm^3, stirring speed at 500 rpm and temperature at 26 °C are shown in Fig. 5.1. As shown in Fig. 5.1, the degradation of MB and 2-NP were observed to increase from 64.4 to 68.1 % for MB and from 59.86 to 61.66 % for 2-NP respectively when the volume of H_2O_2 was increased from 10 to 20 ml. These increases corresponds to an increase in degradation rates from 0.0098 to 0.0109 min^{-1} for MB and from 0.0059 to 0.0072 min^{-1} for 2-NP. The decomposition of H_2O_2 by iron is a crucial step in Fenton's degradation process since it generates the active species required for the degradation of the targeted pollutant (WU et al., 2016). Therefore, an increase in H_2O_2 volume leads to increased amount of hydroxyl radicals formation which also increases the degradation efficiency and degradation rate (KUANG et al., 2013). As the volume of H_2O_2 was increased above 20 ml, the degradation was observed to reduce from 68.1 to 57.4 % when 40 ml of H_2O_2 was added in the case of MB and from 61.66 to 55.28 % for 2-NP. Degradation rates were also observed to

decrease from 0.0109 to 0.0081 min^{-1} for MB and from 0.0072 to 0.0051 min^{-1} for 2-NP when the H_2O_2 volume was increased from 20 to 40 ml.

The catalyst performance was also tested using the R_{45} (mol mol^{-1}) values (RUSEVOVA et al., 2012) which are defined as the amount of H_2O_2 $(n_{H_2O_2})$ consumed per mol of MB (n_{MB}) or 2-NP (n_{2-NP}) degraded in the reaction period between $t = 0$ and $t_{0.45,\text{ MB or 2-NP}}$, meaning the time at which 45 % of the MB or 2-NP was degraded as shown in Eq.(5.1) and (5.2).

$$R_{45} = \left(\frac{n_{H_2O_2}}{n_{MB}} \right)_{t=0.45,MB} \tag{5.1}$$

$$R_{45} = \left(\frac{n_{H_2O_2}}{n_{2-NP}} \right)_{t=0..45,2-NP} \tag{5.2}$$

Stoichiometrically, it will require 36 moles of H_2O_2 to completely decompose 1 mole of MB, while 13.5 moles of H_2O_2 is required to completely neutralize 1 mole of 2-NP. After 45 min of degradation, 59.4, 64.1, 53.9 and 50.4 mg/dm^3 of MB was removed from the reactions when 10, 20, 30 and 40 ml of H_2O_2 were added. This represents the removal of 0.019, 0.02, 0.017 and 0.016 mmol of MB brought about by reacting with 0.669, 0.721, 0.607and 0.567 mmol of H_2O_2. The calculated values of R_{45} (consumption of H_2O_2 per mol of pollutant) were therefore 35.21, 36.05, 35.71, 35.44 mol/mol^{-1} respectively. For 2-NP after 45 min of degradation, 40.44, 41.79, 38.79 and 36.90 mg/dm^3 of 2-NP was removed when 10, 20, 30 and 40 ml of H_2O_2 were added. This represents the removal of 0.043, 0.044, 0.0412 and 0.039 mmol of 2-NP brought about by reacting with 0.580, 0.599, 0.556 and 0.521 mmol of H_2O_2. The corresponding R_{45} values were 13.49, 13.61, 13.56 and 13.36 mol/mol^{-1} respectively. These results indicate that the rate of consumption of H_2O_2 per mole of MB was much higher than for 2-NP and both the reaction rates and % removal

of pollutant was higher for MB than for 2-NP. Yang and Tian (2012) studying the catalysis of MB and 2-NP using Fe-doped sulphated titania (YANG and TIAN, 2012)and Olejnik et al. (2016) degrading MB and 2-NP using Ti/SBA-15 also reported faster kinetics and better degradation for MB as compared with 2-NP (OLEJNIK et al., 2016). This can be attributed to the decolourization of leuco methylene blue, which can be easily converted to MB.

As the volume of H_2O_2 was increased from 10 to 20 ml, the rate of pollutant removal increased and the H_2O_2 consumption per mole of pollutant also increased indicating that an increase in H_2O_2 volume led to an increased formation of hydroxyl radical $\left(\cdot OH\cdot\right)$ as described below (LIAO et al., 2009):

$$Fe^{2+} + H_2O_2 \rightarrow Fe^{3+} + HO^- + HO\cdot \quad (5.3)$$

When the volume of H_2O_2 was increased above 20 ml, the reaction rate constant, degradation and consumption of H_2O_2 per mole of pollutant were observed to reduce. The lower degradation and consumption of H_2O_2 per mole of a pollutant can be attributed to hydroxyl radical scavenging effect (ORTIZ DE LA PLATA et al., 2010) and that the decomposition of H_2O_2 may involve two mechanisms occurring simultaneously (RUSEVOVA et al., 2012). The first mechanism is already explained with Eqn.(5.1) while the second mechanisms involve the reaction of H_2O_2 with the catalyst surface to produce species with low reactivity as shown in Eqns.(5.4-5.6):

$$Fe^{3+} + H_2O_2 \rightarrow Fe^{3+} + O_2^{\cdot -} / HO_2^{\cdot -} + H^+ \quad (5.4)$$

$$Fe^{3+} + H_2O_2 \rightarrow Fe(OOH)^{2+} + H^+ \quad (5.5)$$

$$Fe(OOH)^{2+} \rightarrow Fe^{2+} + HO_2^{\cdot} \quad (5.6)$$

The strong competition of $HO\cdot$ by other species like H_2O_2, Fe^{2+} and Fe^{3+} may also lead to insufficient utilization of H_2O_2 for decomposition of the pollutant as shown in Eqns.(5.3—5.9):

$$Fe^{2+} + {}^{\cdot}OH \rightarrow Fe^{3+} + HO^{-} \quad (5.7)$$

$$Fe^{3+} + 2{}^{\cdot}OH \rightarrow Fe^{2+} + O_2^{\cdot -} / HO_2^{\cdot -} + H^{+} \quad (5.8)$$

$$H_2O_2 + {}^{\cdot}OH \rightarrow O_2^{\cdot -} / HO_2^{\cdot -} + H_2O \quad (5.9)$$

Therefore, the optimum volume of H_2O_2 chosen for the degradation was 20 ml for both MB and 2-NP.

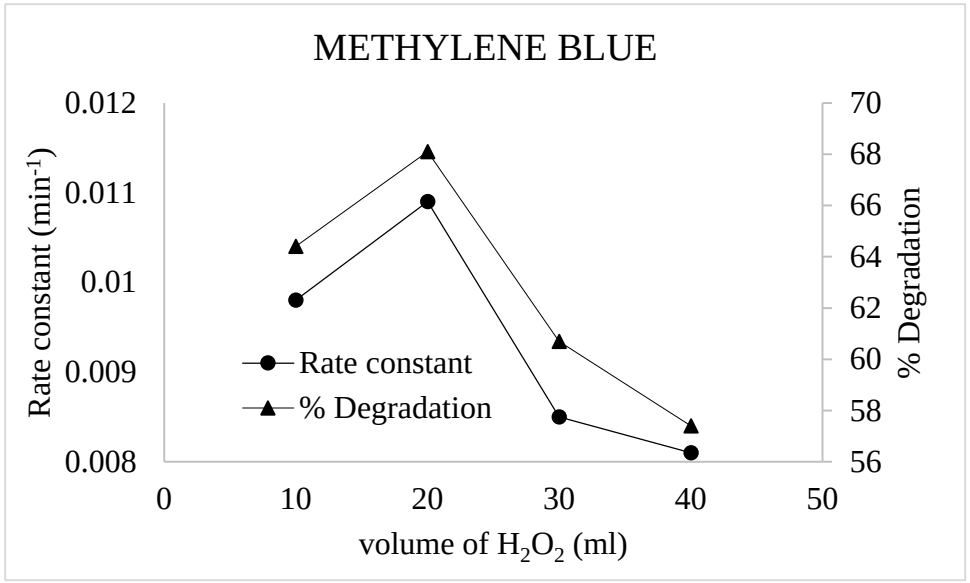

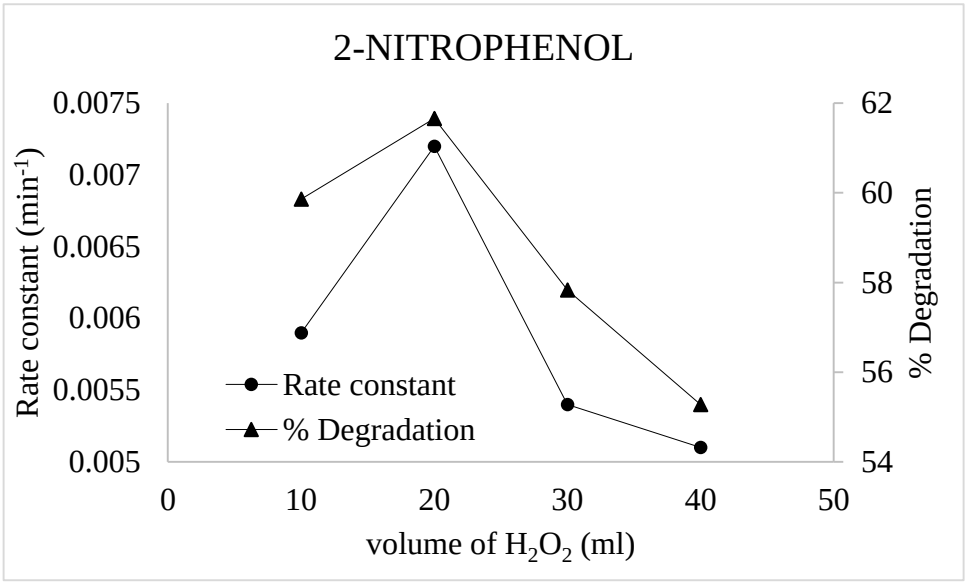

Figure 5. 1: The effect of hydrogen peroxide on the degradation efficiency and rate constant of (a) methylene blue and (b) 2-nitrophenol

5.2 Effect of initial solution pH

In these experiments, the initial solution pH of the MB and 2-NP solutions before the addition of catalyst (PAP-AC-iron oxide) was varied between 3, 7 and 9 to determine the effect of initial solution pH the Fenton-like degradation. The initial solution pH is known to affect the activity of the oxidant and the stability of H_2O_2 in Fenton-like catalysis (SHI et al., 2011). The results indicated that on the addition of the catalyst to MB and 2-NP solutions, the initial solution pH was observed to fall. The degradation and rate constant for the degradation of MB were found to increase from 68.95 to 74.1 % and from 0.0107 to 0.0118 min^{-1} when the MB solution pH was increased from 3 to 7. For 2-NP, the degradation and rate constant increased from 64.09 to 69.08 % and 0.0070 to 0.0084 min^{-1} when initial pH was increased from 3 to 7. As initial solution pH values were increased to 9 for both pollutants, the degradation reduced from 74.1 to 64.85 % for MB and from 69.08 to 60.54 % for 2-NP. The corresponding rate constant were also observed to reduce from 0.0118 to 0.0100 min^{-1} for MB and from 0.0084 to 0.0065 min^{-1} for 2-NP. The decomposition of H_2O_2 brought about by its reaction with iron strongly depends on solution pH. For example, at lower solution pH the formation of $Fe(II)(H_2O)^{2+}$ occurs in solution which reacts more slowly with H_2O_2 and therefore reducing the production of $HO^{\cdot}$ leading to reduced degradation (SHEMER et al., 2006). At higher initial solution pH, conversion of iron oxide to oxyhydroxides occurs which limits the reaction between Fe^{2+} and H_2O_2 leading to the low formation of $HO^{\cdot}$ and therefore reduce % degradation (WU et al., 2016). It is also known that the oxidation potential of $HO^{\cdot}$ reduces with increase in solution pH (PARRA et al., 2001). These reasons will account for the higher performance of the catalyst at solution pH 7 and it's poor performances at lower and higher pHs.

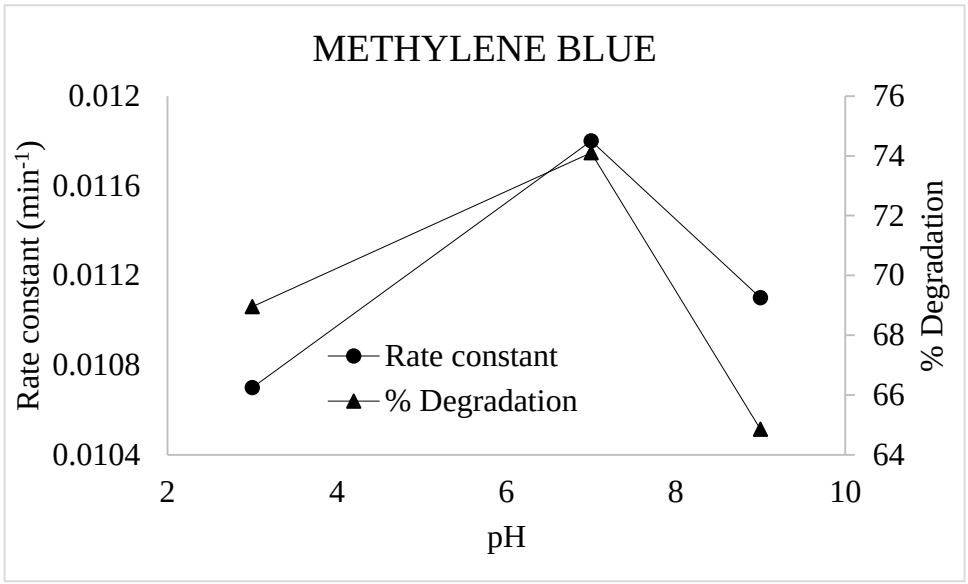

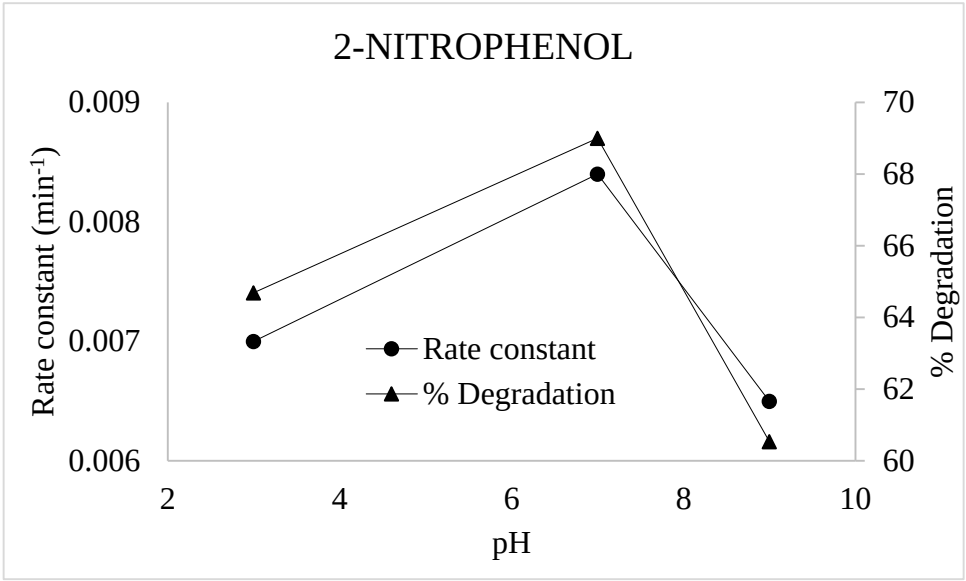

Figure 5. 2: The effect of initial pH on the degradation efficiency and rate constant of (a) methylene blue and (b) 2-nitrophenol

5.3 Effect of Catalyst dose

The influence of catalyst dose on Fenton-like degradation of MB and 2-NP in aqueous solution was studied using catalyst mass of 0.1, 0.2 and 0.3 g, 20 ml of 30 % H_2O_2, at pollutant solution pH of 7, initial concentration of MB and 2-NP at 100 mg/dm^3, stirring speed of 500 rpm and temperature of 26 °C. As observed from Fig. 5.3, the degradation and rate constant were found to increase from 56.1 % and 0.0083 min^{-1} to 74.1 % and 0.0118 min^{-1} for MB and from 64.2 % and 0.0073 min^{-1} to 69.66 % and 0.0082 min^{-1} as the catalyst mass was increased from 0.1 to 0.2 g. The increase in catalyst loading introduces additional sites for increased production of free radical species which eventually increases degradation and reaction rate (BABUPONNUSAMI and MUTHUKUMAR, 2012). When catalyst dose was increased from 0.2 to 0.3 g, the degradation and rate constant for both MB and 2-NP degradation were observed to reduce from 74.1 % and 0.0118 min^{-1} to 47.8 % and 0.0079 min^{-1} for MB and from 69.06 % and 0.0082 min^{-1} to 60.44 % and 0.0069 min^{-1}. A decrease in degradation and rate constant may be attributed to two reasons; (i) agglomeration of solid particles together at higher dose leading to reduction of effective surface (GARRIDO-RAMIREZ et al., 2010) and the increased scavenging of $HO^{\cdot}$ radicals at the surface of the catalyst (CARRIAZO et al., 2005).

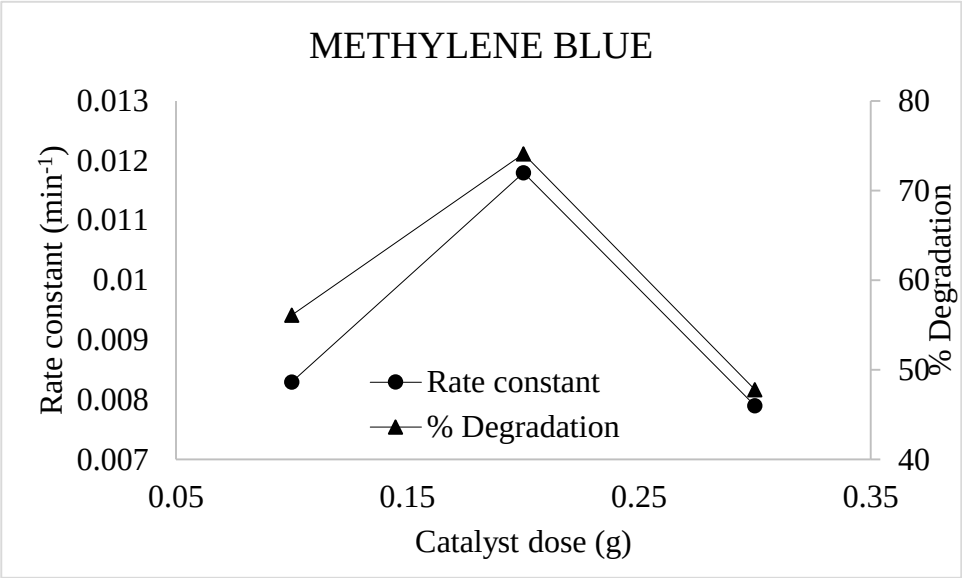

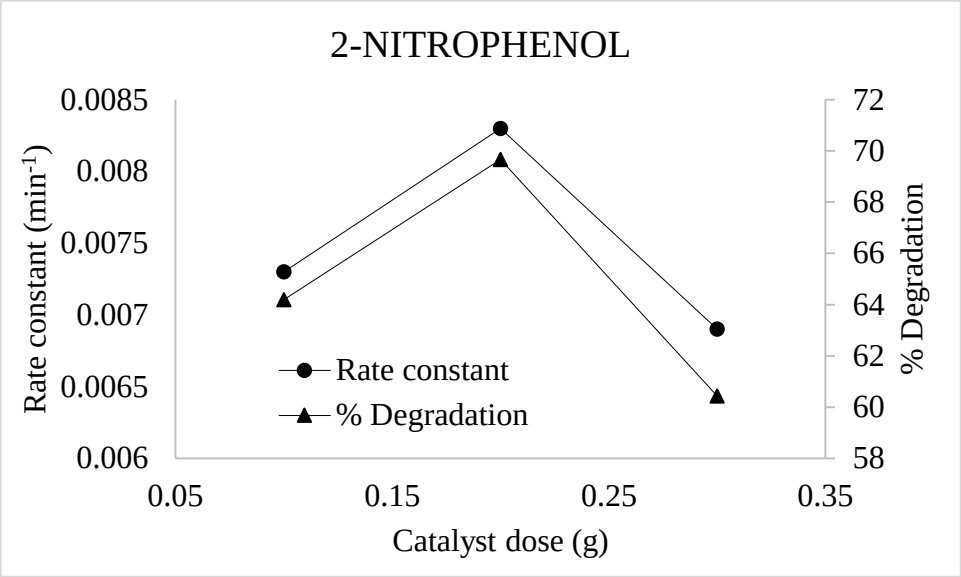

Figure 5. 3: Effect of catalyst dose on the degradation efficiency and rate constants of (a) methylene blue and (b) 2-nitrophenol

5.4 Effect of stirring speed

The influence of stirring speed on Fenton-like degradation of MB and 2-NP in aqueous solution was studied using stirring speeds of 300, 500, 750 and 800 rpm, catalyst mass of 0.2g, 20 ml of 30 % H_2O_2, at pollutant solution pH of 7, initial concentration of MB and 2-NP at 100 mg/dm^3 and temperature of 26 °C. The results revealed that as the stirring speed increased from 300 to 500 rpm the pseudo first rate constant was observed to increase from 0.0099 to 0.0118 min^{-1} for MB and from 0.0064 to 0.0082 min^{-1} for 2-NP while the degradation increased from 66.1 to 74.1 % for MB and from 63.86 to 69.06 % for 2-NP. These increases may be attributed to the fact that the mixture became more homogeneous with an increase in stirring speed and at higher stirring increase the rate of contact between the components of the mixture (CUIPING et al., 2012). These increases in degradation rate for MB and 2-NP with increase stirring speed from 300 to 500 rpm may also indicate that the process was mass transfer limited (SAEED et al., 2015). As the stirring speed was increased from 500 to 750 and 800 rpm, the degradation rates were observed to slightly decreases for MB and 2-NP respectively. Therefore, the resistance due to pollutant mass transfer from solution to the particle surface is believed to have been overcome by stirring at 500 rpm for both pollutants (SAEED and ILYAS, 2013)**.**

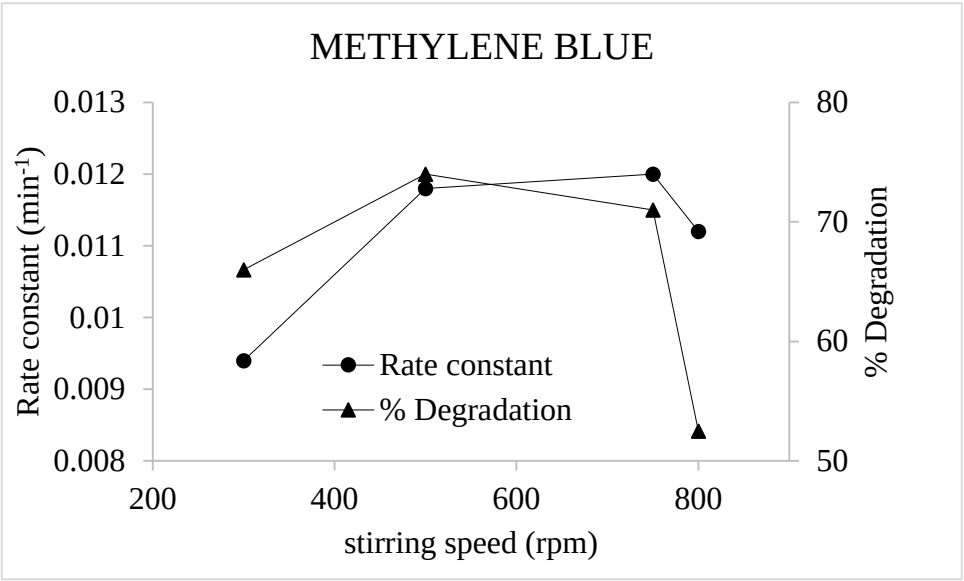

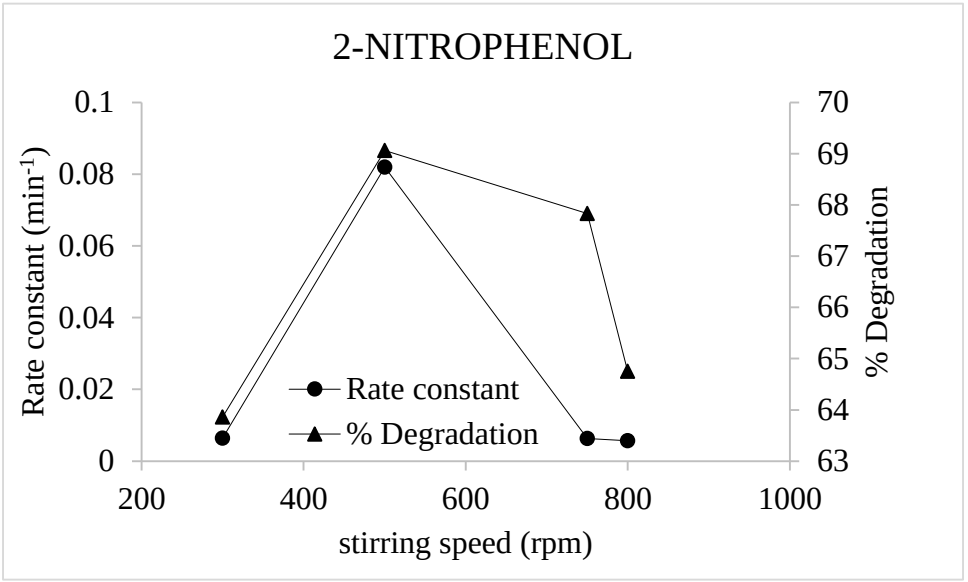

Figure 5. 4: The effect of stirring speed on the degradation efficiency and rate constants of (a) methylene blue and (b) 2-nitrophenol

5.5 Effect of pollutant concentration

The effect of initial pollutant concentration on Fenton-like degradation of MB and 2-NP in aqueous solution was studied varying MB and 2-NP concentrations from 100, 150, 200 and 250 mg/dm^3, catalyst mass of 0.2g, 20 ml of 30 % H_2O_2, at pollutant solution pH of 7, stirring speed of 500 rpm and temperature of 26 °C. The results revealed that as initial MB and 2-NP concentrations were increased from 100 to 250 mg/dm^3, the rate of degradation of MB reduced from 0.0118 to 0.0051 min^{-1} while that of 2-NP reduced from 0.0084 to 0.0042 min^{-1}. These changes in degradation rates corresponds to reduction in degradation from 74.1 % to 60.73, 37.95 and 27.64 % for MB and from 69.06 % to 63.77, 48.74 and 40.75 % for 2-NP as initial pollutant concentration was increased from 100 mg/dm^3 to 150, 200 and 250 mg/dm^3. The decrease in degradation rate with increase in initial MB and 2-NP concentration may be due to site saturation or the blocking of the surface site by MB or 2-NP molecules leading to slower degradation (ZHAO et al., 2012)**.** On the other hand, since the H_2O_2 amounts and the surface active sites remained constant, there will be increased competition of MB or 2-NP molecules for the fixed amounts of hydroxyl radicals produced. Therefore, as initial MB or 2-NP initial concentrations was increased strong competition of pollutant molecule and self-inhibition occurs leading to lower percentage removal with increased initial concentration (CUIPING et al., 2012, MONTEGUDO et al., 2008).

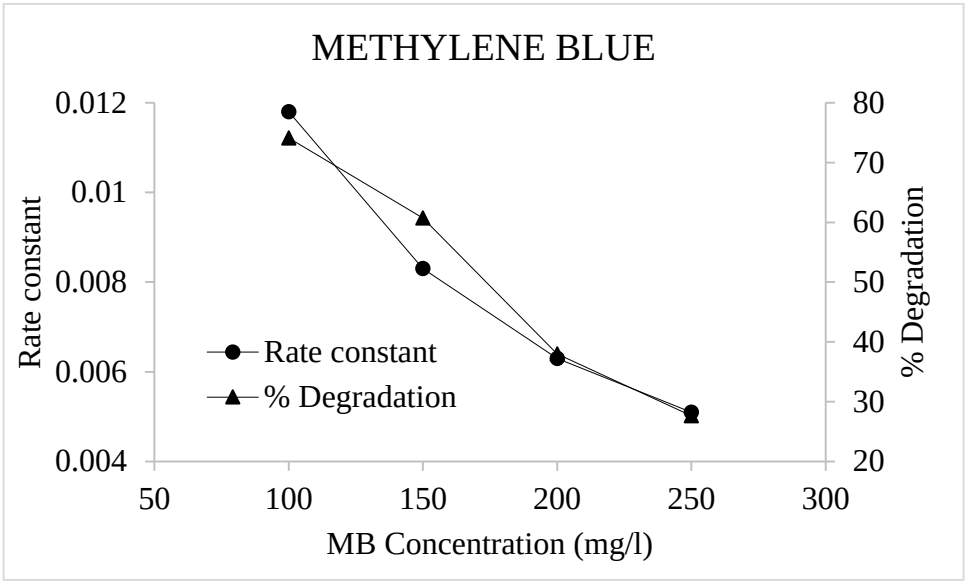

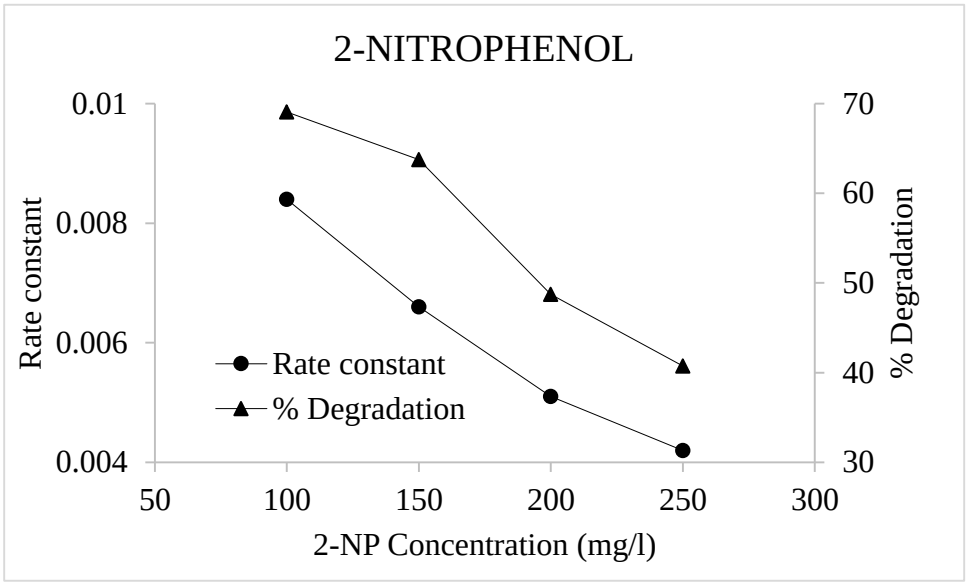

Figure 5. 5: The effect of initial concentration of the pollutants on the degradation efficiency and rate constants of (a) methylene blue and (b) 2-nitrophenol

5.6 Effect of Temperature

The effect of temperature on Fenton-like degradation of MB and 2-NP in aqueous solution was studied varying MB and 2-NP concentrations of 100 mg/dm^3, catalyst mass of 0.2g, 20 ml of 30 % H_2O_2, at pollutant solution pH of 7, stirring speed of 500 rpm and at a temperature of 26 - 56 °C. The results in figure 5.6 revealed the rate of degradation is strongly dependent on temperature and that the degradation rates increased from 0.0118 to 0.0387 min^{-1} for MB and 0.0082 to 0.0245 min^{-1} for 2-NP as temperature was increased from 26 to 56 ^oC respectively. The increase in the rate constant with temperature can be attributed to increase in the interaction between hydrogen peroxide and catalyst in solution which in turn increases the collision frequency of the molecules on the catalyst surface(GARRIDO-RAMIREZ et al., 2010, NAZAMAZADEH-EJHIEH and HUSHMANDRED, 2010).

The effect of temperature was further investigated using the Arrhenius equation to determine the activation energies for the MB and 2-NP degradation. The Arrhenius equation describes the relationship between the rate constant and the temperature applied:

$$\ln k = \ln A - \frac{E_a}{RT} \tag{5.10}$$

where k, is the degradation rate, A is the frequency factor, E_a is the activation energy, R is the ideal gas constant (8.324 J/mol K) and T is the Kelvin temperature. The rate limiting step of a heterogeneous reaction can be a chemical reaction at the surface or diffusion of the reactant (LIEN and ZHANG, 2007) and this is determined by the relationship between the reaction temperature and the rate constant. Surface controlled reactions in solutions have activation energies that are greater than 29 kJ/mol while diffusion controlled reactions have lower activation energies between 8 to 21 kJ/mol (CHEN and ZHU, 2007). A good relationship was observed between ln k and 1/T for MB (r^2 = 0.9981) and 2-NP (r^2 = 0.9888). The calculated values of E_a for MB and 2-NP were

32.03 and 30.48 kJ/mol respectively. Activation energies in these range indicate that the degradation reaction is a surface-controlled reaction (WU et al., 2016). The results also show that the activation energy for MB degradation was higher than that for 2-NP. Activation energies for most thermal reaction processes are generally in the range of 60 to 250 kJ/mol (CHEN and ZHU, 2007, SUN et al., 2012), these results, therefore, imply that the decompositions of MB and 2-NP in solution by PCP-AC-iron oxide lowers the activation energies making the decompositions possible.

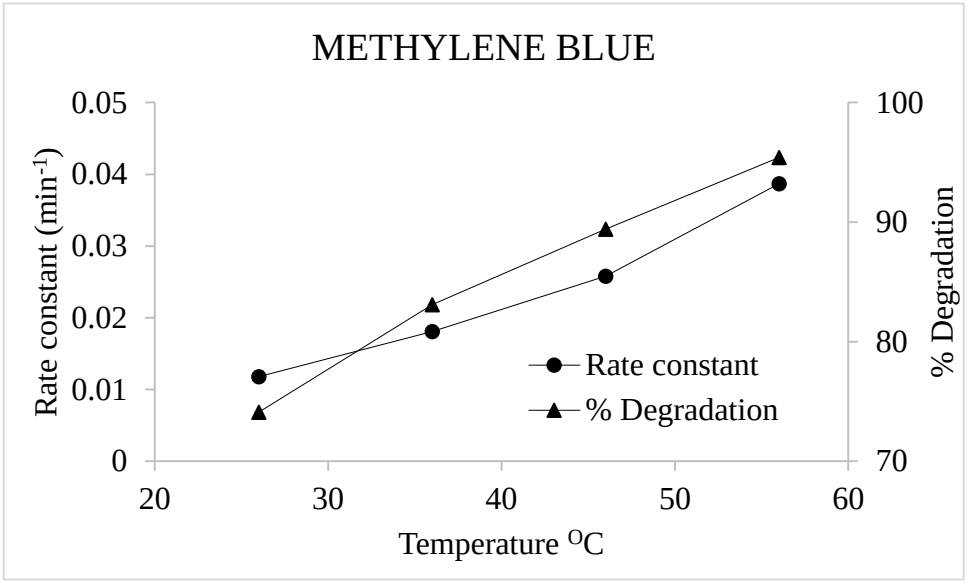

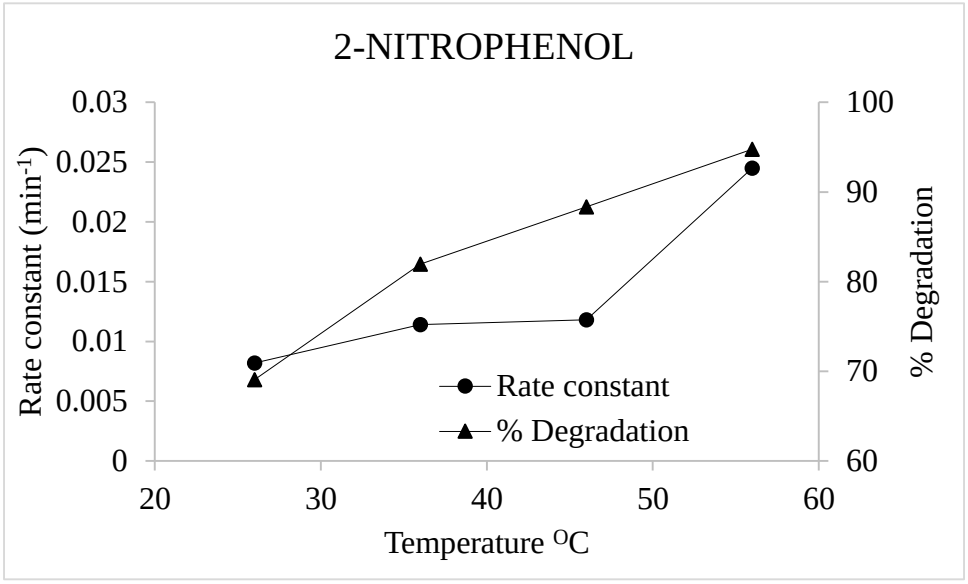

Figure 5. 6: The effect of temperature on the degradation efficiency and rate constants of (a) methylene blue and (b) 2-nitrophenol

5.7 Comparison of PCP-AC-Iron oxide and PCP-AC as radicals initiator

A set of experiment was also done to discriminate the effect of adsorption, degradation by hydrogen peroxide alone, or degradation by PCP-AC with hydrogen peroxide since it was reported that hydrogen peroxide can also act as radicals initiator as compared to the degradation by PCP-AC-Iron oxide composite with hydrogen peroxide. In table 5.7 it was observed that the degradation rate constant when using the PCP-AC-iron oxide was higher as compared to adsorption, degradation by hydrogen peroxide and PCP-AC with hydrogen peroxide. Hence it can be said the more removal of MB and 2-NP was through heterogeneous Fenton oxidation process, were adsorption and degradation with hydrogen peroxide only shown to be negligible. Also to confirm that activated carbon can act as a radical initiator, hydroxyl scavenger was added at the begining of adsorption, degradation by hydrogen peroxide only, PCP-AC with hydrogen peroxide, and degradation by PCP-AC-Iron oxide composite with hydrogen peroxide. The PCP-AC-Iron oxide with hydrogen peroxide had a higher reduction in degradation rate constant when radicals scarvenger was added, followed by the degradation of 2-NP and MB by PCP-AC with hydrogen peroxide and adsorption showed no difference, suggesting that more of hydroxyl radical are produced when using the PCP-AC-Iron oxide composite. Hence this shows that indeed activated carbon can act as a radical scavenger. Also the degradation of both 2-NP and MB were hydroxyl radical driven. The high degradation rate constant of MB and 2-NP can be attributed to the synergistic effect of adsorption and both activated carbon and iron oxide as radical initiators.

Table 5.7: Comparison of PCP-AC-Iron oxide and PCP-AC as radicals initiator

Methylene Blue					2-Nitrophenol				
Adsorption in the dark					Adsorption in the dark				
1st order	r^2	2nd order	r^2		1st order	r^2	2nd order	r^2	
0.0054	0.9992	0.00004	0.9989	Without Scavenger	0.0020	0.9993	0.00002	0.9990	Without Scavenger
0.0056	0.9994	0.00004	0.9993	With Scavenger	0.0019	0.9938	0.00001	0.9930	With Scavenger
H_2O_2 Alone					H_2O_2 Alone				
1st order	r^2	2nd order	r^2		1st order	r^2	2nd order	r^2	
0.0008	0.9993	0.000006	0.9991	Without Scavenger	0.0003	0.9997	0.000002	0.9995	Without Scavenger
0.0002	0.9991	0.000003	0.9989	With Scavenger	0.00005	0.9993	0.000001	0.9990	With Scavenger
PCP-AC + H_2O_2					PCP-AC + H_2O_2				
1st order	r^2	2nd order	r^2		1st order	r^2	2nd order	r^2	
0.0063	0.9997	0.00006	0.9978	Without Scavenger	0.0029	0.9994	0.00003	0.9998	Without Scavenger
0.0027	0.9996	0.00002	0.9989	With Scavenger	0.0006	0.9998	0.000004	0.9995	With Scavenger
PCP-AC-iron oxide + H_2O_2					PCP-AC-iron oxide + H_2O_2				
1st order	r^2	2nd order	r^2		1st order	r^2	2nd order	r^2	
0.0083	0.9985	0.0001	0.9970	Without Scavenger	0.0051	0.9988	0.00006	0.9975	Without Scavenger
0.0043	0.9998	0.00003	0.9988	With Scavenger	0.0015	0.9998	0.000009	0.9980	With Scavenger

5.8 Conclusions

The experimental parameters were successfully optimized. The parameters value that gave the highest degradation efficiency were, 20 ml of hydrogen peroxide at pH 7, a catalyst dose of 0.2 g, stirring speed of 500 rpm, initial concentration of 100 mg/l and temperature of 26 ^{o}C. The lowest temperature was chosen as the operating temperature to energy conservation. The results also showed that the activation energy for MB degradation was higher than that for 2-NP. MB and 2-NP showed to be highly degraded at these operating conditions. Both MB and 2-NP showed the same trend.

5.9 References

BABUPONNUSAMI, A. & MUTHUKUMAR, K. 2012. Removal of phenol by heterogeneous photo electron Fenton-like process using nano-zero valent iron. *Separation and Purification Technology*, 98**,** 130-135.

CARRIAZO, J., GUÉLOU, E., BARRAULT, J., TATIBOUÉT, J. M., MOLINA, R. & MORENO, S. 2005. Synthesis of pillared clays containing AL, Al-Fe, or Al-Ce-Fe from bentonite: Characterization and catalytic activity. *Catalysis Today,* 126**,** 107-108.

CHEN, J. & ZHU, L. 2007. Heterogeneous UV-Fenton catalytic degradation of dyestuff in water with hydroxyl-Fe pillared bentonite. *Catalysis Today,* 126**,** 463-470.

CUIPING, B., WENQI, G., DEXIN, F., MO, X., QI, Z., SHAOHUA, C., ZHONGXUE, G. & YANSHUI, Z. 2012. Natural graphite tailings as heterogeneous Fenton catalyst for the decolorization of rhodamine B. *Chemical Engineering Journal,* 197**,** 306-313.

GARRIDO-RAMIREZ, E., THENG, B. & MORA, M. 2010. Clays and oxides minerals as catalysts and nanocatalysts in the Fenton-like reactions- a review. *Applied Clay Science,* 47**,** 182-192.

KUANG, Y., WANG, Q., CHEN, Z., MEGHARAJ, M. & NAIDU, R. 2013. Heterogeneous Fenton-like oxidation of monochlorobenzene using green synthesis of iron nanoparticles. *Journal of Colloid and Interface Science,* 410**,** 67-73.

LIAO, Q., SUN, J., H & GAO, L. 2009. Degradation of phenol by heterogeneous Fenton reaction using multi-walled carbon nanotube supported Fe_2O_3 catalysts. *Colloids and Surfaces A: Physicochemical and Engineering Aspects,* 345**,** 95-100.

LIEN, H. L. & ZHANG, W. X. 2007. Nanoscale Pd/Fe bimetallic particles : Catalytic effects of palladium in hydrodechlorination *Applied Catalysis B: Environment,* 177**,** 110-116.

MONTEGUDO, J. M., DURAN, A. & LOPEZ-ALMODOVAR, C. 2008. Homogeneous ferrioxalate-assisted solar photo-Fenton degradation of orange II in aqueous solutions. *Applied Catalysis B: Environment,* 83**,** 46-55.

NAZAMAZADEH-EJHIEH, A. & HUSHMANDRED, S. 2010. Solar photodecolorization of methylene blue by CuO/X zeolite as a heterogeneous catalyst. *Applied Catalysis A: General,* 388**,** 149-159.

OLEJNIK, T., PASIECZNA-PATKOWSKA, S., LESIUK, A. & RYCZKOWSKI, J. 2016. Phenol and methylene blue photodegradation over Ti/SBA-15 materials under UV light. *Polish Journal of Chemical Technology,* 18**,** 30-38.

ORTIZ DE LA PLATA, G. B., ALFANO, O. M. & CASSANO, A. E. 2010. Decomposition of 2-chlorophenol employing goethite as Fenton catalyst: Proposal of a feasible, combined reaction scheme of heterogeneous and homogeneous reactions. *Applied Catalysis B: Environment,* 95**,** 1-13.

PARRA, S., MALATO, S., BLANCO, J., PERINGER, P. & PULGARIN, C. 2001. Concentrating versus non-concentrating reactors for solar photocatalytic degradation of p-nitrotoluene-o-sulfonic acid. *Water Science and Technology,* 44**,** 219.

RUSEVOVA, K., KOPINKE, F. & GEORGI, A. 2012. Nano-sized magnetic iron oxides as catalysts for heterogeneous Fenton-like reactions - Influence of Fe(II)/Fe(III) ratio on catalytic performance. *Journal of Hazardous Materials,* 241**,** 433-440.

SAEED, M., ADEEL, S., ILYAS, M., SHAHZAD, M. A., USMAN, M., HAQ, E. & HAMAYUN, M. 2015. Oxidative degradation of methyl orange catalysed by lab prepared nickel hydroxide in aqueous media. *Desalination and Water Treatment,* 54**,** 1-10.

SAEED, M. & ILYAS, M. 2013. Oxidative removal of phenol from water catalysed by lab prepared nickel hydroxide. *applied Catalysis B: Environment,* 129**,** 247-254.

SHEMER, H., KUNNUKCU, Y. K. & LINDEN, K. G. 2006. Degradation of the pharmaceutical metronidazole via UV, Fenton and photo-Fenton processes. *Chemosphere,* 63**,** 269.

SHI, L., LIN, Y., ZHANG, X. & CHEN, Z. 2011. Synthesis, characterization and kinetics of bentonite supported nZVI for the removal of Cr (VI) from aqueous solution. *Chemical Engineering Journal,* 171**,** 612-617.

SUN, J. H., FENG, J. L. & SHI, S. H. 2012. Degradation of the antibiotic sulfamonomethoxine sodium in aqueous solution by photo-Fenton oxidation. *Chinese Science Bulletin,* 57**,** 558-564.

WU, Q., ZHANG, H., ZHOU, L., BAO, C., ZHU, H. & ZHANG, Y. 2016. Synthesis and application of rGO/$CoFe_2O_4$ composite for catalytic degradation of methylene blue on heterogeneous Fenton-like oxidation. *Journal of Taiwan Institute Chemical Engineering,* 67**,** 484-494.

YANG, Y. & TIAN, C. 2012. Photocatalytic degradation of methylene blue and phenol on Fe-doped sulfated titania. *Research on Chemical Intermediates Journal,* 38**,** 693-703.

ZHAO, H., WANG, Y., WANG, Y., CAO, T. & ZHAO, G. 2012. Electro-Fenton oxidation of pesticides with a novel Fe_3O_4@Fe_2O_3/activated carbon aerogel cathode: High activity, wide pH ranges and catalytic mechanism. *Applied Catalysis B: Environment,* 125**,** 120-127.

CHAPTER 6: KINETICS STUDIES

6.1. Kinetics modeling of data

Researchers often determine the potential of the catalyst by kinetics models. The experimental data is analyzed using kinetic models to establish the mechanism and efficiency of the catalytic degradation process. Degradation reaction orders were studied using pseudo-first-order, pseudo-second order, and Langmuir-Hinshelwood models.

6.1.1 Pseudo-first and pseudo-second kinetic models

The kinetics of the catalytic degradation of MB and 2-NP using Fenton-like catalysts have been modeled using pseudo-first and pseudo-second kinetic models. For example, the pseudo first-order was used in the modeling of methylene blue degradation by magnetic carbon composites (WU et al., 2016) and by rGO/$CoFe_2O_4$ (ZHOU et al., 2015). The pseudo-first and second order kinetics can be presented as:

$$r = \frac{dC}{dt} = k_1 C_t \qquad (6.1)$$

$$r = \frac{dC}{dt} = k_2 C_t^2 \qquad (6.2)$$

Integrating Eqs(6.1) and (6.2) with respect to the limits of $C = C_t$ at time $t = 0$, the non-linear form of the equations become:

$$C = C_t \exp^{k_1 t} \qquad (6.3)$$

$$C = \frac{C_t}{k_2 C_t + 1} \qquad (6.4)$$

where r is the rate of methylene blue degradation ($min^{-1}mg/dm^3$), C is the initial concentration of methylene blue and C_t is the methylene blue concentration at any time (mg/dm^3), k_1 (min^{-1}) and k_2 (dm^3/mg min) are the pseudo first and pseudo second order rate constants.

6.1.2 Langmuir-Hinshelwood

Langmuir-Hinshelwood model was applied to describe the kinetic data since the Langmuir-Hinshelwood kinetics written in terms of initial concentration rate for $KC_0 << 1$, reduces to the pseudo first order kinetics (KUMAR et al., 2009).

$$\ln\left(\frac{C_0}{C}\right) + K(C_0 + C_t) = k_r K t \tag{6.5}$$

Therefore, if the term $KC_0 << 1$, then Eq.(5) reduces to:

$$r = k_r K C_t \tag{6.6}$$

making Eq.(6) to reduce to Eq.(2)

Therefore, the pseudo first-order rate constant, k_1 is then taken as k_{app}, where $k_{app} = k_r K$. Langmuir-Hinshelwood equation for degradation rate can be written as:

$$r = -\frac{dC}{dt} = k_r \times \theta_L \times \theta_{HO^\cdot} \tag{6.7}$$

Where k is the surface reaction rate constant, θ_L is the fraction of surface sites covered by MB molecules, $\theta_{HO^\cdot}$ is the fraction of the surface covered by $HO^\cdot$ which are assumed to degrade MB. The amount of $HO^\cdot$ radicals is considered to be constant during the degradation process.

Therefore Eq.(6) can be written as:

$$r = k\theta_L \tag{6.8}$$

Where k is the new rate constant and it is equal to $r = k\theta_{HO^\cdot}$

According to the Langmuir-Hinshelwood model, the fraction of the surface site covered by MB will be:

$$\theta_L = \frac{n_{ads}}{n_0} = \frac{K_L C_0}{1 + K_L C_0} \tag{6.9}$$

$$\frac{1}{n_{ads}} = \frac{1}{n_0} + \left[\left(\frac{1}{n_0 K_L}\right)\left(\frac{1}{C_0}\right)\right] \tag{6.10}$$

Where K_L is the adsorption equilibrium constant of MB and C_0 is the initial concentration of MB, n_{ads} is the number of MB molecules adsorbed and n_0 is the initial number of MB molecules.

Therefore, substituting the expression for θ_L from Eq.(6.9) into Eq.(6.8) we get:

$$r = \frac{k K_L C}{(1 + K_L C_0)} = k_{app} C \tag{6.11}$$

$$\frac{1}{r} = \left(\frac{1 + K_L C_0}{k K_L C}\right) = \frac{1}{k_{app} C} \tag{6.12}$$

$$\frac{1}{k_{app}} = \left(\frac{1 + K_L C_0}{k K_L}\right) \tag{6.13}$$

$$\frac{1}{k_{app}} = \frac{1}{k K_L} + \frac{C_0}{k} \tag{6.14}$$

The values of k and K_L for MB degradation for samples prepared with different iron precursor amounts and constant iron precursor amount with different microwave power were determined from the slope $FeCl_3$ adeded during synthesis and intercept of the plots $1/k_{app}$ versus C_0 (Eq.(6.14)) and the values of fraction of surface covered by MB molecules was calculated using Eq.(6.9).

The values of k and K_L for MB degradation for samples prepared with different iron precursor amounts and constant iron precursor amount with different microwave power were determined

from the slope $FeCl_3$ and intercept of the plots $1/k_{app}$ versus C_0 (Eq.(6.14)) and the values of fraction of surface covered by MB molecules was calculated using Eq.(6.9). These parameters along with the correlation coefficient, r^2, values are shown in Tables 6.1 and 6.1a. The values of the parameters k and K_L and the relationship between these parameters and the amount of $FeCl_3$ applied in the catalyst preparation are shown in Table 6.1 and Figure 6.1b. From the results obtained, it was observed that both values of surface degradation constant, k, and Hinshelwood adsorption constant, K_L, increased as the amount of iron precursor applied for catalyst preparation increased from 0.01 g to 0.20 g. The r^2 values for the relationships were all reasonable high suggesting the applicability of the model to the experimental data, signifying that the degradation was carried out on the catalyst surface. As the amount of iron precursor was increased to 0.30 g, the values of k and K_L were also found to decrease. The values of the parameters, k and K_L and the relationship between these parameters and the microwave power applied in the catalyst preparation are shown in Table 6.1 and Fig. 6.3. The reasonably high values of the r^2 show the applicability of the model to the experimental data. As the microwave power was increased from 600 to 1200 W both values of k and K_L were observed to decrease. Although it was observed from section 4.7 that the percentage iron content of the samples increased with the increasing microwave power, this increase in percentage iron content did not produce an increase in k and K_L.

The fraction of surface site covered by MB, $\theta_{L,}$ for both sets of samples were calculated at the different MB concentrations applied (100 to 250 mg/dm^3) and the results shown in Tables 6.2 and 6.3 while the relationship between fraction of surface covered by MB, $\theta_{L,}$ versus the amounts of iron precursor and microwave power applied for the catalyst preparation are displayed in Figure 6.2a and b. The results showed that for any particular mass of iron precursor applied for the catalyst

preparation, the fractional surface coverage, $\theta_{L,}$ increased with initial MB concentration and the increase being rapid at lower concentrations and less rapidly at higher concentrations. The less rapid increase at high initial MB concentration may be due to site saturation or the blocking of the surface site by MB molecules (KUMAR et al., 2009). The values of θ_L increased with increase in the iron precursor mass applied for catalyst preparation from 0.01 to 0.20g and then fell when iron precursor mass was raised to 0.30 g. This increase in fraction of surface covered by MB, θ_L, is therefore responsible for the observed increase in the degradation rate constant, *k*, observed on increasing the iron precursor mass for catalyst preparation from 0.01 g to 0.20 g and the observe decrease of θ_L, when 0.30 g of iron precursor was applied led to a decrease in degradation rate constant, *k*.

Figure 6.2b shows that for any particular MB concentration, the fraction of surface covered by MB, θ_L had their highest values at low concentrations and the θ_L values were observed to decrease sharply from 600 to 940 W before becoming almost constant at 1200 W. This trend was repeated for all other MB concentration and at the different microwave power. The rapid decrease between 600 and 960 W was observed to reduce as the initial concentration was increased from 100 to 250 mg/dm^3. The reduction with increasing initial concentration confirms site saturation at higher MB concentration.

6.2 Conclusions

It was observed that both the values of surface degradation constant, *k*, and Hinshelwood adsorption constant, K_L, increased as the amount of iron precursor applied for catalyst preparation increases, suggesting an increased surface degradation. However as the microwave power increases from 600 to 1200 W both values of surface degradation constant, *k*, and Hinshelwood adsorption constant, K_L decreases, suggesting the degradation of methylene blue is more likely to

take place on the solution. It was observed that for any particular mass of iron precursor applied for the catalyst preparation, the fractional surface coverage, $\theta_{L,}$ increased with initial MB concentration, thus increasing the rate. However as the microwave power increases fractional surface coverage, $\theta_{L,}$ decrease, hence the decrease in rate constant was observed.

Table 6. 1: Pseudo-first and pseudo-second-order rate constants

Mass of $FeCl_3$ added (g)	r^2	Var. Error	r^2	Var. Error
0.01	0.9993	2.8	0.9985	5.9
0.05	0.9995	3.1	0.9968	18.5
0.10	0.9995	3.7	0.9964	27.7
0.20	0.9993	6.5	0.9877	12.7
0.30	0.9991	9.3	0.9911	93.4
Microwave Power (W)				
600	0.9993	6.5	0.9977	120.6
720	0.9995	9.0	0.9977	39.4
840	0.9996	6.0	0.9981	29.4
960	0.9995	6.3	0.9982	20.8
1200	0.9986	13.0	0.9980	18.5

Table 6. 2: The relationship between the iron precursor and Langmuir-Hinshelwood constant and surface coverage.

Mass of $FeCl_3$ (g)	k_1	K_L	r^2	θ_L			
				100 ppm	150 ppm	200 ppm	250 ppm
0.01	0.531	0.045	0.9985	0.818	0.870	0.900	0.918
0.05	0.662	0.069	0.9998	0.873	0.912	0.935	0.947
0.10	0.877	0.072	0.9957	0.878	0.915	0.935	0.947
0.20	1.343	0.077	0.9998	0.884	0.920	0.939	0.950
0.30	1.156	0.069	0.9968	0.873	0.912	0.932	0.945

Table 6. 3: The relationship between microwave power and Langmuir-Hinshelwood constant and surface coverage.

Microwave Power (W)	k_1	K_L	r^2	θ_L			
				100 ppm	150 ppm	200 ppm	250 ppm
600	1.343	0.077	0.9987	0.884	0.920	0.939	0.950
720	1.020	0.065	0.9891	0.867	0.907	0.929	0.942
840	0.888	0.043	0.9947	0.810	0.865	0.895	0.914
960	0.769	0.034	0.9968	0.772	0.836	0.871	0.894
1200	0.673	0.033	0.998	0.768	0.852	0.869	0.892

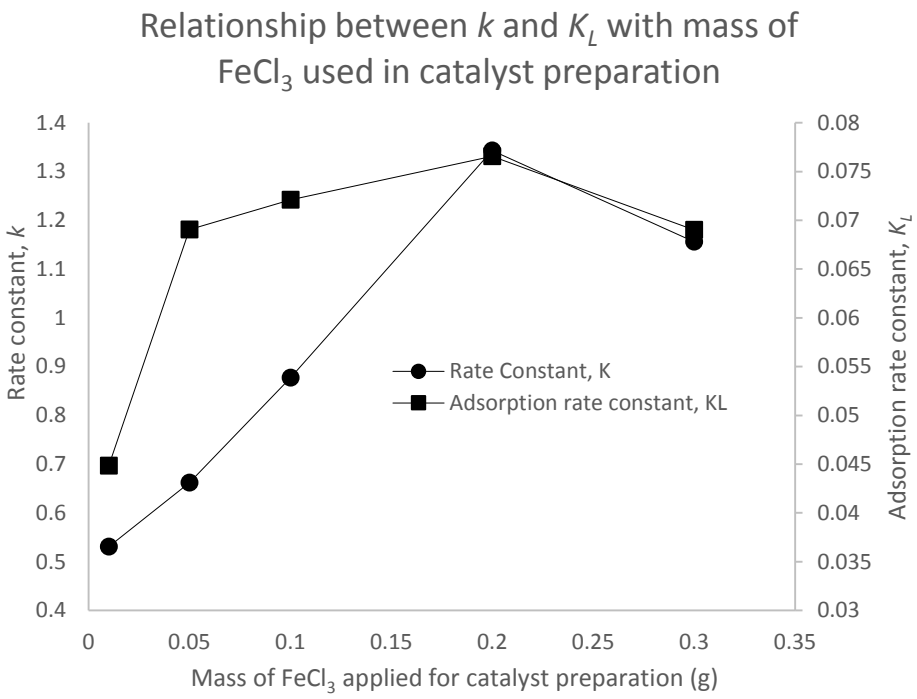

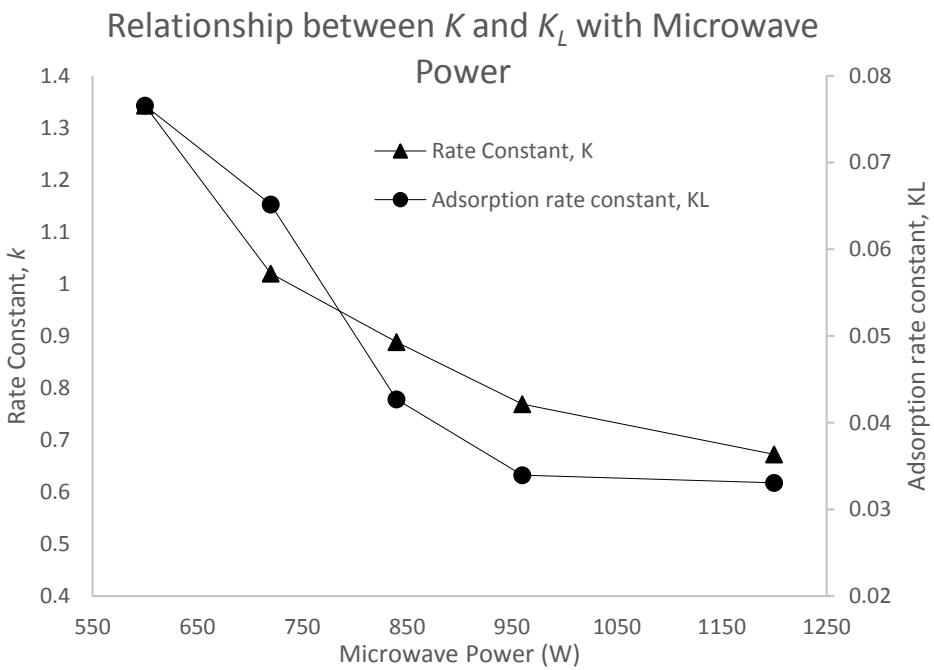

Figure 6. 1: The relationship between degradation rate constant, k, adsorption rate constant, K_L versus (a) mass of $FeCl_3$ at 600 W used for catalyst preparation and (b) microwave power using 0.20 g $FeCl_3$.

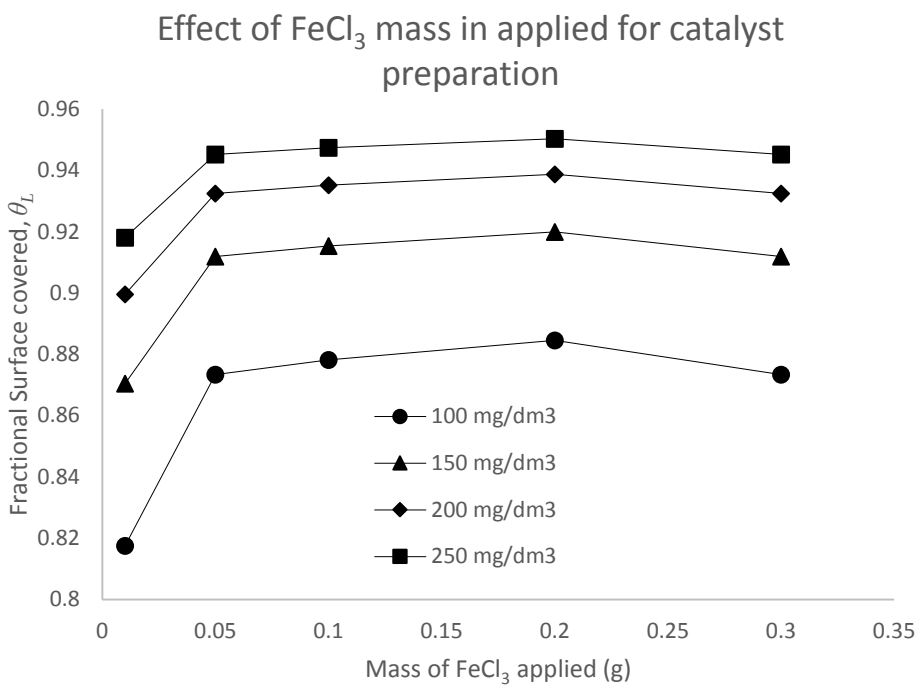

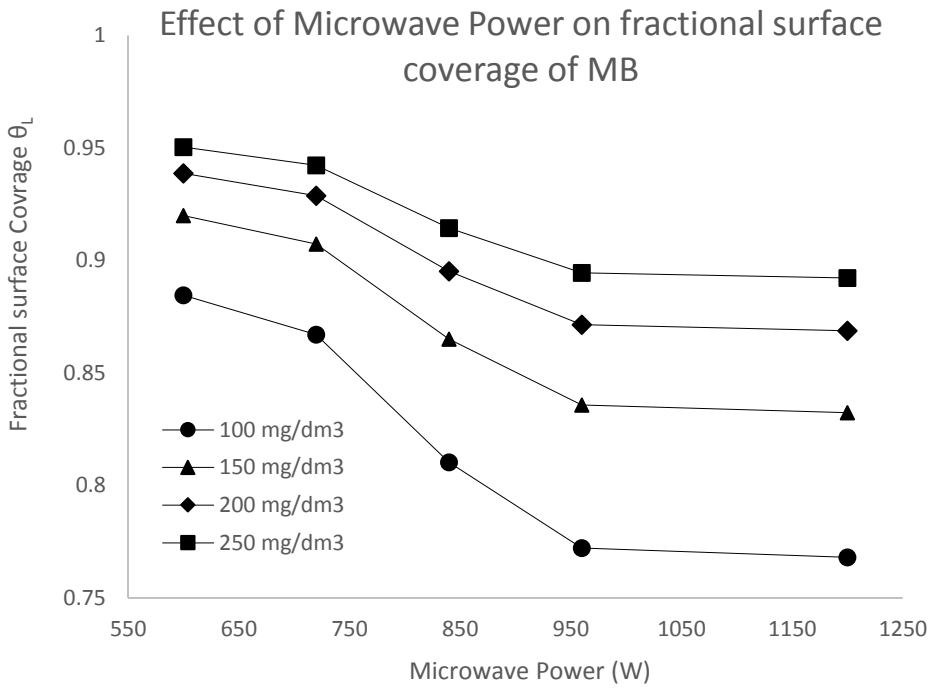

Figure 6. 2: The relationship between fractions of surface covered by MB versus (a) mass of $FeCl_3$ at 600 W used for catalyst preparation and (b) microwave power using 0.20 g $FeCl_3$.

6.3 References

KUMAR, K. V., PORKODI, K. & ROCHA, F. 2009. Langmuir-Hinshelwood kinetics - A theoretical study. *Catalysis Communications,* 9**,** 82-84.

WU, Q., ZHANG, H., ZHOU, L., BAO, C., ZHU, H. & ZHANG, Y. 2016. Synthesis and application of rGO/CoFe2O4 composite for Catalytic degradation of methylene blue on heterogeneous Fenton-like oxidation. *Journal of Taiwan Institute Chemical Engineering,* 67**,** 484-494.

ZHOU, L., MA, J., ZHANG, H., SHAO, Y. & LI, Y. 2015. Fabrication of magnetic carbon composites from peanut shells and its application as a heterogeneous Fenton catalyst in removal of methylene blue. *Applied Surface Sciences,* 324**,** 490-498.

CHAPTER 7: THERMODYNAMICS

This chapter presents and discusses the thermodynamics of the degradation process of 2-NP. The temperatures were varied during the degradation of 2-NP so that rate constants and activation energies were calculated. The thermodynamics parameters such as Gibbs free energy (ΔG), change in enthalpy (ΔH), and change in entropy (ΔS) were also determined.

7.1 Activation energy

The effect of temperature on the degradation of 2-NP was studied at varying temperature from 26 to 56 ^{o}C. The results were fitted the pseudo-first order suggesting that the degradation of 2-NP is a surface driven reaction. The results showed that the degradation of 2-NP strongly depends on the temperature applied, thus increases the degradation rate as temperature increases. The increase in the rate constant can be due to increased interaction of H_2O_2 and Fe^{2+}, which increases the production of hydroxyl radicals that degrades 2-NP.

In Table 7.1 & 7.3, it was observed that for all samples prepared at different $FeCl_3$ of 0.01, 0.05, 0.10, 0.20 and 0.30 g at a microwave power of 600 W, for all temperature employed during degradation of 2-NP, the pseudo first order rate constant increased with increasing temperature from 26 to 56 ^{o}C. This trend can be attributed to the increased molecules collision frequency leading to more interaction of H_2O_2 and Fe^{2+}, hence resulting in more degradation of 2-NP. When the mass of $FeCl_3$ increased from 0.01 to 0.20 g the pseudo first order rate increased, for all temperatures. This trend is due to the increase in active sites on the surface of the support as the mass of $FeCl_3$ increased. In contrast when the mass of $FeCl_3$ further increases from 0.20 to 0.30 g, could not further increase the degradation, hence it was observed a decrease in the degradation rate

of 2-NP. This is because of the increased Fe^{2+} on the surface of the support that acts as hydroxyl radical's scavenger, hence decreasing the catalytic activity.

It was observed also that degradation rate decreases as the microwave power increase for all temperature applied during the degradation of 2-NP. This trend may be due to a decrease in the active surface sites as microwave power increases during catalyst synthesis, as shown by the EDX results in figure 4.6.5. The effect of temperature was further investigated by using the Arrhenius equation to obtain the activation energies for the degradation of 2-NP using catalyst prepared at different microwave power. Arrhenius explains the relationship between the activation energy and temperature applied.

$$\ln k = \ln A - \frac{E_a}{RT}$$

Where k, is the degradation rate, A is the frequency factor, E_a is the activation energy, R is the ideal gas constant (8.324 J/mol K) and T is the Kelvin temperature. The rate limiting step of a heterogeneous reaction can be either chemical reaction at the surface or the diffusion of pollutant (LIEN and ZHANG, 2007), and this is determined by the relationship between reaction temperature and the rate constant. Surface controlled reactions in solutions have activation energies that are greater than 29 kJ/mol while diffusion controlled reactions have lower activation energies between 8 to 21 kJ/mol (CHEN and ZHU, 2007).

For all the degradation reactions of 2-NP using the catalyst prepared at the different mass of $FeCl_3$ at a constant microwave power of 600 W and different microwave power at a constant mass of 0.20g, their activation energies were found to be greater than 29 kJ/mol suggesting that the degradation of 2-NP is surface controlled for all the catalyst. Activation energies for samples prepared at mass of 0.01, 0.05, 0.10, 0.20, and 0.30 were found to be 32.20, 31.88, 31.21, 30.84,

and 31.61 kJ/mol. The activation energies showed to decrease from 32.20 to 30.84 kJ/mol as the mass of $FeCl_3$ increases from 0.01 to 0.20 g due to the increasingly active site on the surface of the support. Further increases of $FeCl_3$ from 0.20 to 0.30 g resulted in a decrease in activation energy. Indicating the optimum for the degradation of 2-NP could be the sample prepared at 0.20g of $FeCl_3$ since further increase results in a catalyst with a lower catalytic activity.

Also as the microwave power increases during catalyst synthesis, there is an increase in the activation in the activation energies. Activation energies for the sample prepared at a microwave power of 600, 720, 840, 960 and 1200 W were 30.18, 32.15, 33.71, 34.81 and 36.38 kJ/mol respectively as shown in table 7.3. This trend implies that as the microwave power increase during catalyst synthesis, the minimum energy required to start the degradation of 2-NP increases, hence it was observed a decrease in % 2-NP degradation as the microwave power increases from 600 to 1200 W, since for the sample prepared at higher will need a higher minimum energy to start the reaction as compared to samples prepared at a lower microwave power. This also implies that sample prepared at a microwave power of 600W is an ideal catalyst since it needs low activation energy, to conserve energy. The low activation energy for the sample prepared at 600 W, confirms the high catalytic activity as compared to the sample prepared at 1200 W that has higher activation energy. Therefore the optimum catalyst could be proposed to be synthesized at a microwave power of 600 W with a mass of 0.20 g $FeCl_3$ since it has shown to have low activation energy and higher degradation rate.

7.2 Thermodynamic parameters

Further studies were done to confirm the optimum condition for the synthesis of PCP-AC-Iron oxide catalyst. Thermodynamics parameters such as Gibbs free energy (ΔG), change in enthalpy

(ΔH), and change in entropy (ΔS) were determined for the degradation of 2-NP by using Eyring equation

$$\ln \frac{Rate}{T} = \ln\left(\frac{k}{w}\right) + \frac{\Delta S^{\#}}{R} - \frac{\Delta H^{\#}}{RT} \qquad (30)$$

where rate is the rate constant or rate coefficient of the various processes, *T* is the Kelvin temperature, *k* and *w* are the Boltzmann's and Planck's constants respectively. The change in entropy of activation ($\Delta S^{\#}$) and enthalpy of activation ($\Delta H^{\#}$), for this step, was evaluated from the intercept and slope of each linear plot. The free energies of activation ($\Delta G^{\#}$) for the degradation of 2-NP using catalyst prepare at different microwave power was computed using the Eq. (31)(FAYOUMI et al., 2012):

$$\Delta G^{\#} = \Delta H^{\#} - T\Delta S^{\#}$$

As shown in Table 7.2 and 7.4, ΔG indicates the spontaneity of the degradation process, ΔH is used to determine the nature of the reaction, whether its endothermic or exothermic and ΔS is used to determine the degree of randomness of the reaction that is the tendency to enter into solution phase(IBOUKHOULEFA et al., 2014, OLAJIRE and OLAJIDE, 2014). For all the reactions with the catalyst prepared at different microwave power at the mass of 0.20 g $FeCl_3$ and different mass of $FeCl_3$ at 600 W during catalyst synthesis, the enthalpy change was found to be positive, suggesting that all the reaction were endothermic. Enthalpy change values were found to be decreasing from 29. 56 to 27. 90 kJ/mol when mass increases from 0.01 to 0.20g of $FeCl_3$. The trend implies that the more of $FeCl_3$ added during catalyst synthesis, results in the catalyst that needs less energy to start the reaction. Even so, when the mass of $FeCl_3$ was further increased from 0.20g to 0.30g the enthalpy change increased from 27. 90 to 29.02 kJ/mol. This signifies that the further increase of $FeCl_3$ mass has a negative impact on the catalytic activity.

However as the microwave power increases from 600 to 1200 W the ΔH increases from 29.70 to 33.70 kJ/mol, implying that the energy needed to start the reaction increases as the microwave power increases. Also, this trend indicates that as the microwave power increases the energy needed to start the reaction hence higher microwave radiation of the catalyst is will not be advised since energy conservation is of significant on catalysis (YOUSEF et al., 2011).

Moreover, for all the catalyst prepared at different microwave power at the constant mass of $FeCl_3$ and at different $FeCl_3$ at constant microwave power for all temperatures, ΔG is negative, suggesting that the reactions are spontaneous and favors the formation of products. Hence, in this case, it favors the interaction of Fe^{2+} and H_2O_2 to form hydroxyl radicals to degrade 2-NP. When temperature increases from 26 to 56 ^{0}C for all sample synthesized at the different mass of $FeCl_3$, ΔG increases. This trend indicates the increase spontaneity and feasibility of the reaction as temperature increases (YOUSEF et al., 2011). In the same manner as the mass of $FeCl_3$ increases from 0.01 to 0.20 g during synthesis, ΔG increases for all temperature used during degradation of 2-NP. This can also be attributed to the increased surface active sites on the support. At the same time ΔG decreases when the mass of $FeCl_3$ increases from 0.20 to 0.30g for all temperature employed due to more of Fe^{2+} that act as hydroxyl radicals scavenger.

When temperature increases from 26 to 56 ^{o}C, ΔG increases, this means that the interaction of Fe^{2+} and H_2O_2 to form hydroxyl radicals to degrade 2-NP increases hence the degradation of 2-NP increases as temperature increases. However, when microwave power increases from 600 to 1200 W, ΔG decreases for all temperatures applied during degradation. Suggesting that the spontaneity and the ability of formation of products by its self without external help decreases with an increase in microwave power, hence the degradation efficiency decreases as the microwave power decreases from 600- 1200 W(ATKINS and DE PAULA, 2006).

ΔS is used to determine the degree of randomness. ΔS is observed to be positive for all samples prepared at different $FeCl_3$ at a constant microwave power and at different microwave power and mass of 0.20g $FeCl_3$, expressing increase randomness on the solid-liquid interface. The degree of randomness was found to be 189.1, 190.1, 190.3, 191.8, and 189.6 J/K for sample synthesized at a mass of 0.01, 0.05, 0.10, 0.20, and 0.30 g $FeCl_3$ respectively. When $FeCl_3$ mass increases from 0.01 to 0.20 g during synthesis, the degree of randomness (ΔS) increases. This implies that the more random the molecules are, at the solid-liquid interface the higher the catalytic activity. Whereas when the mass of $FeCl_3$ increases from 0.20 to 0.30 g the degree of randomness (ΔS) decreases from 191.8 to 189.6 J/K. This trend implies that the more of $FeCl_3$ is been added during catalyst synthesis it yields to a catalyst with less randomized molecules at the solid-liquid interface.

When microwave power increases the degree of randomness (ΔS), decreases with microwave power (KARTHIKEYAN et al., 2011). For sample prepared at a microwave power of 600, 720, 840, 960 and 1200 W, the degree of randomness were 191.8, 186.9, 178.1, 179.1 and 174,7 J/K mol respectively. This trend conveys that for the samples prepared a lower microwave power, there is a high degree of randomness, hence increased the excitement of the molecules as compared to the sample prepared at higher microwave power. Furthermore, for the sample prepared at lower microwave power, it will require low energy to excite the molecules as compared to the sample prepared at higher microwave power. Hence sample prepared at 600 W would be an ideal catalyst for the degradation of 2-NP.

7.3 Conclusions

For the Fenton oxidation process of 2-NP, an increase in the temperature was observed to increase the degradation rate constant. However, an increase in mass from 0.01g to 0.20g showed to have increased rate constants, spontaneity and the degree of randomness also decreased activation

energies and enthalpy change which were endothermic. This implies that the feasibility of the reaction increase with an increase in mass of $FeCl_3$. However a further increase of mass of $FeCl_3$ could not further increase the feasibility and catalytic activity. Coupled with that, when microwave power increases from 600 to 1200 W the decreased rate constants, spontaneity and the degree of randomness also increased activation energies and enthalpy change which were endothermic. As a result decreasing the feasibility as the microwave power increases. Hence it can be concluded that the catalyst to give high feasibility and high catalytic activity should be prepared at a microwave power of 600 W with a mass of 0.20 g $FeCl_3$.

Table 7. 1: Rate constants and activation energies for degradation of 2-NP using catalyst prepared at different masses of $FeCl_3$ using microwave of 600 W

Catalyst mass (g)	Temperature (°K)				Activation Energy (kJ/mol)	r^2
	299	309	319	329		
	Pseudo first order rate (min^{-1})	Pseudo first order rate (min^{-1})	Pseudo first order rate (min^{-1})	Pseudo first order rate (min^{-1})		
0.01	0.0054	0.0090	0.0120	0.0182	32.20	0.9916
0.05	0.0062	0.0090	0.0133	0.0201	31.88	0.9962
0.10	0.0075	0.0101	0.0162	0.0229	31.21	0.9905
0.20	0.0082	0.0114	0.0178	0.0245	30.84	0.9952
0.30	0.0069	0.0093	0.0148	0.0215	31.63	0.9904

Table 7. 2: Thermodynamics parameter for the degradation of 2-NP using catalyst prepared at different masses of $FeCl_3$ using microwave power of 600 W

Catalyst mass (g)	Temperature (°K)				ΔH (kJ/mol)	ΔS (J/K mol)	r^2
	299	309	319	329			
	-ΔG (kJ/mol)						
0.01	26.96	28.85	30.75	32.64	29.56	189.1	0.9899
0.05	27.68	29.58	31.49	33.39	29.27	190.1	0.9957
0.10	28.29	30.19	32.10	34.00	28.60	190.3	0.9984
0.20	29.47	31.39	33.30	35.22	27.90	191.8	0.9944
0.30	27.67	29.57	31.47	33.36	29.02	189.6	0.9888

Table 7. 3: Rate constants and activation energies for degradation of 2-NP using catalyst prepared at different microwave power with 0.20 g mass of $FeCl_3$

Microwave Power (W)	Temperature (°K)				Activation Energy (kJ/mol)	r^2
	299	309	319	329		
	Pseudo first order rate (min^{-1})	Pseudo first order rate (min^{-1})	Pseudo first order rate (min^{-1})	Pseudo first order rate (min^{-1})		
600	0.0082	0.0114	0.178	0.0245	30.48	0.9952
720	0.0075	0.0110	0.0240	0.0240	32.15	0.9983
840	0.0070	0.0108	0.0164	0.0238	33.71	0.9987
960	0.0065	0.1000	0.0161	0.0229	34.81	0.9982
1200	0.0058	0.0093	0.0153	0.0216	36.38	0.9971

Table 7. 4: Thermodynamics parameter for the degradation of 2-NP using catalyst prepared at different microwave power with a mass of 0.20 g of $FeCl_3$

Microwave Power (W)	Temperature (°K)				ΔH (kJ/mol)	ΔS (J/K mol)	r^2
	299	309	319	329			
	-ΔG (kJ/mol)						
600	29.47	31.39	33.32	35.22	27.90	191.8	0.9944
720	26.33	28.20	30.07	31.94	29.50	186.9	0.9980
840	23.34	25.16	26.98	28.80	32.21	178.1	0.9984
960	21.34	23.14	24.93	26.72	32.21	179.1	0.9979
1200	18.48	20.23	21.97	23.72	33.77	174.7	0.9965

7.4 References

ATKINS, P. & DE PAULA, J. 2006. *Physical Chemistry, Eighth Edition,* Great Britain Oxford University Press.

CHEN, J. & ZHU, L. 2007. Heterogeneous UV-Fenton catalytic degradation of dyestuff in water with hydroxyl-Fe pillared bentonite. *Catalysis Today,* 126**,** 463-470.

FAYOUMI, L. M. A., EZZEDINE, M. A., AKEL, H. H. & EL JAMAL, M. M. 2012. Kinetic Study of the Degradation of Crystal Violet by $K_2S_2O_8$. Comparison with Malachite Green. *Portugaliae Electrochimica Acta* 30**,** 121-133.

IBOUKHOULEFA, H., AMRANEB, A. & KADIA, H. 2014. Removal of phenolic compounds from olive mill wastewater by a Fenton-like system H_2O_2/ Cu(II)—thermodynamic and kinetic modeling. *Desalination and Water Treatment,* 57**,** 1874-1879.

KARTHIKEYAN, S., TITUS, A., GNANAMANI, A., MANDAL, A. B. & SEKARAN, G. 2011. Treatment of textile wastewater by homogeneous and heterogeneous Fenton oxidation processes. *Desalination,* 281**,** 438-445.

LIEN, H. L. & ZHANG, W. X. 2007. Nanoscale Pd/Fe bimetallic particles : Catalytic effects of palladium in hydrodechlorination *Applied Catalysis B: Environment,* 177**,** 110-116.

OLAJIRE, A. A. & OLAJIDE, A. J. 2014. Kinetic Study of Decolorization of Methylene Blue with Sodium Sulphite in Aqueous Media: Influence of Transition Metal Ions. *Journal of Physical Chemistry & Biophysics,* 4**,** 136.

YOUSEF, R. I., EL-ESWED, B. & AL-MUHTASEB, A. H. 2011. Adsorption characteristics of natural zeolites as solid adsorbents for phenol removal from aqueous solutions: Kinetics, mechanism, and thermodynamics studies. *Chemical Engineering Journal,* 171**,** 1143-1149.

CHAPTER 8: DEGRADATION MECHANISM, CATALYST STABILITY & DEGRADATION PRODUCTS

This chapter presents and discusses the degradation mechanism, catalyst stability and degradation products of MB and 2-NP by Fenton oxidation process. It reports on the effect of radical scavenging on the degradation %, the amount of iron oxide leached during catalyst reuse.

8.1 Degradation mechanism

The mechanism of Fenton's oxidation is known to be hinged on the decomposition of H_2O_2 catalyzed by the iron oxide species producing radicals that promote degradation of the pollutants. To confirm the degradation mechanism, the degradation was measured in the absence and presence of radical scavenger, for example with 10 ml of 1 mM isopropanol which acts as a scavenger for hydroxyl radicals $\left(\cdot OH\cdot\right)$ and 10 ml of 1mM of Benzoquinone that acts as a radical scavenger for superoxide radicals $(O_2^{\cdot-})$. The degradation of MB and 2-NP without and with isopropanol and benzoquinone using catalyst prepared with different masses of the iron precursor at 600 W and those prepared with 0.20 g iron precursor at different microwave power are displayed in figure 8.1a and b for MB and figure 8.2a and b for 2-NP. The results displayed in figure 8.1a and b revealed that there was a rapid increase in MB degradation with an increase in the amount of iron precursor applied for catalyst preparation from 0.01 to 0.20g and then the values reduced slightly at 0.30 g. On the other hand, the MB degradation was observed to decrease rapidly from microwave power 600 to 960 W and became constant at microwave power 1200 W. Also the results in figure 8.2a and b displayed a similar trend that there was an increase in 2-NP degradation as the amount of iron precursor applied for catalyst preparation increases from 0.01 to 0.20g and further in from 0.20 g to 0.30 g there was a decrease in 2-NP degradation. However, the 2-NP

degradation was shown to decrease rapidly as the microwave power increases from 600 to 1200 W. These results revealed that when both scavengers (isopropanol and benzoquinone) were added at the beginning of the experiments, the % MB and 2-NP degradation reduced in value when compared with that in the absence of radical scavenger. This, therefore, suggests that both $\left(OH^{\cdot}\right)$ and $(O_2^{\cdot-})$ radicals were involved in the degradation mechanism. The reduction in MB degradation were observed to be higher for experiments where isopropanol was added as compared with experiments where benzoquinone was added. This suggests that the hydroxyl radicals $\left(OH^{\cdot}\right)$were more active in the MB and 2-NP degradation than the superoxide radicals $(O_2^{\cdot-})$ (ZHAO et al., 2012, LIOU et al., 2005).

Since both $\left(OH^{\cdot}\right)$ and $(O_2^{\cdot-})$ radicals were observed to affect the mechanism of the catalytic reaction, the following reactions were proposed for the radical production (Eqs.(13-16))

$$Fe^{2+} + H_2O_2 \rightarrow Fe^{3+} + OH^- + {}^{\cdot}OH \quad (13)$$

$$Fe^{3+} + H_2O_2 \rightarrow Fe^{3+} + O_2^{\cdot-} / HO_2^{\cdot-} + H^+ \quad (14)$$

$$Fe^{3+} + 2{}^{\cdot}OH \rightarrow Fe^{2+} + O_2^{\cdot-} / HO_2^{\cdot-} + H^+ \quad (15)$$

$$H_2O_2 + {}^{\cdot}OH \rightarrow O_2^{\cdot-} / HO_2^{\cdot-} + H_2O \quad (16)$$

It was observed that as the amount of iron precursor applied for catalyst preparation, the fraction of the surface covered by MB or 2-NP and the MB and 2-NP degradation increased, the reduction in degradation caused by the addition of scavengers decreased (Figure 8.1a and 8.2a). Since the amount of hydroxyl radicals (${}^{\cdot}OH$) produced should increase with increasing amount $FeCl_3$ added (% iron content) for catalyst preparation, the addition of constant amount isopropyl scavenger to all experiments should produce a smaller reduction in degradation as the amount $FeCl_3$ increases.

It is, therefore, logical to infer that a higher proportion of the radicals ($^{\cdot}OH$) produced will be scavenged for samples with lower amounts of iron precursor (leading to a higher reduction in MB and 2-NP degradation) than for samples with a higher amount of iron precursor (leading to a lower reduction in degradation). Hydroxyl radicals have the higher oxidation potential of the two radicals $^{\cdot}OH$ and $O_2^{\cdot-}$ produced. The degradation mechanism shows that $O_2^{\cdot-}$ radicals can be produced from undesirable side reactions according to Eqs.(14 - 16). A higher reduction in degradation (25.6 to 18.8 %) for benzoquinone addition was observed when 0.01 g of $FeCl_3$ was applied for catalyst preparation than when 0.20 g of the iron precursor was applied (70.5 to 66.6 %). In the same manner, a higher reduction in 2-NP degradation (18.3-15.1 %) for benzoquinone addition was observed when 0.01 g of $FeCl_3$ was applied for catalyst preparation than when 0.20 g of the iron precursor was applied (69.06-63.3 %). The higher production of $O_2^{\cdot-}$ radicals when lower iron precursor amounts was applied for catalyst preparation can be attributed to the lower levels of decomposition of H_2O_2 owing to the low iron content (0.3 %) of the sample. Therefore producing fewer $^{\cdot}OH$ radicals which then react with excess H_2O_2 and Fe^{3+} in the system according to Eqs.(14-16) forming $O_2^{\cdot-}$. As the iron content of the catalyst increases, decomposition of H_2O_2 by Fe^{2+} increases and hydroxyl radicals produced degrades more MB & 2-NP in solution, however further increase results in the production of hydroxyl radicals (GUO et al., 2014, SABHI and KIWI, 2001).

Although the iron content of the catalysts increased with increasing microwave power from 600 to 1200 W, a reducing trend was observed in the fraction of the surface covered by MB or 2-NP and MB and 2-NP degradation (Figure 8.1b and 8.2b). The addition of the scavengers to each experiment led to a further reduction in the degradation for both MB and 2-NP as microwave

power increases from 600 to 1200 W during catalyst synthesis. The addition of isopropanol scavenger produced decreases in MB degradation that were lower at lower microwave power and higher at higher microwave power. Identical to that, the addition of isopropanol scavenger produced a decrease in 2-NP degradation that was lower at lower microwave power and higher at higher microwave power. This result suggests that hydroxyl radical ($^{\cdot}OH$) production decreased with increasing microwave power. Since the fraction of the surface covered by MB reduced although the % iron content increased with microwave power, the decomposition of H_2O_2 by Fe^{2+} and Fe^{3+} (Eqs. (13-14)) becomes low due to low reaction rates. Benzoquinone addition was observed to reduce the MB degradation as the microwave power was increased. The addition of benzoquinone scavenger produced a decrease in MB degradation that was higher at lower microwave power and zero at higher microwave power. In the same manner, surface covered by 2-NP reduced although the iron content increased with microwave power, the decomposition of H_2O_2 by Fe^{2+} and Fe^{3+} (Eqs. (13-14)) becomes low due to low reaction rates. This also means that as the microwave power increases the (Eqn. 2) side chain reaction that is driving the degradation of 2-NP, hence there is a decrease in 2-NP degradation as the microwave power increases. Benzoquinone addition was observed to reduce the 2-NP degradation as the microwave power was increased from 600 to 1200 W. The reduction in MB degradation were from 59.9 to 58 % for 720 W, 53.4 to 51.7 % for 840 W, 45.3 to 44.2% for 960 W and 45.3 to 45.3 % at 1200 W. The 2-NP decreased from 65.06 to 64.30 % for 600 W, 59.9 to 57.9 % for 720 W, 53.4 to 50.7 % for 840 W, 45.3 to 40.9 % for 960 W and 45.3 to 40.1 % for 1200 W. This trend suggest that superoxide radicals produced increases with the increase in microwave power, this can also attribute to the lower 2-NP degradation as the microwave power increases from 600 W to 1200 W, since superoxide radicals has a lower oxidation potential as compared to hydroxyl radicals.

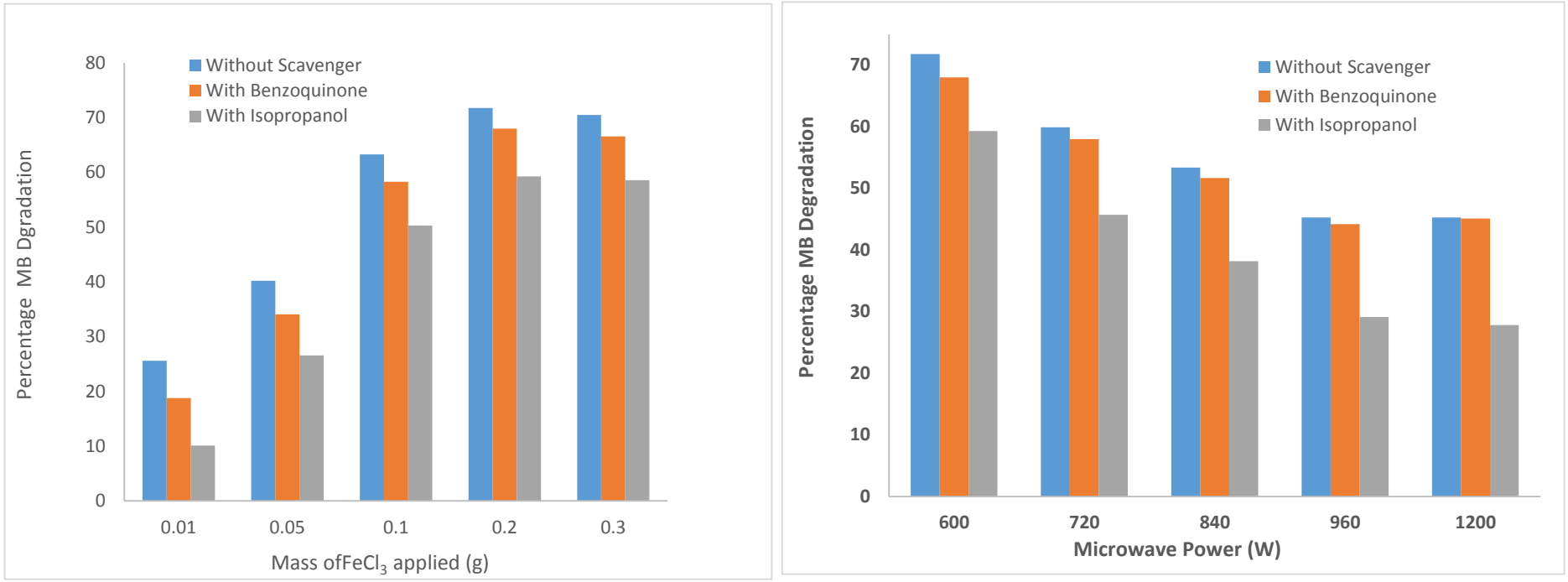

Figure 8. 1: The relationship between degradation of MB with scavengers and without scavengers on the MB % degradation (a) mass of $FeCl_3$ at 600 W used for catalyst preparation and (b) microwave power using 0.20 g $FeCl_3$

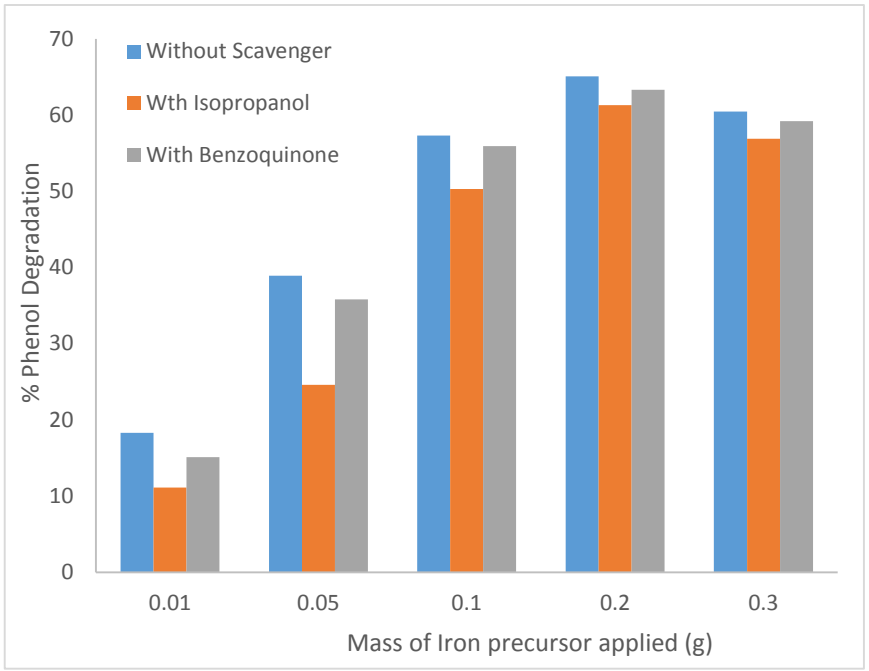

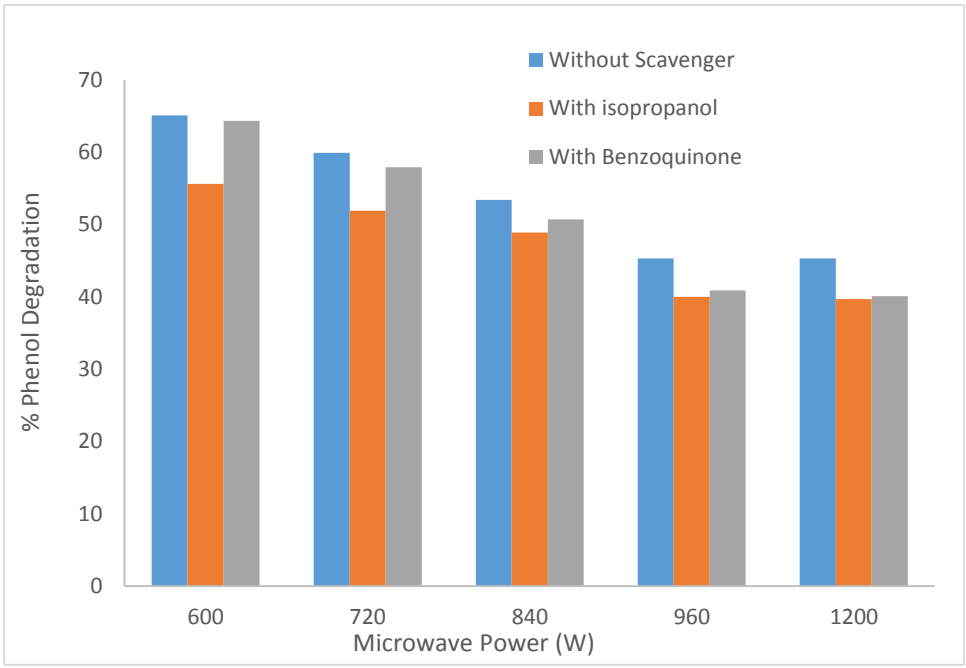

Figure 8. 2: The relationship between degradation of 2-NP with scavengers and without scavengers on the 2-NP % degradation (a) mass of $FeCl_3$ at 600 W used for catalyst preparation and (b) microwave power using 0.20 g $FeCl_3$.

8.2 Catalyst resuse and leaching

The PCP-AC-iron oxide catalysts prepared using different masses of iron precursor and at different microwave power were applied for MB and 2-NP degradation in three consecutive runs. Between each run, the catalyst was separated from the solution by filtration, washed with deionized water, and dried at 100°C in a vacuum oven overnight before reuse. Figure 8.3 and 8.4 show the degradation for the first, second and third cycle for samples prepared using different amounts of $FeCl_3$ at 600 W and samples prepared using 0.20 g iron precursor at different microwave power.

The results in figure 8.3a and 8.4a, shows that decreases were observed in the degradation for MB and 2-NP from the first to the third cycle for all samples and that iron oxide was leached out into the solution during the repeated cycles. Factors that may lead to these changes include (i) deactivation of the catalyst surface by adsorption of MB or 2-NP molecules and degradation products and (ii) oxalic acid molecules formed during catalytic degradation of MB or 2-NP causing leaching of iron oxide from the catalyst surface into solution (REY et al., 2009). For the set of samples in Fig. 9a, the fraction of the surface covered by MB, θ_L increased with the % iron content and this led a higher degradation of MB and 2-NP in solution. As MB and 2-NP molecules are degraded, the concentration of oxalic acid in solution increases leading to leaching of iron oxide from the catalyst surface (Fig. 9a).

According to the XRF results, the percentage iron contents for the samples prepared using 0.01, 0.05, 0.10, 0.20 and 0.30 g iron precursor were 0.3, 1.6, 2.1, 2.7 and 3.2 % respectively and the amount of iron leached into solution after three cycles were 0.02, 0.09, 0.35, 0.90 and 1.29 ppm of Fe was respectively for MB and 0.03, 0.1960, 0.2640, 0.5051, and 0.7749 ppm for 2-NP. Comparing the amount of iron leached for MB and 2-NP, during MB degradation it was observed that leached iron oxide leached more as compared to 2-NP degradation for all samples prepared

using different masses of the iron precursor. This can suggest that during degradation process of MB and 2-NP, formation of oxalic acid increased during the degradation of MB as compared to 2-NP, this can also be supported by the degradation of MB and 2-NP, where it showed MB has a higher degradation than 2-NP. The levels of iron leached into solution were low as compared to the European Union permissible values of < 2 ppm (REY et al., 2009, XAVIER et al., 2015). Although the concentration of iron leached into solution was highest for the samples with 2.7 and 3.2 % iron content, these samples also had the least reduction in degradation after the third run for both MB and 2-NP. This may be due to higher iron content and fraction of the surface covered by MB molecules, θ_L (active iron oxide sites) of these samples as compared with samples having lower θ_L values and lower % iron content. Although a high amount of iron oxide was lost by leaching, sufficient active sites were still available for degradation. Therefore, these samples are deemed to be better reusable and stable catalyst for heterogeneous Fenton reaction (ZHOU et al., 2015).

The effect of microwave power on the MB degradation for samples prepared with the constant amount of iron precursor in the first, second and third cycle of degradation along with the concentration of iron oxide leached into solution is shown in Fig. 9b. The MB degradation was observed to increase as the fraction of the surface covered by MB, θ_L, increased and this led to a higher production of oxalic acid which produced a higher level of iron oxide leaching (REY et al., 2009). According to the XRF results, the iron contents for the samples prepared using microwave power of 600, 720, 840, 960 and 1200 W were 2.7, 3.2, 3.5, 3.6 and 3.7 % and the amount of iron leached into solution after three runs were 0.90, 0.82, 0.24, 0.13 and 0.12 ppm of Fe was respectively for MB and 0.5051, 0.3983, 0.2729, 0.1743, and 0.1069 ppm respectively for 2-NP. The result also suggests that the iron content did not increase with a fraction of the surface covered

by MB or 2-NP, but as iron content increased the reduction in degradation in the third stage decreased. The reason for this observed trend may be due to the modification of the iron oxide nanoparticles in the activated carbon matrix by higher microwave power heating.

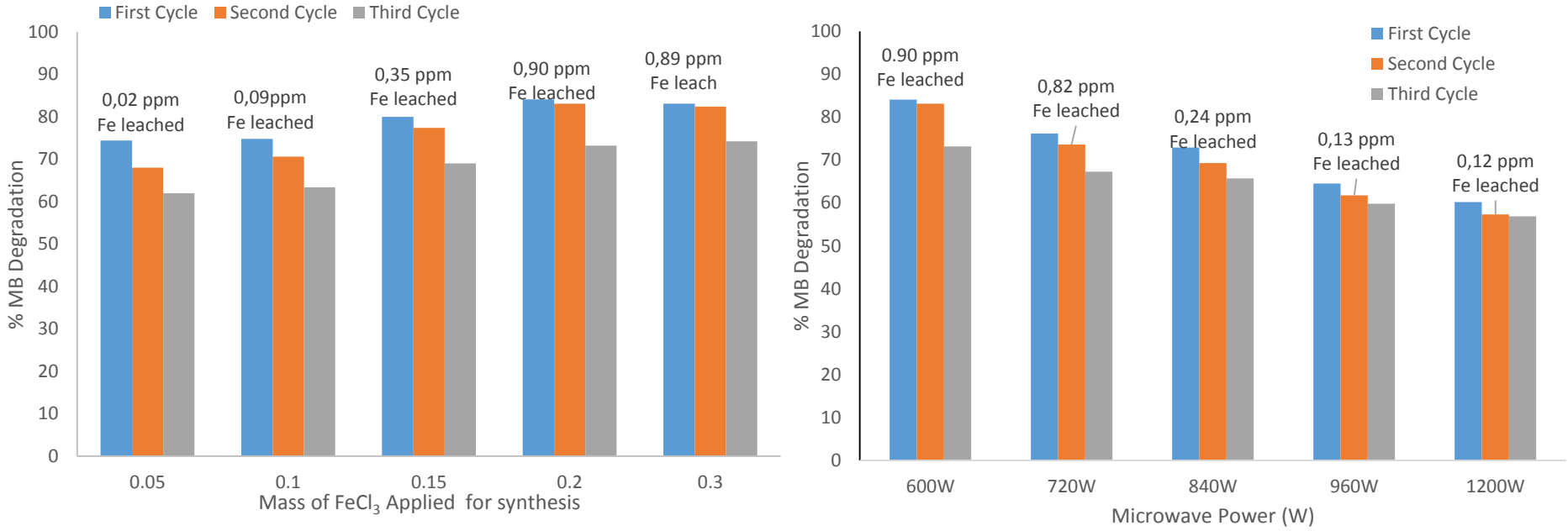

Figure 8. 3: The relationship between MB % degradation after three cycles along with the concentration of iron leached versus (a) mass of $FeCl_3$ at 600 W used for catalyst preparation and (b) microwave power using 0.20 g $FeCl_3$.

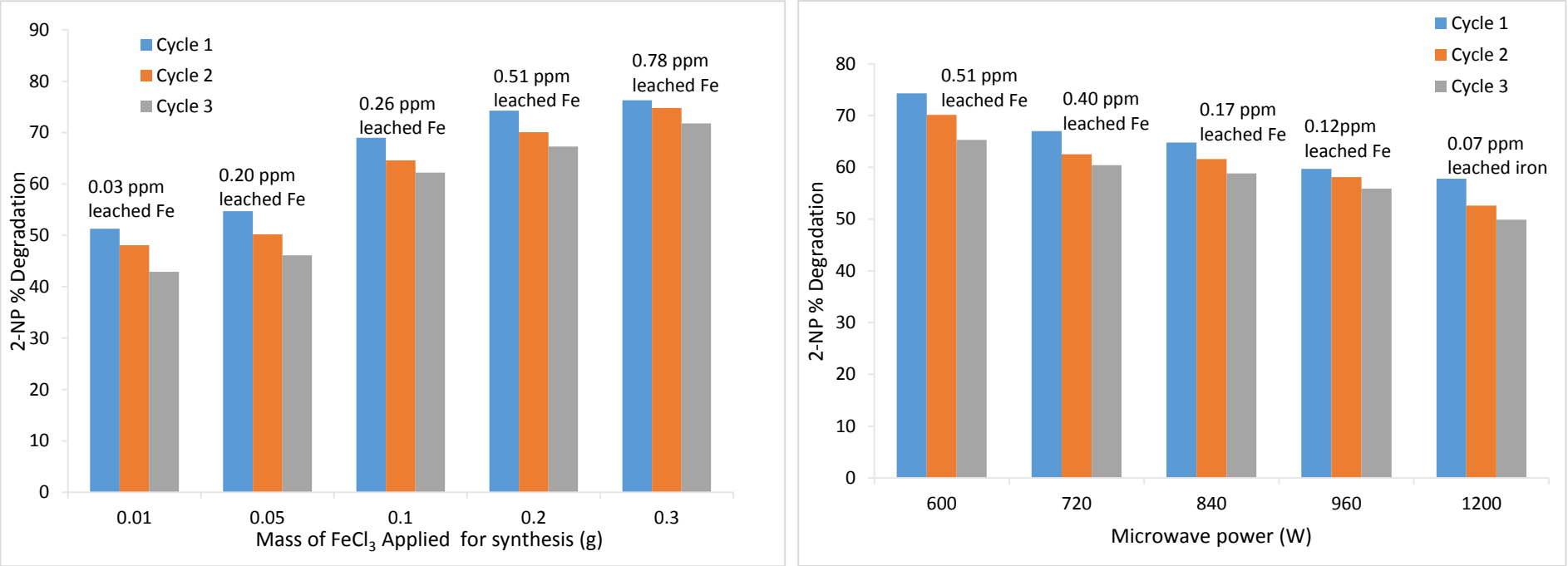

Figure 8.4: The relationship between 2-NP % degradation after three cycles along with the concentration of iron leached versus (a) mass of $FeCl_3$ at 600 W used for catalyst preparation and (b) microwave power using 0.20 g $FeCl_3$.

8.3 Degradation products for MB AND 2-NP

Fenton oxidation process mainly involves the production of hydroxyl radicals from the reaction of Fe^{2+} and H_2O_2. These hydroxyl radicals are used to degrade the MB and 2-NP. However in the degradation of MB, decolorization of MB it does not mean the complete mineralization to non-toxic molecules. MB is blue in color and leuco MB (LMB), the reduced form of methylene blue is colorless. LMB can be converted back to MB (BOKER et al., 2014, GNASER et al., 2005), hence it should be confirmed that the decolorization of the MB is not due to the formation of LMB.

Studies of the products formed were performed by the Gas chromatography-mass spectrometry (GC/MS) to confirm the degradation intermediates as shown in figure 8.5-8.13. The peak at 284 m/z in Figure 8.5 corresponds to the molecular ion of the undegraded MB. Figures 8.7a,b,c show the degraded MB, which shows the disappearance of the peak m/z = 284, which corresponds to MB (HOUAS et al., 2001), however it showed peaks at 270, 256 and 227 m/z which corresponds to azure B, azure A, and thionin respectively, due to the loss of methyl groups (RAUF et al., 2010, WANG et al., 2014). Azure B, azure A, and thionin could be further oxidized to form single ring molecules. In turn, they may have been subjected to further degradation, eventually leading to a ring opening and the formation of a series of aliphatic mono- and di-carboxylic acid. Among the carboxylic acids formed, malonic acid, oxalic acid, and formic acid were identified, which corresponded to 106, 91, 44 m/z respectively (LIOTTA et al., 2009). The carboxylic acids can be further degraded to CO_2, H_2O, SO_4^{2-} and NO_3^- (HUANG et al., 2010).

In the analysis of 2-NP, the undegraded 2-NP showed an intense peak at m/z = 139 which corresponds to the m/z of 2-NP in figure 8.10 (SAMUEL et al., 2014). However, with the degraded 2-NP, the distinct peak at m/z =139 disappeared, with intense peaks at m/z = 44, 58, 91, 106 which corresponds to formic acid, acetic acid, oxalic acid and malonic acid respectively (LIOTTA et al.,

2009). The study confirms that 2-NP was degraded by the Fenton-like oxidation process. The carboxylic acids can be further degraded to CO_2, H_2O, and NO_3^- (DI PAOLA et al., 2003). The proposed reaction mechanism for MB and 2-NP was also shown in figure 8.9 & 8.13 respectively.

PURE METHYLENE BLUE

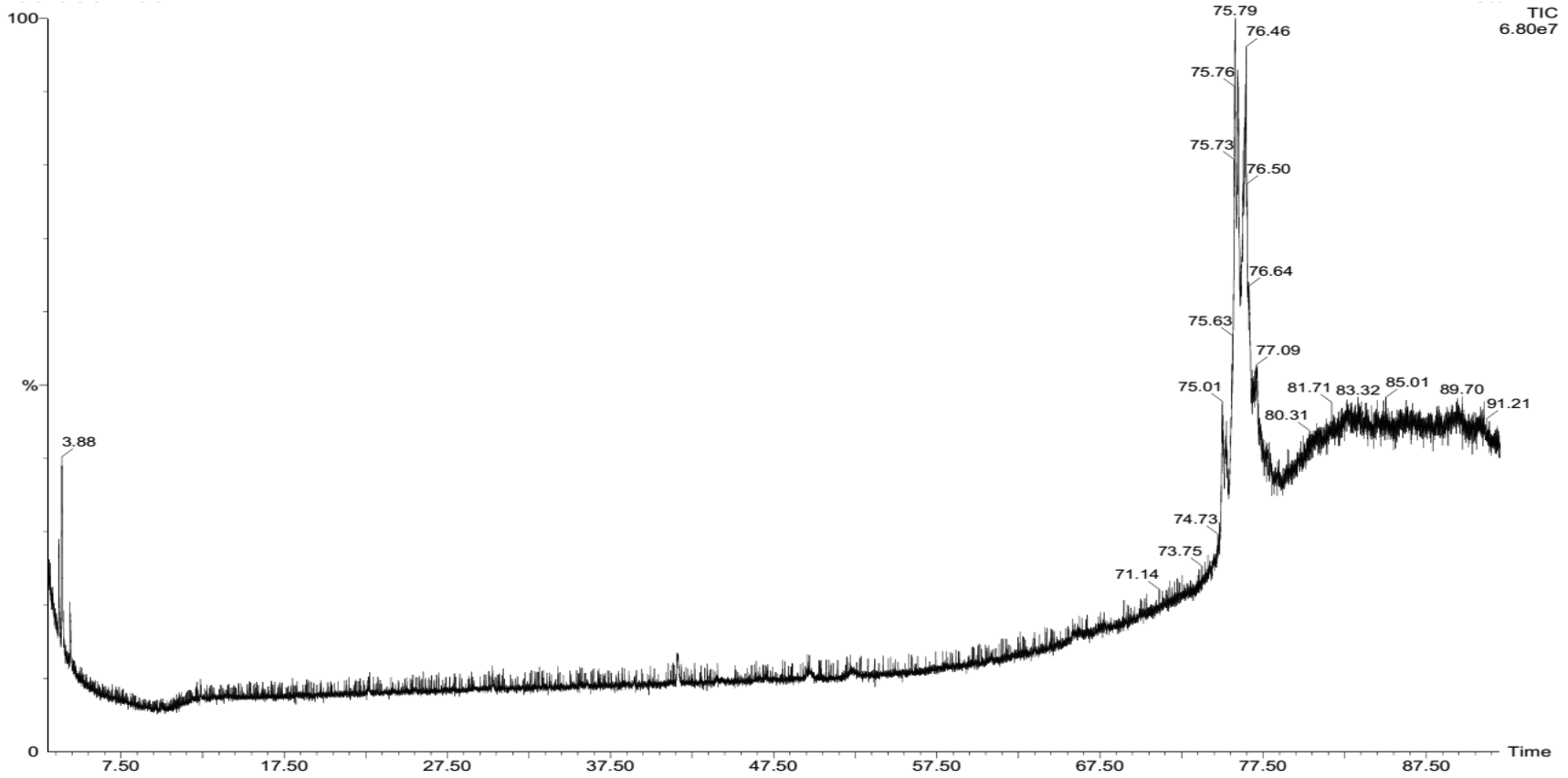

Figure 8. 4: GC Spectrum for un-degraded MB

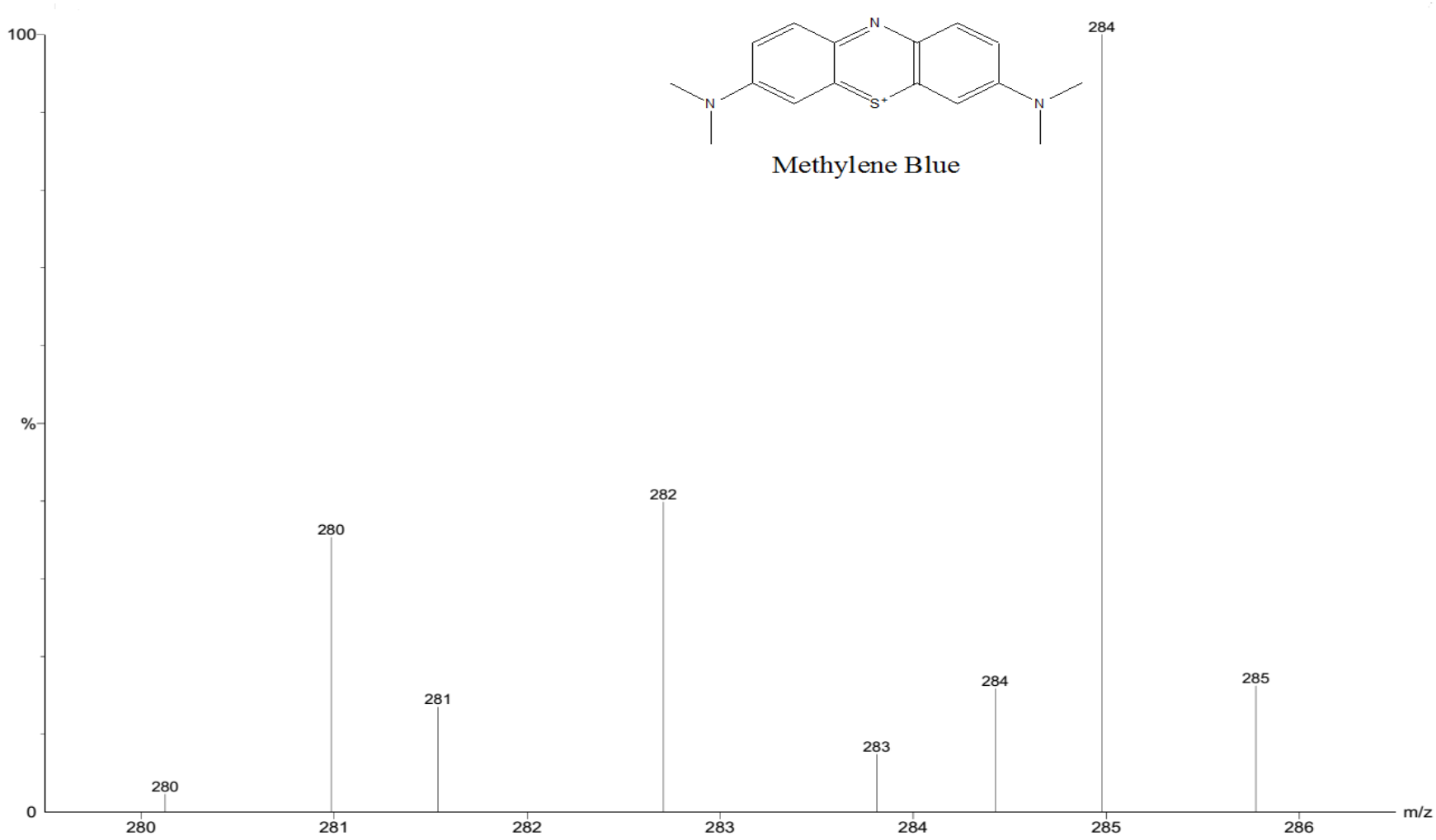

Figure 8. 5: Mass spectrum of un-degraded MB

METHYLENE BLUE DEGRADATION PRODUCTS

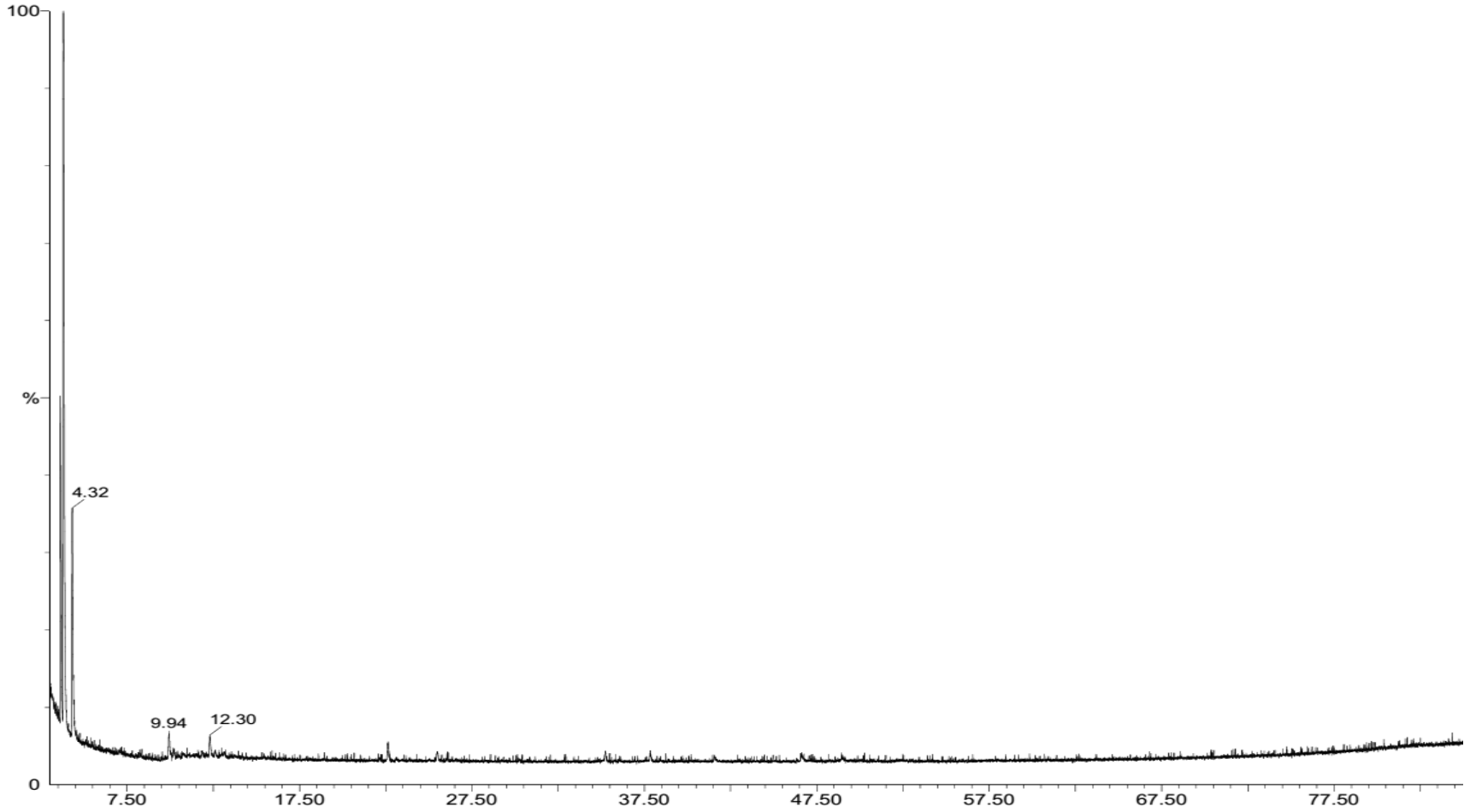

Figure 8. 6: GC Spectrum for degradation products

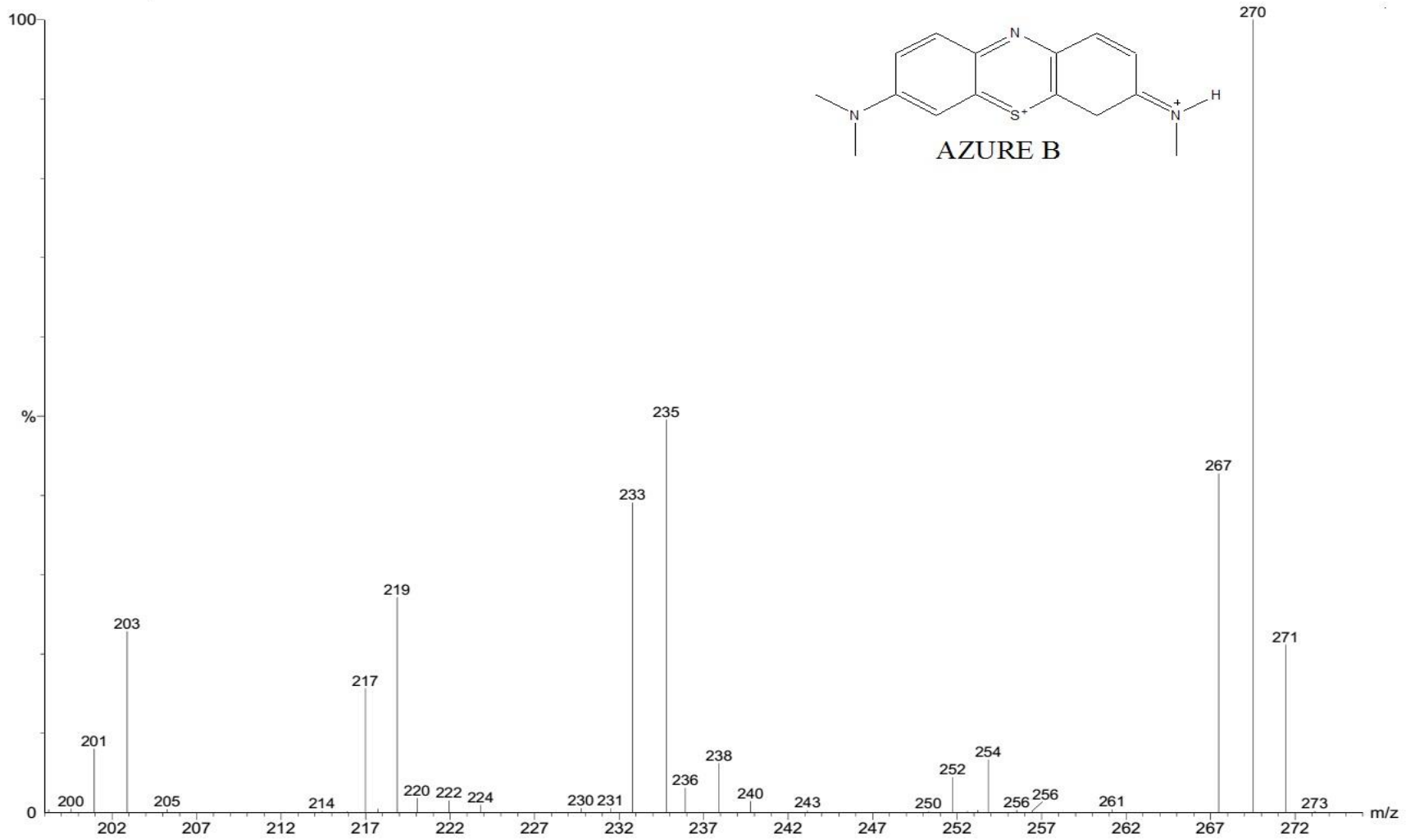

Figure 8. 7: Mass spectrum of the degradation products of MB

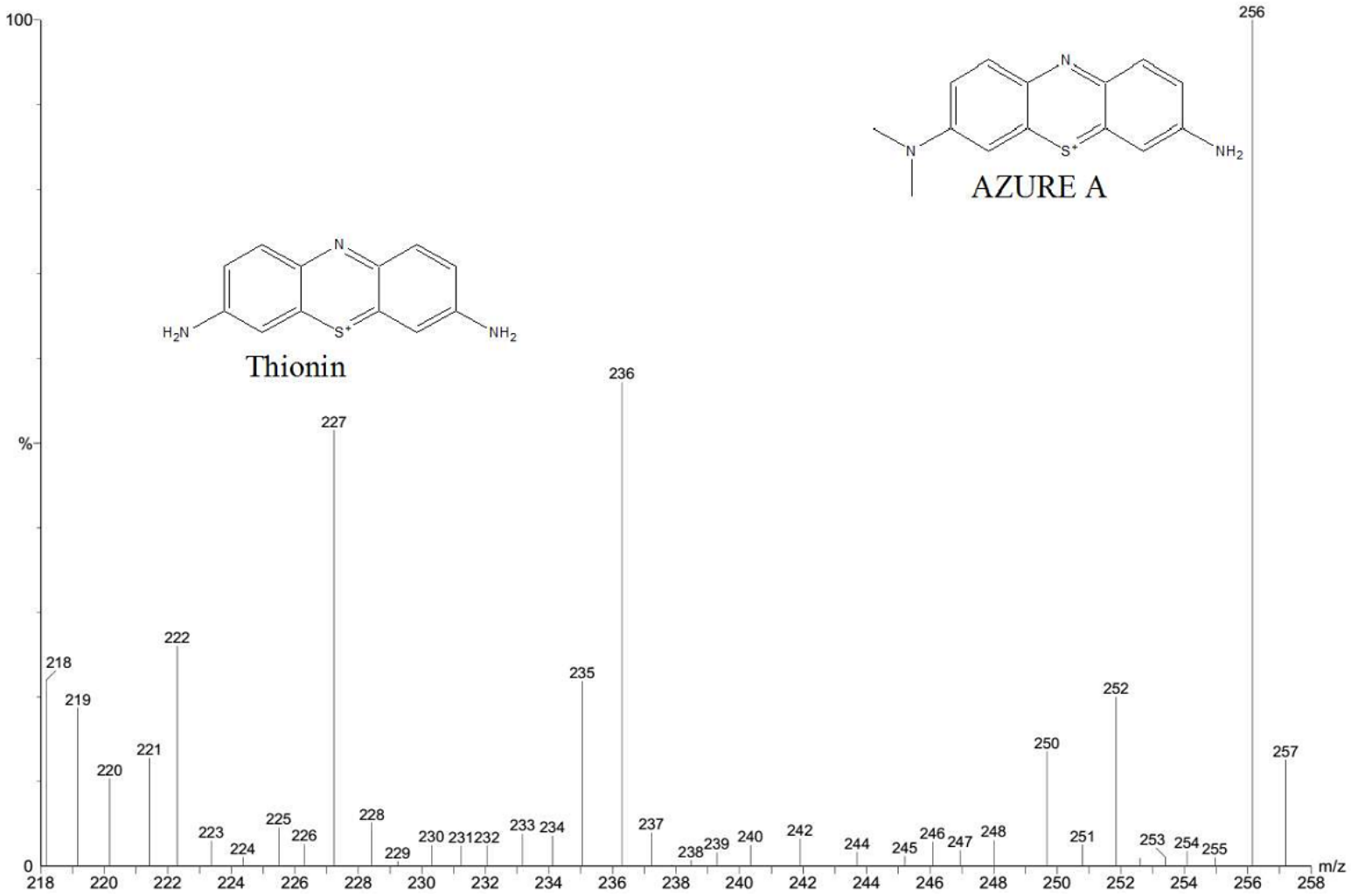

Figure 8.7b: Mass spectrum of the degradation products of MB

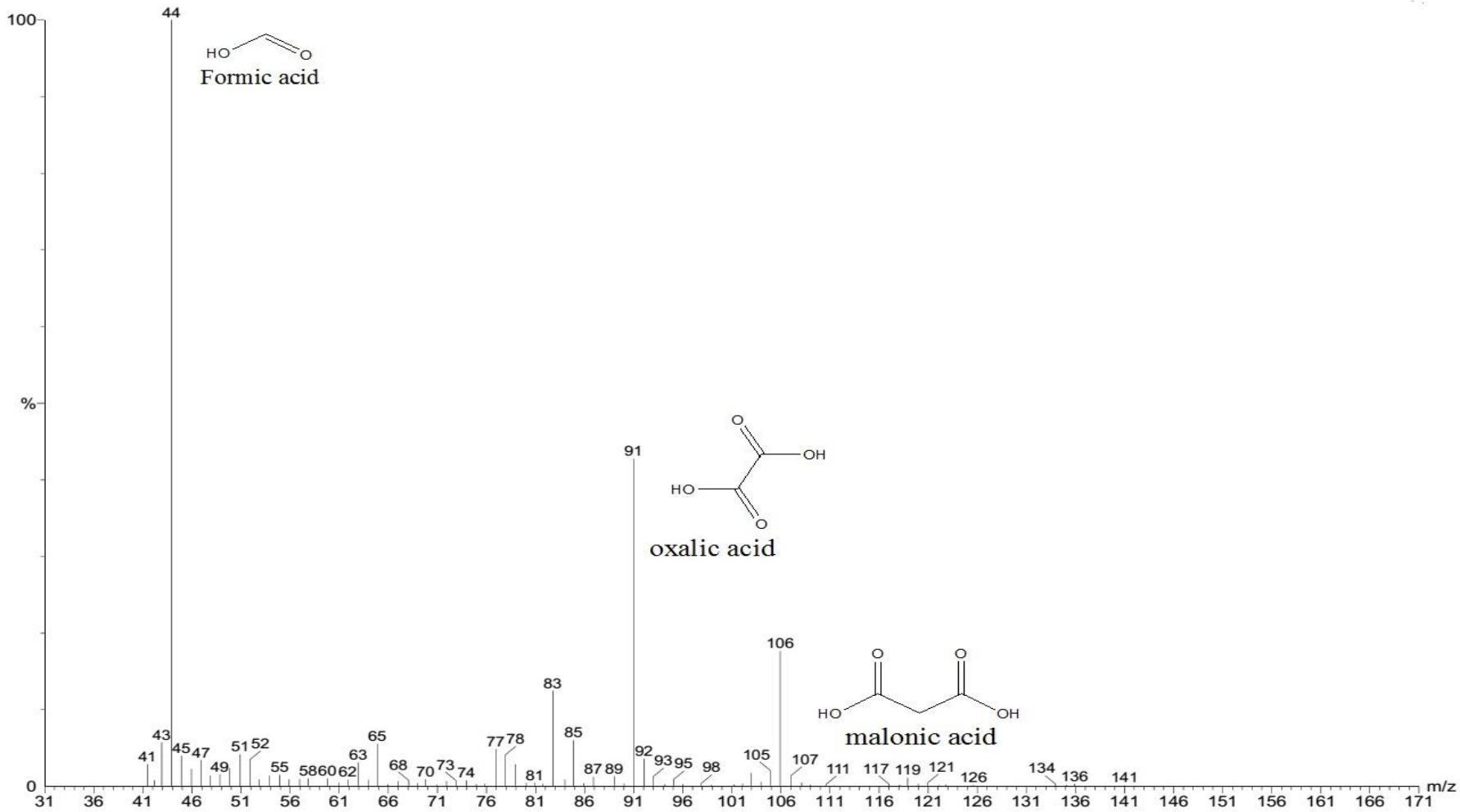

Figure 8.7c: Mass spectrum of the degradation products of MB

Table 8. 1: GC retention time and mass to charge ratio for MB

Retention time	**m/z**	**Name**
77.79	284	Methylene blue
61.552	270	Azure B
	256	Azure A
	236	Thionin
3.69	106	Malonic acid
	91	Oxalic acid
	44	Formic acid

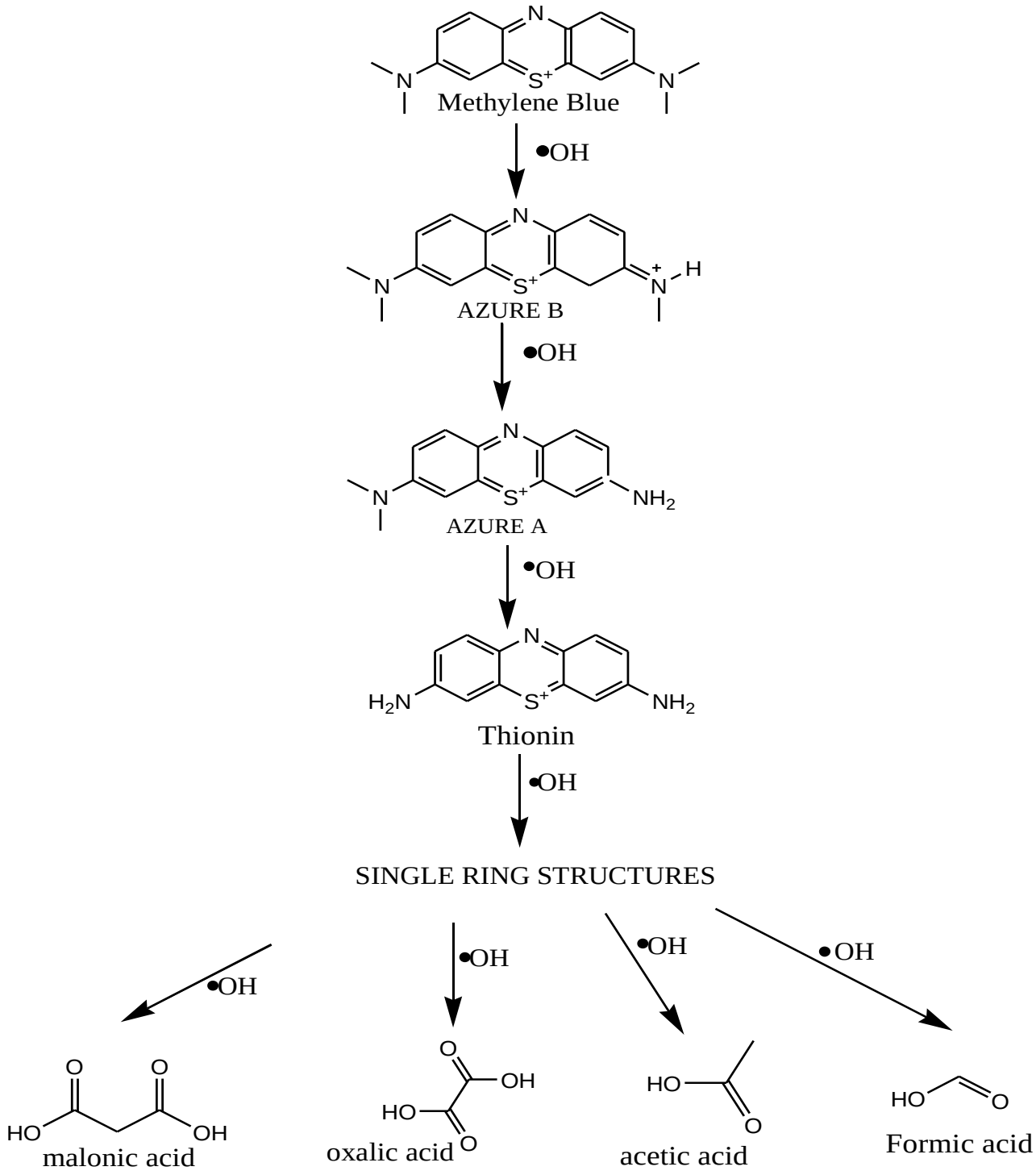

Figure 8. 8: Proposed reaction mechanism for MB

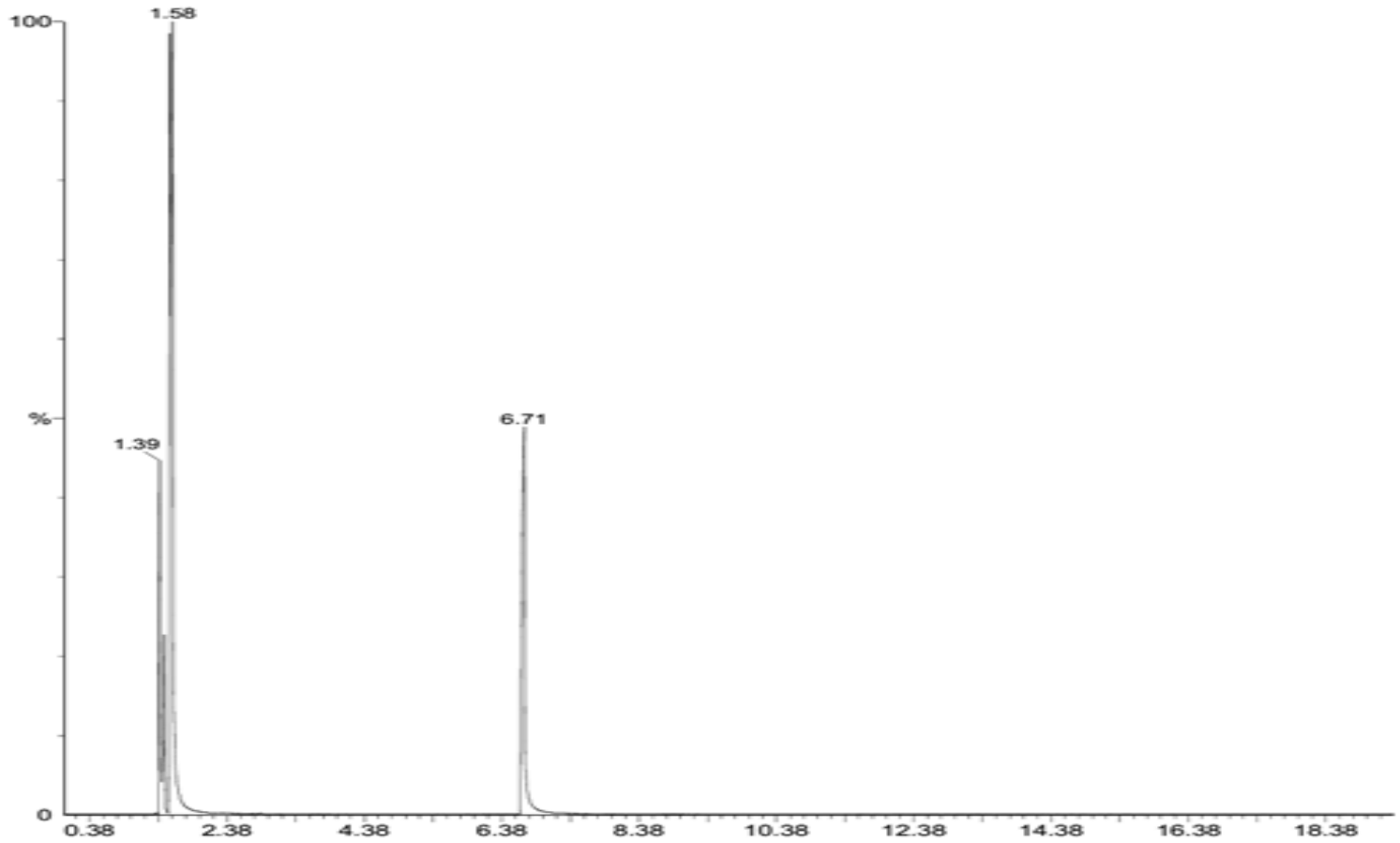

Figure 8. 9: GC Spectrum for the un-degraded 2-NP

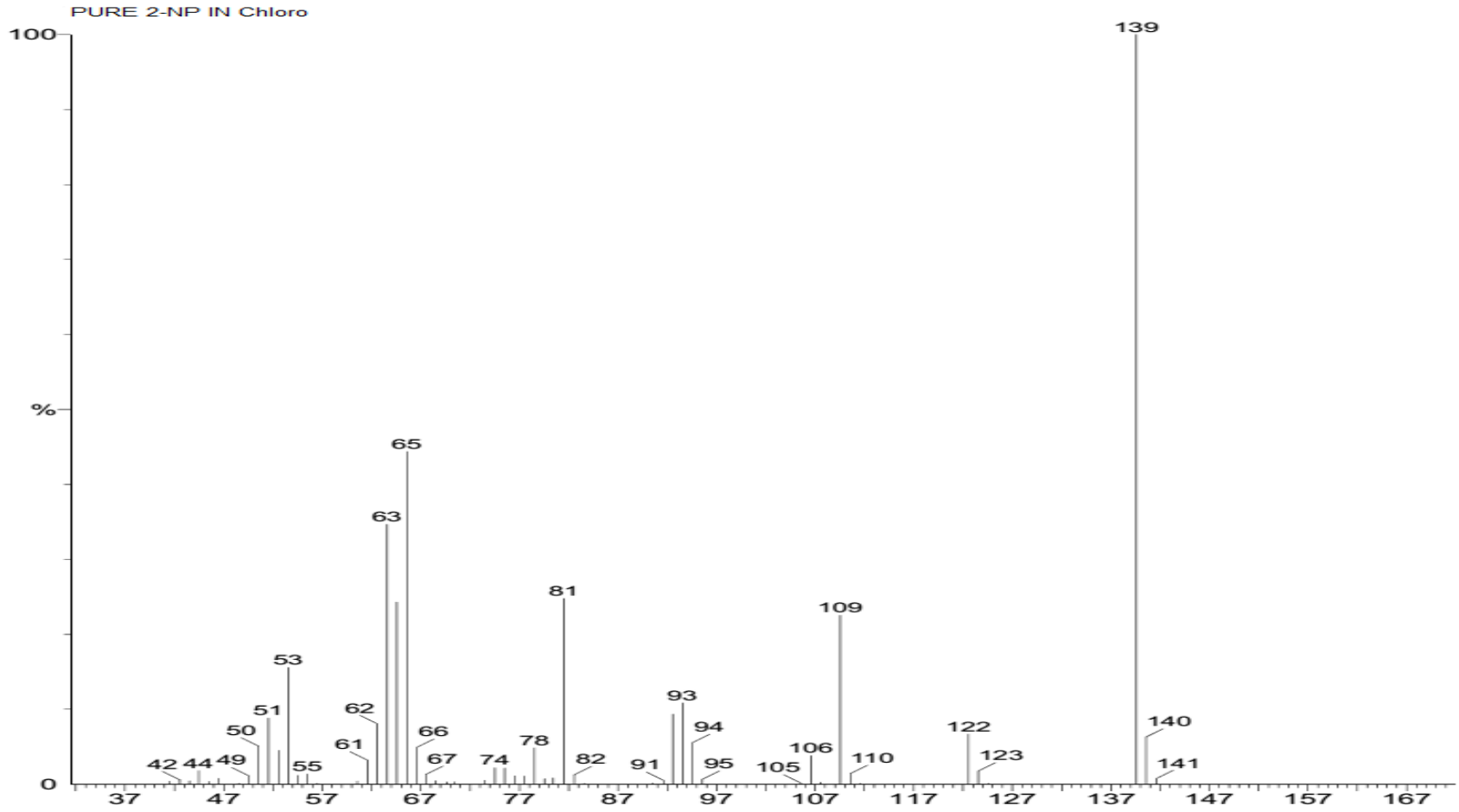

Figure 8. 10: Mass spectrum for the un-degraded 2-NP

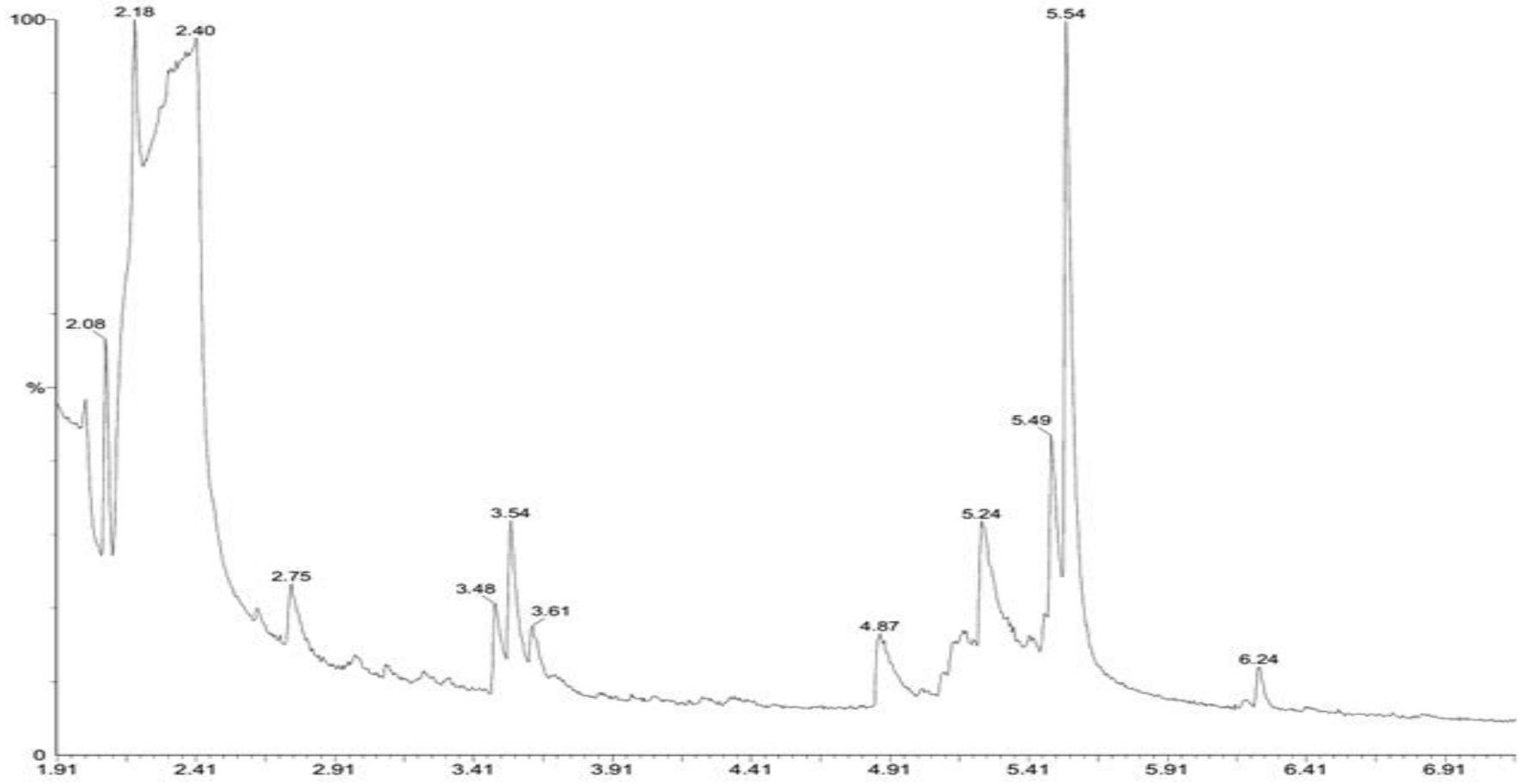

Figure 8. 11: GC Spectrum for the degradation products

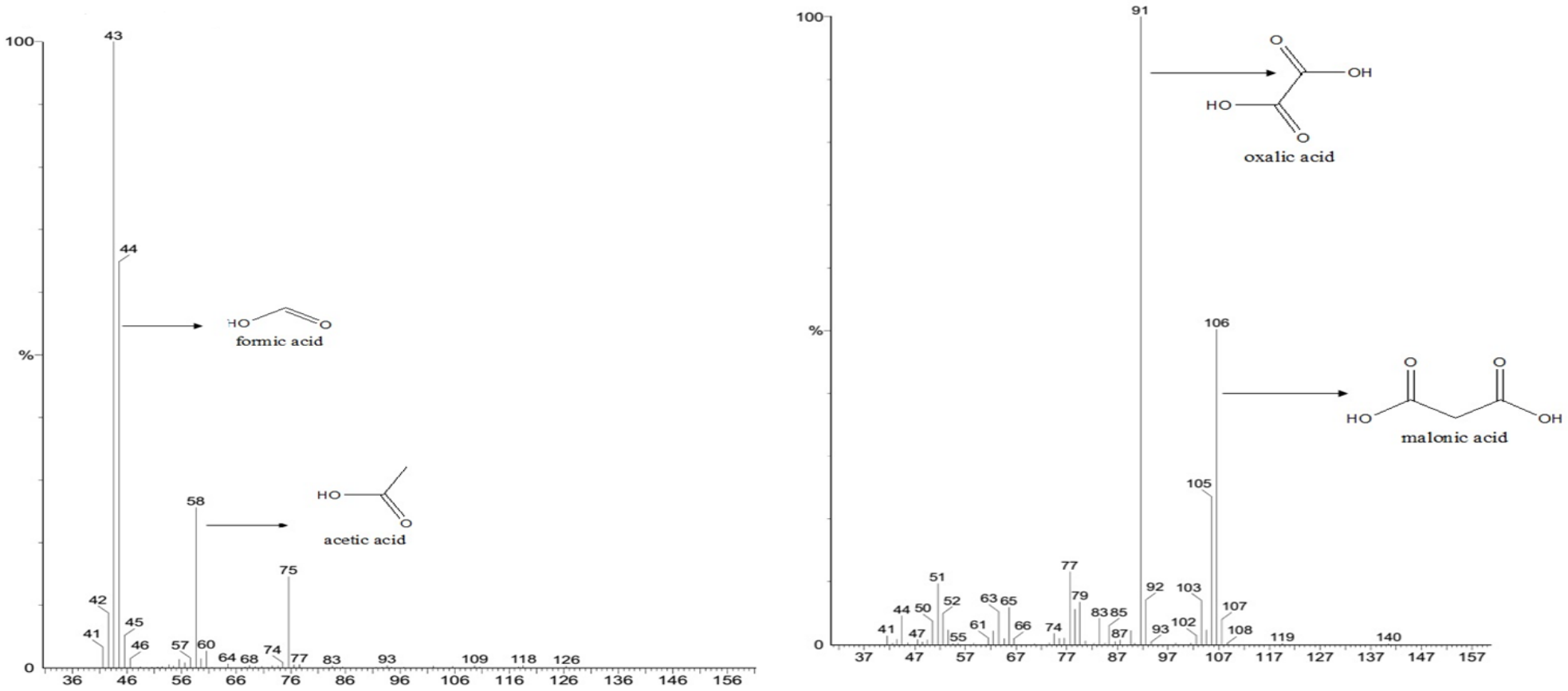

Figure 8. 12: Mass spectra for the degradation products

Table 8. 2: GC retention time and mass to charge ratio for 2-NP

Retention time (min)	m/z	Name
6.71	139	2-nitrophenol
2.840	106	Malonic acid
	91	Oxalic acid
	43	Formic acid

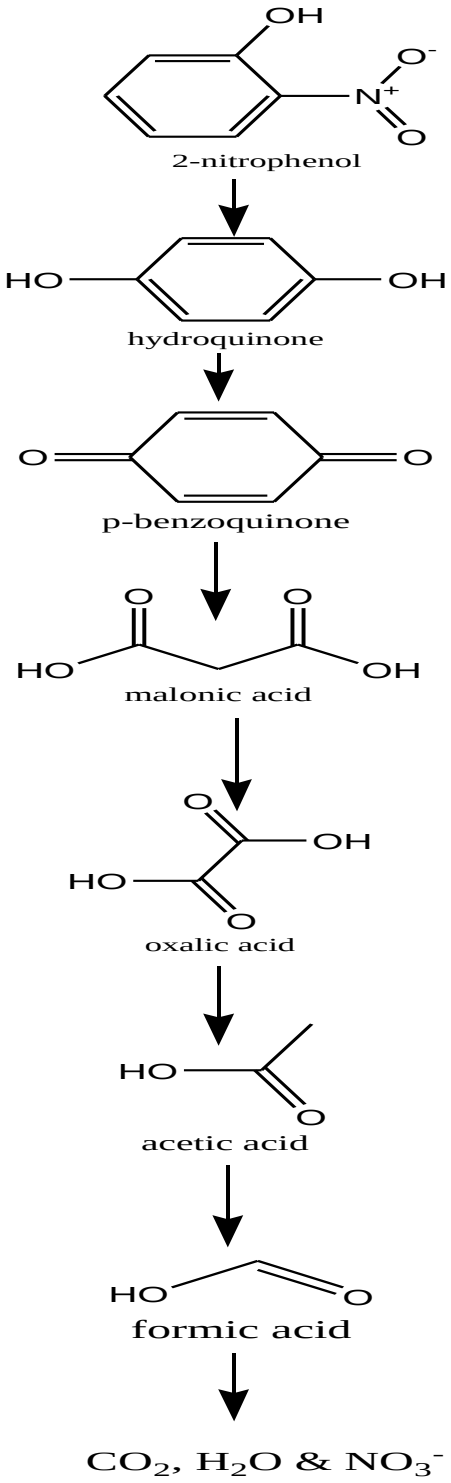

Figure 8. 13: Proposed reaction mechanism for 2-Nitrophenol

8.4 Conclusions

The Fenton oxidation process mechanism is known to be driven by the hydroxyl radicals and the super oxides radicals also contributed to the degradation of MB and 2-NP. The catalytic stability was also tested, and it was observed that for all catalyst the degradation decreased from the first run to the third run for both MB and 2-NP due to leaching of iron oxide. The leached iron was found to be less that the permissible limit of 2 ppm in water. It was observed that MB and 2-NP were degraded to smaller carboxylic acid. Hence it can be confirmed that the catalyst prepared can be used in the Fenton oxidation to degrade recalcitrant organic molecules to smaller molecules.

8.5 References

BOKER, V., KARMALI, R. & RANE, K. 2014. Comparison of degradation of methylene blue dye by ZnO, N doped ZnO and iron ore rejects. *European Chemical Bulletin,* 3**,** 520-529.

DI PAOLA, A., AUGUGLIARO, V., PALMISANO, L., PANTALE, G. & SAVINOV, E. 2003. Heterogeneous photocatalytic degradation of nitrophenols. *Journal of Photochemistry and Photobiology A: Chemistry,* 155 207-214.

GNASER, H., SAVINA, M. R., CALAWAY, W. F., TRIPA, E. C., VERYOVKIN, I. V. & PELLIN, M. J. 2005. Photocatalytic degradation of methylene blue on nanocrystalline TiO2: Surface mass spectrometry of reaction intermediates. *International Journal of Mass Spectrometry,* 245**,** 61-67.

GUO, S., ZHANG, G. K. & WANG, J. Q. 2014. Photo-Fenton degradation of rhodamine B using Fe_2O_3-kaolin as heterogeneous catalyst: characterization, process optimization and mechanism. *Journal of Colloid and Interface Science,* 433 1-8.

HOUAS, A., LACHHEB, H., KSIBI, M., ELALOUI, E., GUILLARD, C. & HERRMANN, J. M. 2001. Photocatalytic degradation pathway of methylene blue in water. *Applied Catalysis B: Environmental* 31**,** 145-157.

HUANG, F., CHEN, L., WANG, H. & YAN, Z. 2010. Analysis of the degradation mechanism of methylene blue by atmospheric pressure dielectric barrier discharge plasma. *Chemical Engineering Journal,* 162**,** 250-256.

LIOTTA, L. F., GRUTTADAURIA, M., DI CARLO, G., PERRINI, G. & LIBRANDO, V. 2009. Heterogeneous catalytic degradation of phenolic substrates: Catalysts activity. *Journal of Hazardous Materials,* 162**,** 588-606.

LIOU, R. M., CHEN, S. H., HUNG, M. Y., HSU, C. S. & LAI, J. Y. 2005. Fe (III) supported on resin as effective catalyst for the heterogeneous oxidation of phenol in aqueous solution. *Chemosphere,* 59**,** 117.

RAUF, M. A., MOHAMMED, A., MEETANI, M. A., KHALEEL, A. & AHMED, A. 2010. Photocatalytic degradation of Methylene Blue using a mixed catalyst and product analysis by LC/MS. *Chemical Engineering Journal,* 157 373-378.

REY, A., FARALDOS, M., CASAS, J. A., ZAZO, J. A., BAHAMONDE, A. & RODRı´GUEZ, J. J. 2009. Catalytic wet peroxide oxidation of phenol over Fe/AC catalysts: Influence of iron precursor and activated carbon surface. *Applied Catalysis B: Environmental,* 86**,** 69-77.

SABHI, S. & KIWI, J. 2001. Degradation of 2,4-dichlorophenol by immobilized iron catalysts. *Water Research,* 35**,** 1994-2002.

SAMUEL, M. S., SIVARAMAKRISHNA, A. & MEHTA, A. 2014. Bioremediation of p-Nitrophenol by Pseudomonas putida 1274 strain. *Journal of Environmental Health Science & Engineering.,* 12**,** 53.

WANG, L., MEI, L., XING, X., LIAO, L., LV, G., LI, Z. & WU, L. 2014. Mechanism and process of methylene blue degradation by manganese oxides under microwave irradiation. *Applied Catalysis B: Environmental* 160-161**,** 211-216.

XAVIER, S., GANDHIMATHI, R., NIDHEESH, P. V. & RAMESH, S. T. 2015. Comparative removal of Magenta MB from aqueous solution by homogeneous and heterogeneous photo-Fenton processes. *Desalination and Water Treatment***,** 1-10.

ZHAO, H., WANG, Y., WANG, Y., CAO, T. & ZHAO, G. 2012. Electro-Fenton oxidation of pesticides with a novel Fe_3O_4@Fe_2O_3/activated carbon aerogel cathode: High activity,

wide pH range and catalytic mechanism. *Applied Catalysis B: Environmental* 125**,** 120-127.

ZHOU, G., CHEN, Z., FANG, F., HE, Y., SUN, H. & SHI, H. 2015. Fenton-like degradation of Methylene Blue using paper mill sludge-derived magnetically separable heterogeneous catalyst: Characterization and mechanism. *Journal of Environmental Sciences*, 35**,** 20-26.

CHAPTER 9: CONCLUSIONS AND RECOMMENDATIONS

9.1 Conclusions

There have been efforts by researchers to synthesize heterogeneous Fenton catalyst that is cost effective. The current synthesis of the heterogeneous Fenton oxidation catalyst has shown to be time and energy constraining. The main aim of this study was to prepare non-toxic and low-cost heterogeneous Fenton oxidation from iron oxide catalyst supported on activated carbon produced from an agricultural waste via microwave synthesis for the Fenton oxidation of 2-nitro phenol and methylene blue.

The characterization results showed a successful synthesis of the PCP-AC-Iron oxide catalyst by microwave single step synthesis, as it was shown by FTIR, XRD, EDX, XPS, SEM, elemental mapping, iodine and methylene blue number. The catalyst synthesized at 600 W with 0.20g of the iron precursor was observed to produce the moderate amount of micropores and mesopores, as it was also shown the SEM images, IN and MBN. The elemental mapping also showed the high dispersion of iron oxide on the surface of the support, hence the optimum synthesis conditions were found to be at 600 W microwave treatment using 0.20 g of the iron precursor. The XPS showed the iron oxide formed on the surface of the support was found to be Fe_2O_3, with an average size of 1.72 nm as shown by the TEM. It can be concluded that both the iron precursor and microwave power had an effect on the porosity, thermal stability, chemical composition and dispersion of iron oxide on the surface of the support material.

The catalyst prepared at 600 W with 0.20g of the iron precursor was then applied in the degradation of 2-NP and MB. The experimental parameters were successfully optimized. The optimum conditions that gave the highest degradation efficiency were, for the volume of hydrogen peroxide

was found to be 20 ml at pH 7, a catalyst dose of 0.2 g, stirring speed of 500 rpm, initial concentration of 100 mg/l and temperature of 26 ^{o}C. The lowest temperature was chosen as the operating temperature to energy conservation. The results also showed that when using the PCP-AC-Iron oxide for the degradation of 2-NP and MB lowered the activation. Both MB and 2-NP showed similar degradation trend.

The degradation kinetics were also fitted to the pseudo-first-order, pseudo-second-order, and Langmuir-Hinshelwood models. The coefficient of determination and the percent variable error methods were used to determine which kinetic model gave the best fit. The data fitted the pseudo-second-order model, implying that the degradation of 2-NP and MB are surface reaction driven. Therefore Langmuir-Hinshelwood model was fitted since in order for the Langmuir-Hinshelwood model to be applied the data has to fit the pseudo-first-order model. It was observed that both the values of surface degradation constant, k, and Hinshelwood adsorption constant, K_L, increased as the amount of iron precursor applied for catalyst preparation increases, suggesting an increased surface degradation. However as the microwave power increases from 600 to 1200 W both the values of surface degradation constant, k, and Hinshelwood adsorption constant, K_L decreases, suggesting the degradation of methylene blue is more likely to take place on the solution. It was observed that for any particular mass of iron precursor applied for the catalyst preparation, the fractional surface coverage, θ_L, increased with initial MB concentration, thus increasing the rate. However as the microwave power increases the fractional surface coverage, θ_L, decrease, hence the decrease in rate constant was observed.

The thermodynamics parameters were also studied for the degradation of 2-NP. For the Fenton oxidation process of 2-NP, an increase in the temperature was observed to increase the degradation rate constant. However, an increase in mass from 0.01g to 0.20g showed to have increased rate

constants, spontaneity and the degree of randomness also decreased activation energies and enthalpy change which were endothermic. This implies that the feasibility of the reaction increase with an increase in mass of $FeCl_3$. However a further increase in mass of $FeCl_3$ could not further increase the feasibility and catalytic activity. Coupled with that, when microwave power increases from 600 to 1200 W the decreased rate constants, spontaneity and the degree of randomness also increased activation energies and enthalpy change which were endothermic. As a result decreasing the feasibility as the microwave power increases. Hence it can be concluded that the catalyst to give high feasibility and high catalytic activity should be prepared at a microwave power of 600 W with a mass of 0.20 g $FeCl_3$.

Fenton oxidation process mechanism, catalyst leaching and degradation products were studied. The Fenton oxidation process mechanism was found to be driven by the hydroxyl radicals and the super oxides radicals also contributed to the degradation of MB and 2-NP since the addition of isopropanol and benzoquinone resulted in the reduced degradation percentage of 2-NP and MB. The catalytic stability was also tested, and it was observed that for all catalyst the degradation % decrease from the first run to the third run for both MB and 2-NP due to leaching of iron oxide. The leached iron was found to be less that the permissible limit of 2 ppm in water. The Fenton oxidation process by the synthesized PCP-AC-Iron oxide composite showed to degrade MB and 2-NP to smaller carboxylic acid. Hence it can be confirmed that the catalyst prepared can be used in the Fenton oxidation to degrade recalcitrant organic molecules to smaller organic molecules.

9.2 Recommendations

This work describes the preparation and application of PCP-AC-Iron oxide on the heterogeneous Fenton oxidation of MB and 2-NP. Future works may explore using different size of the pine cone powder (smaller) as it may produce the PCP-AC-Iron oxide composite that has an increased surface area. Also exploring the use of different iron salt as a chemical activator and source of iron oxide, which may result in the PCP-AC-Iron oxide composites with different characteristics. The pre-treatment of the pine cone powder can be explored to remove the organic oils and resin acids in the carbonaceous material. For the application of the PCP-AC-iron oxide on the Fenton oxidation process, the degradation to be monitored with HPLC or TOC analyzer, especially for nitrophenols since they are colorless at low pH. And also the degradation products should be analyzed by HPLC-MS or LC-MS, since GC-MS requires volatile smaple.